Supplementary Information

Conformational Isomerization as a Key Selectivity-Determining Step

Kazuma Muto, Miho Hatanaka,* Fumitoshi Kakiuchi, and Takuya Kochi*

Table of Contents

I. General Information

Unless otherwise noted, all reactions were carried out under nitrogen, and all commercial reagents were used as received. Anhydrous Et_2O and THF were purchased from Kanto Chemical Co. Inc. and used as received. Anhydrous acetone was purchased from Wako Pure Chemical Industries, Ltd. and used as received. 1,2-Dichloroethane was distilled from P_2O_5. Dichloromethane was purified by passing through a Glass Contour solvent purification system. THF for LDA was distilled from sodium and benzophenone. Diisopropylamine for LDA was distilled from CaH_2. Methyl-d_3-triphenyl-phosphonium bromide was synthesized according to the literature procedure.[1] ^1H, and $^{13}C\{^1H\}$ NMR spectra were recorded on a JEOL ECS-400, ECX-400 or ECX-800 spectrometer. IR spectra were recorded on a JASCO FT/IR-410 infrared spectrometer. ESI-MS and DART-MS was performed on a JEOL JMS-T100LCS. Gel permeation chromatography (GPC) was carried out with JAI LC-9201 with JAIGEL 2.5H. Flash column chromatography was carried out with silica gel 60N (Kanto Chemical Co., Inc.).

II. Computational Details

All the calculations for structure optimization and vibrational frequency calculation were performed by using Gaussian 09 (revision D.01) program,[2] by M06 method[3] using SDD basis sets[4] with ECP for palladium and cc-pVDZ basis sets[5] for other atoms, with empirical dispersion correction (DFT-D3[6]). Single point PCM correction using SMD method[7]-[9] (1,2-dichloroethane) was adopted for single point calculation. All the values of free-energy change are at 298.15 K. To explore TS of the associative alkene exchange, we applied the artificial force induced reaction (AFIR) method[10]-[12] and The locally updated planes (LUP) method[13], [14] in GRRM17 program.[15], [16]

III. Structural and Electronic Parameters of Palladium Hydride Intermediates/TSs Containing 1,10-Phenanthroline and Propene Ligands.

Table S1. Energy Decomposition Analyses of Propene Hydride Palladium Intermediates/TSs (kcal/mol)[a]

	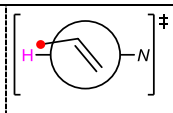 TS(**1**-**2**)	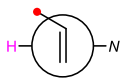 **2**	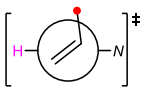 TS(**2**-**3**)	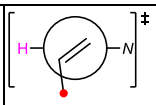 TS(**1**-**4**)	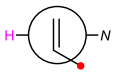 **4**	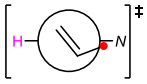 TS(**4**-**3**)
Δ*G*	8.5	4.6	5.9	6.0	4.0	9.7
ΔE_0	9.3	5.9	7.0	7.1	6.1	11.0
INT[a]	-37.8	-39.6	-39.2	-38.6	-39.3	-38.9
DEF_{alkene}[a]	4.8	3.2	4.1	3.5	3.2	6.9
$DEF_{[Pd]}$[a]	0.9	1.0	0.8	0.9	1.0	1.6

a) For energy decomposition analysis (EDA), the optimized structure is divided into the catalyst fragment [Pd] and the alkene, whose energies are calculated without further structural optimization. Separately, the two fragments are structurally optimized and then their energies are calculated. The interaction energy, INT, is defined as the difference between the total electronic energy (ΔE_0) of the original palladium complex and the sum of ΔE_0 of the structurally-unoptimized fragments. The deformation energy, DEF, is defined as the difference between ΔE_0 of the structurally-optimized and -unoptimized fragment.

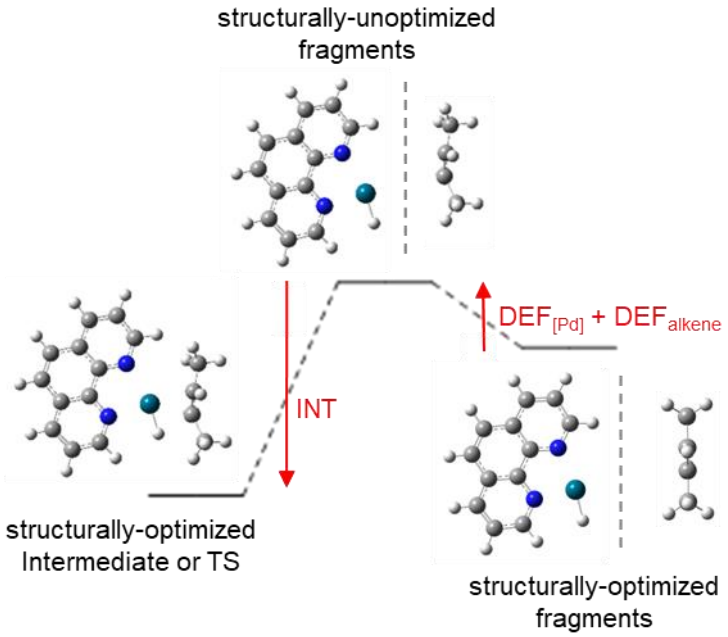

Table S2. Structural Parameters around the Propene Ligand of the Hydride Palladium Intermediates/TSs

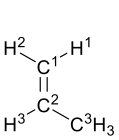

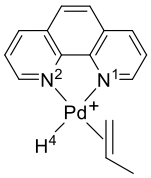

	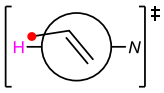 TS(**1**-**2**)	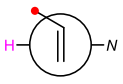 **2**	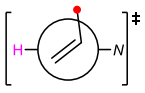 TS(**2**-**3**)	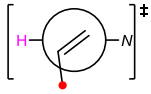 TS(**1**-**4**)	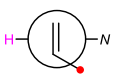 **4**	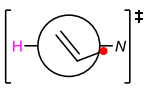 TS(**4**-**3**)
$H^1–C^1=C^2–H^3$ 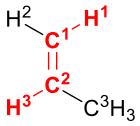	167.9°	165.4°	161.4°	160.2°	164.4°	168.5°
$H^2–C^1=C^2–C^3$ 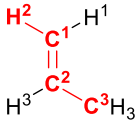	153.9°	162.8°	165.3°	163.7°	163.7°	148.6°
$C^1=C^2$ 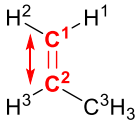	1.381 Å	1.380 Å	1.380 Å	1.382 Å	1.380 Å	1.384 Å
$C^3–C^2–H^3$ 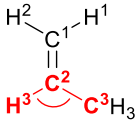	115.9°	115.5°	116.3°	116.3°	115.9°	116.0°
$H^1–C^1–H^2$ 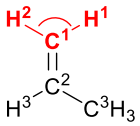	116.8°	116.5°	116.5°	117.0°	116.4°	115.9°
Pyramidalization angle (C^1H_2)[a]	17.1°	14.4°	14.5°	17.3°	15.1°	17.1°
Pyramidalization angle (C^2HMe)[a]	14.3°	11.4°	12.8°	12.6°	10.9°	18.1°

a) The pyramidalization angle is defined as the angle between the C=C bond and the plane formed by one of the alkene carbon, the hydrogen substituent, and the ligating atom of the R substituent (R = Me or H).

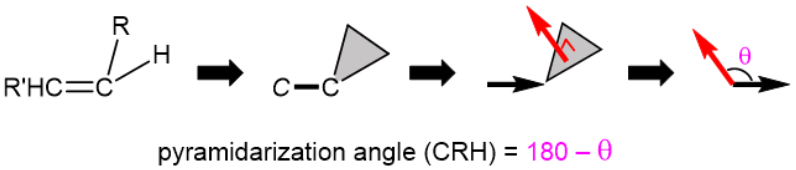

pyramidarization angle (CRH) = 180 – θ

Table S3. Structural Parameters Concerning the Relationship between Propene and the Palladium Center

	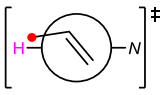 TS(**1**-**2**)	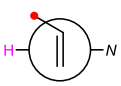 **2**	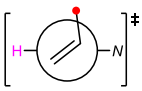 TS(**2**-**3**)	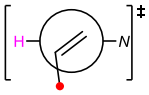 TS(**1**-**4**)	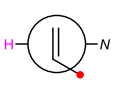 **4**	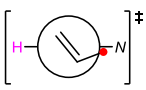 TS(**4**-**3**)
Pd–C^1 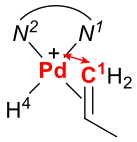	2.175 Å	2.186 Å	2.213 Å	2.166 Å	2.174 Å	2.214 Å
Pd–C^2 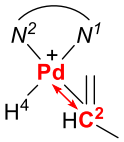	2.297 Å	2.232 Å	2.217 Å	2.276 Å	2.252 Å	2.239 Å
Pd–centroid 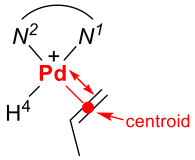	2.128 Å	2.099 Å	2.105 Å	2.111 Å	2.103 Å	2.116 Å
Pd–alkene distance 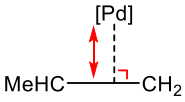	2.119 Å	2.097 Å	2.105 Å	2.104 Å	2.100 Å	2.116 Å
N^1–Pd–centroid 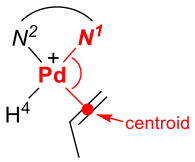	109.3°	101.4°	107.5°	109.8°	104.6°	117.0°
C^4–N^1–Pd–centroid 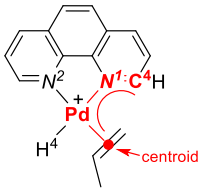	-5.8°	-3.4°	0.6°	8.2°	5.4°	-1.6°
Pd–centroid–C^1 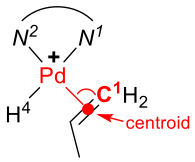	95.3°	92.0°	90.2°	94.8°	93.4°	91.1°

Table S4. Structural Parameters Concerning the Relationship between the Hydride/1,10-Phenanthroline Ligands and the Palladium Center of the Propene Complex

	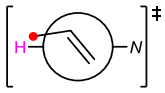 TS(**1**-**2**)	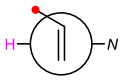 **2**	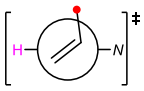 TS(**2**-**3**)	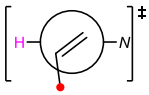 TS(**1**-**4**)	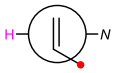 **4**	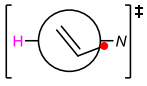 TS(**4**-**3**)
Pd–H^4 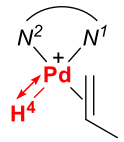	1.531 Å	1.542 Å	1.537 Å	1.541 Å	1.540 Å	1.528 Å
N^2–Pd–H^4 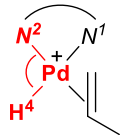	90.7°	94.7°	91.6°	91.6°	93.7°	89.3°
Pd–N^1 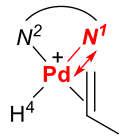	2.226 Å	2.206 Å	2.230 Å	2.211 Å	2.222 Å	2.266 Å
Pd–N^2 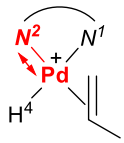	2.100 Å	2.107 Å	2.103 Å	2.105 Å	2.105 Å	2.123 Å

Table S5. NBO analyses of the Propene Hydride Palladium Intermediates/TSs

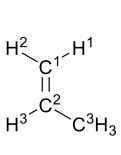

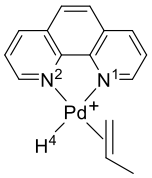

	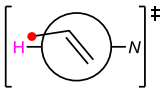 TS(**1**-**2**)	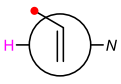 **2**	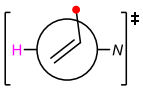 TS(**2**-**3**)	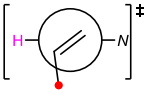 TS(**1**-**4**)	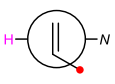 **4**	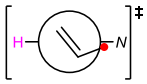 TS(**4**-**3**)
σ(C^1=C^2) [a]	1.99	1.99	1.99	1.99	1.99	1.99
σ*(C^1=C^2) [a]	0.01	0.01	0.01	0.01	0.01	0.01
p(C^1) of σ(C^1=C^2) [b]	65.2%	65.3%	64.9%	65.3%	65.3%	64.5%
p(C^2) of σ(C^1=C^2) [b]	65.5%	65.7%	65.7%	65.5%	65.4%	65.9%
π(C^1=C^2) [a]	1.67	1.67	1.66	1.66	1.66	1.65
π*(C^1=C^2) [a]	0.19	0.18	0.20	0.21	0.18	0.22
p(C^1) of π(C^1=C^2) [b]	96.1%	96.4%	96.9%	96.1%	96.2%	97.2%
p(C^2) of π(C^1=C^2) [b]	96.9%	96.7%	96.6%	97.4%	97.2%	96.5%
bond index (Pd–C^1)	0.37	0.32	0.31	0.39	0.33	0.30
bond index (Pd–C^2)	0.27	0.28	0.28	0.26	0.26	0.29
bond index (C^1=C^2)	1.57	1.57	1.56	1.55	1.57	1.54
Mulliken Charge (alkene)	0.35	0.38	0.35	0.36	0.38	0.33
Mulliken Charge (Pd)	0.20	0.14	0.18	0.17	0.15	0.22
Natural Charge (alkene)	0.18	0.21	0.19	0.18	0.21	0.17
Natural Charge (Pd)	0.28	0.27	0.27	0.27	0.26	0.28

a) The occupancy of the natural bond orbital.

b) The p character of the orbitals of the corresponding atom in the natural bond orbital.

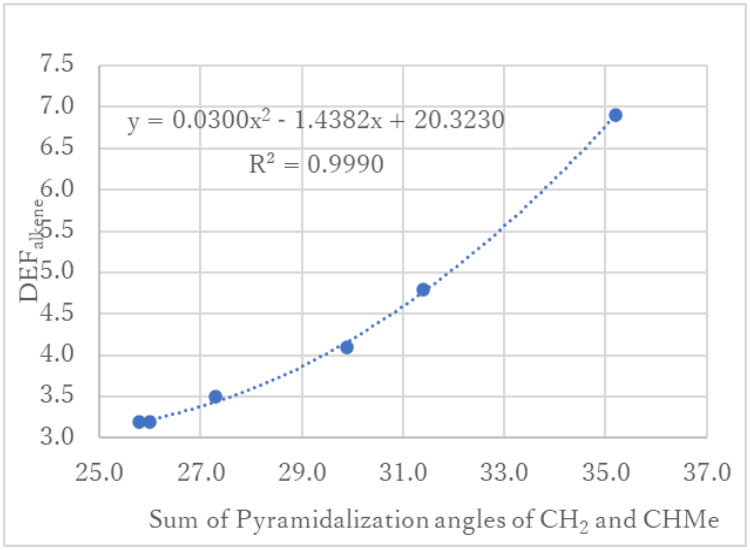

Figure S1. The quadratic regression of the strain energy of the propene (DEF_{alkene}) on the sum of the propene pyramidalization angles of the intermediates/TSs.

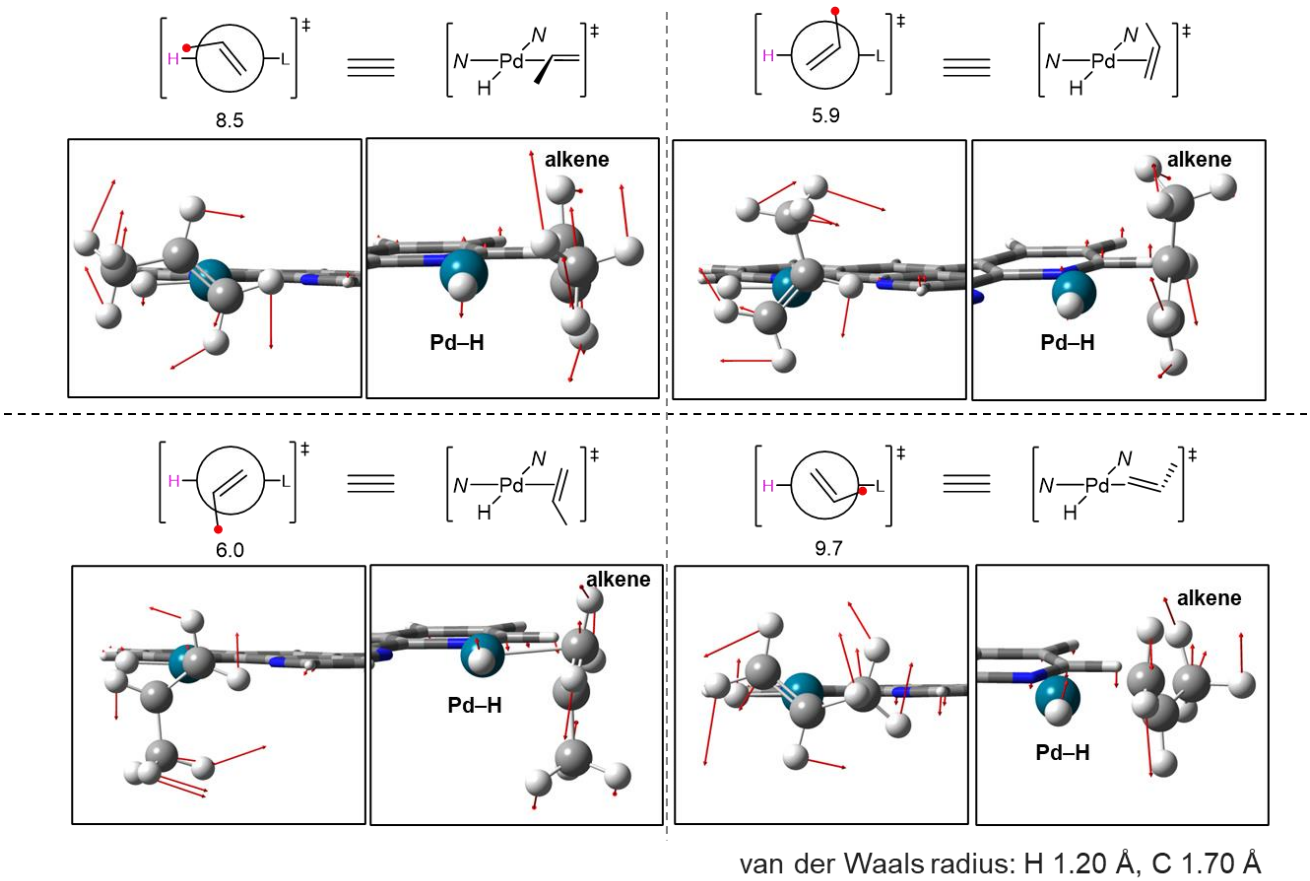

Figure S2. The direction of the vibration vectors of imaginary frequencies at the transition states during the chain walking over the three-carbon alkyl chain.

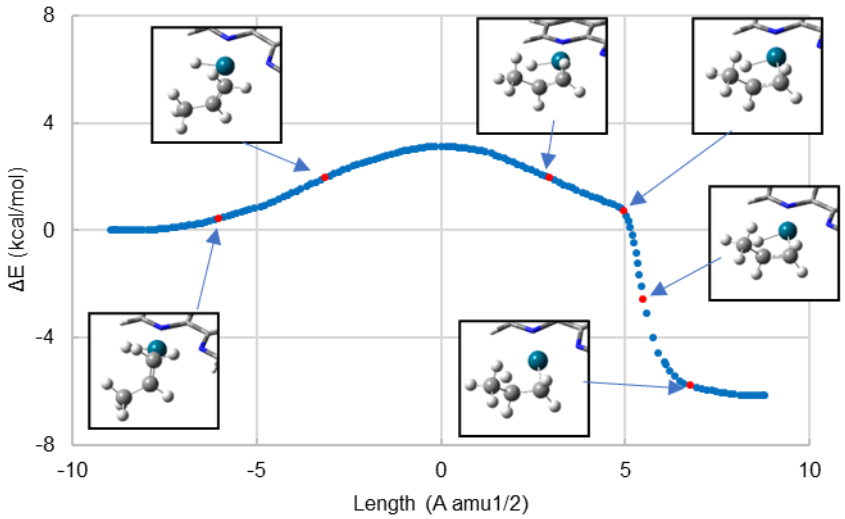

Figure S3. The changes of the Gibbs free energy along the intrinsic reaction coordinate for the pathway from **2** to **1** and some structures of the palladium complexes on the IRC.

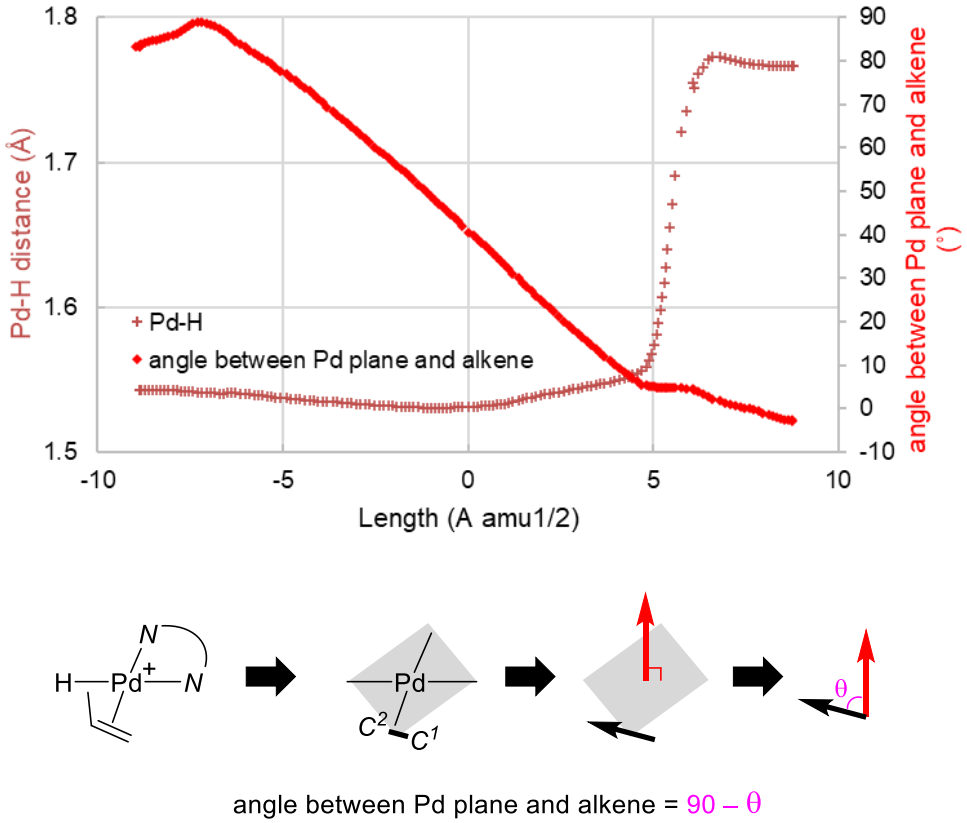

Figure S4. The changes of the Pd–H bond length and the angle between the Pd plane (square plane) and the C^1–C^2 bond along the intrinsic reaction coordinate for the pathway from **2** to **1**.

IV. Calculated Reaction Pathways of the Palladium Chain Walking on the Three-Carbon Alkyl Chain and Alkene Exchange

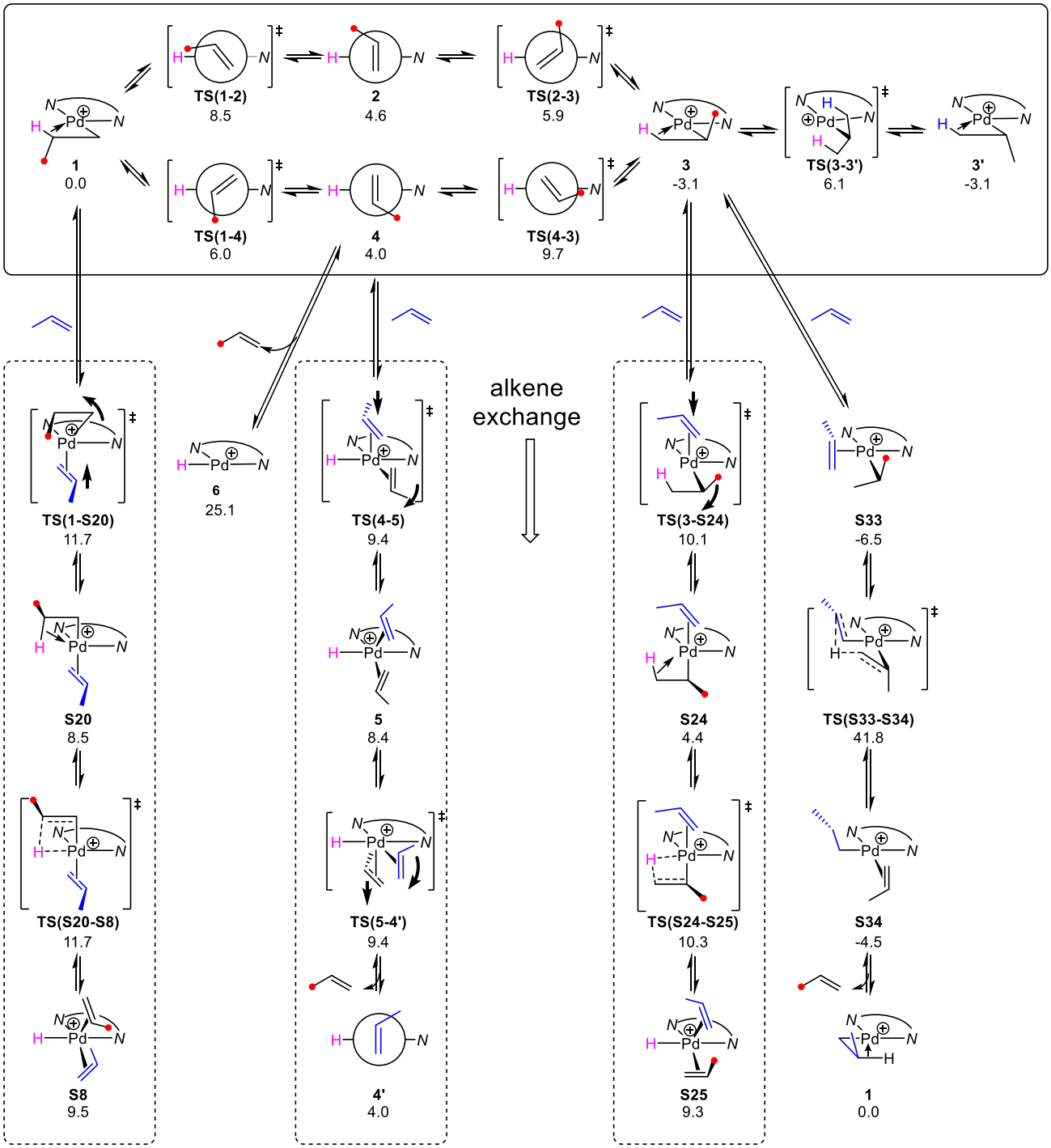

Figure S5. Comparison of the alkene exchange pathways in the (phen)Pd chain walking in the three-carbon chain. The number associated with each structure is the Gibbs free energy (ΔG, kcal/mol).

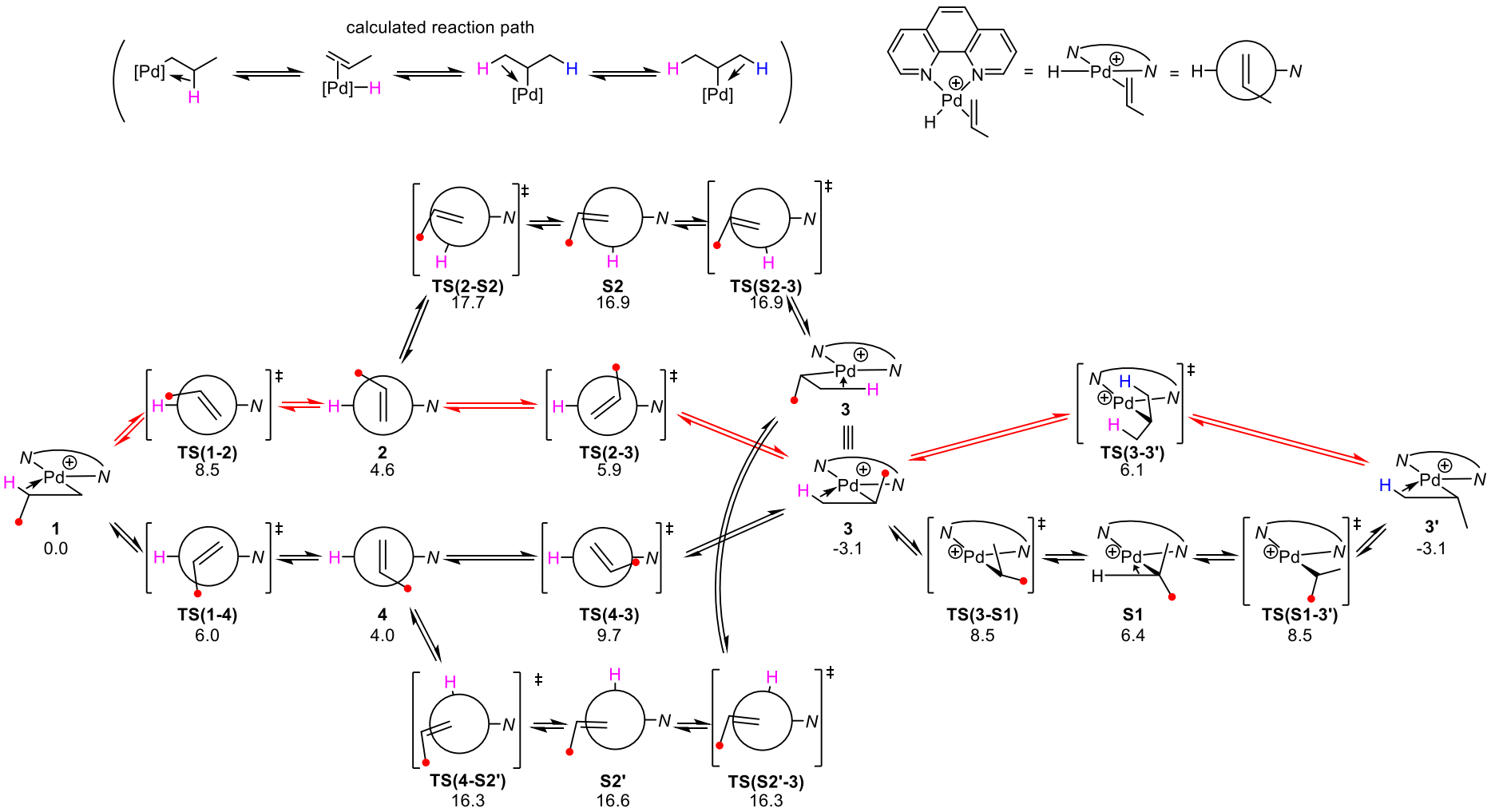

Figure S6. The calculated pathways in the (phen)Pd chain walking on the three carbon chain. The number associated with each structure is the Gibbs free energy (ΔG, kcal/mol).

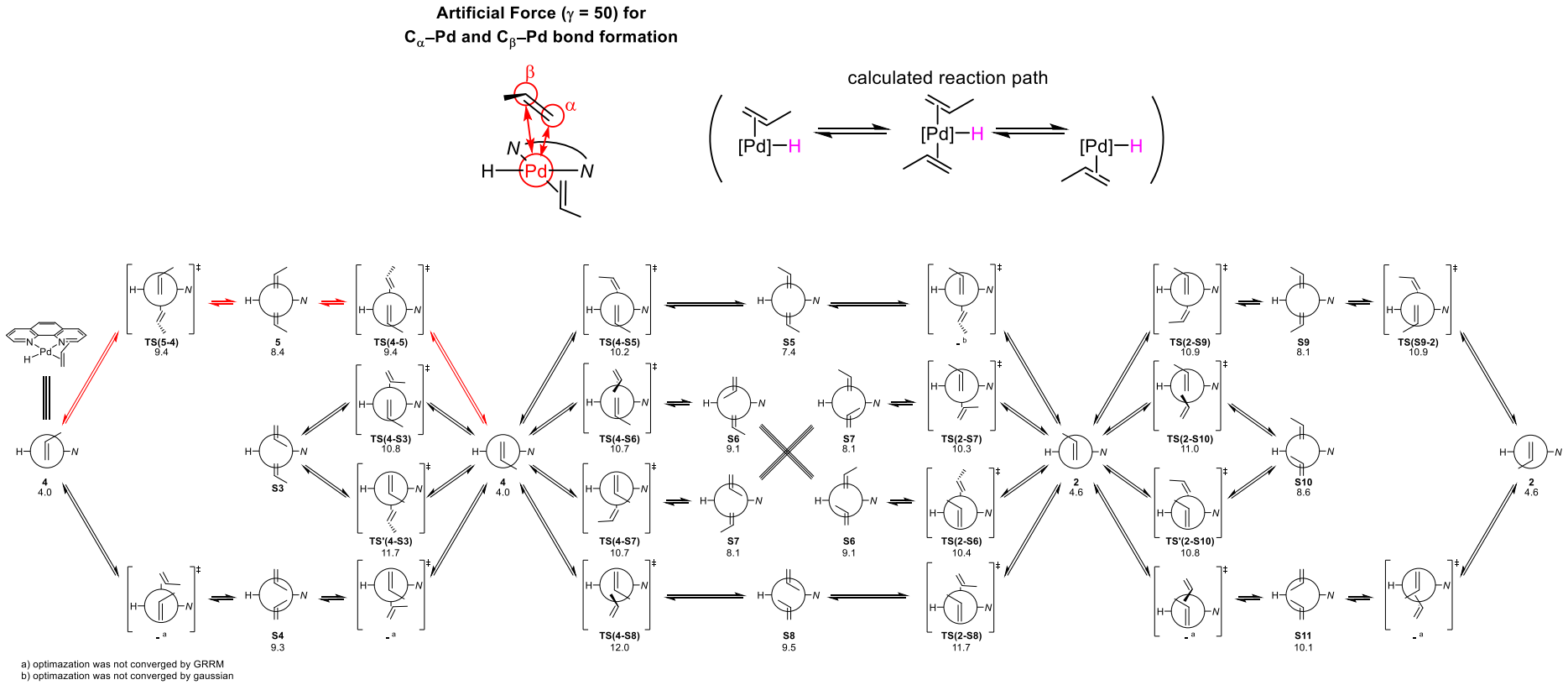

Figure S7. Comparison of the associative alkene exchange pathways in the (phen)Pd chain walking in the three carbon chain. The pathways differ by the orientation of the propene ligands. The number associated with each structure is the Gibbs free energy (Δ*G*, kcal/mol).

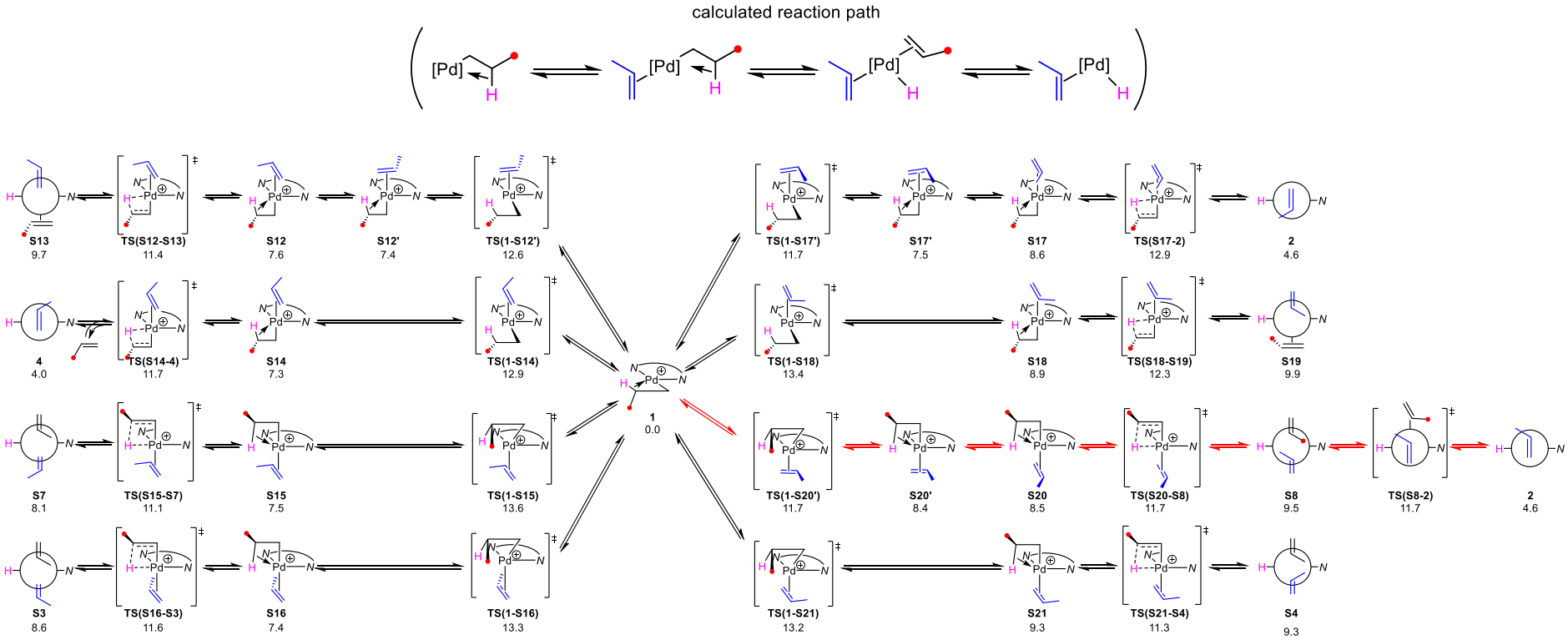

Figure S8. Examination of the associative alkene exchange pathways via direct association of the incoming propene with the (phen)Pd^{n}Pr complex. The number associated with each structure is the Gibbs free energy (ΔG, kcal/mol).

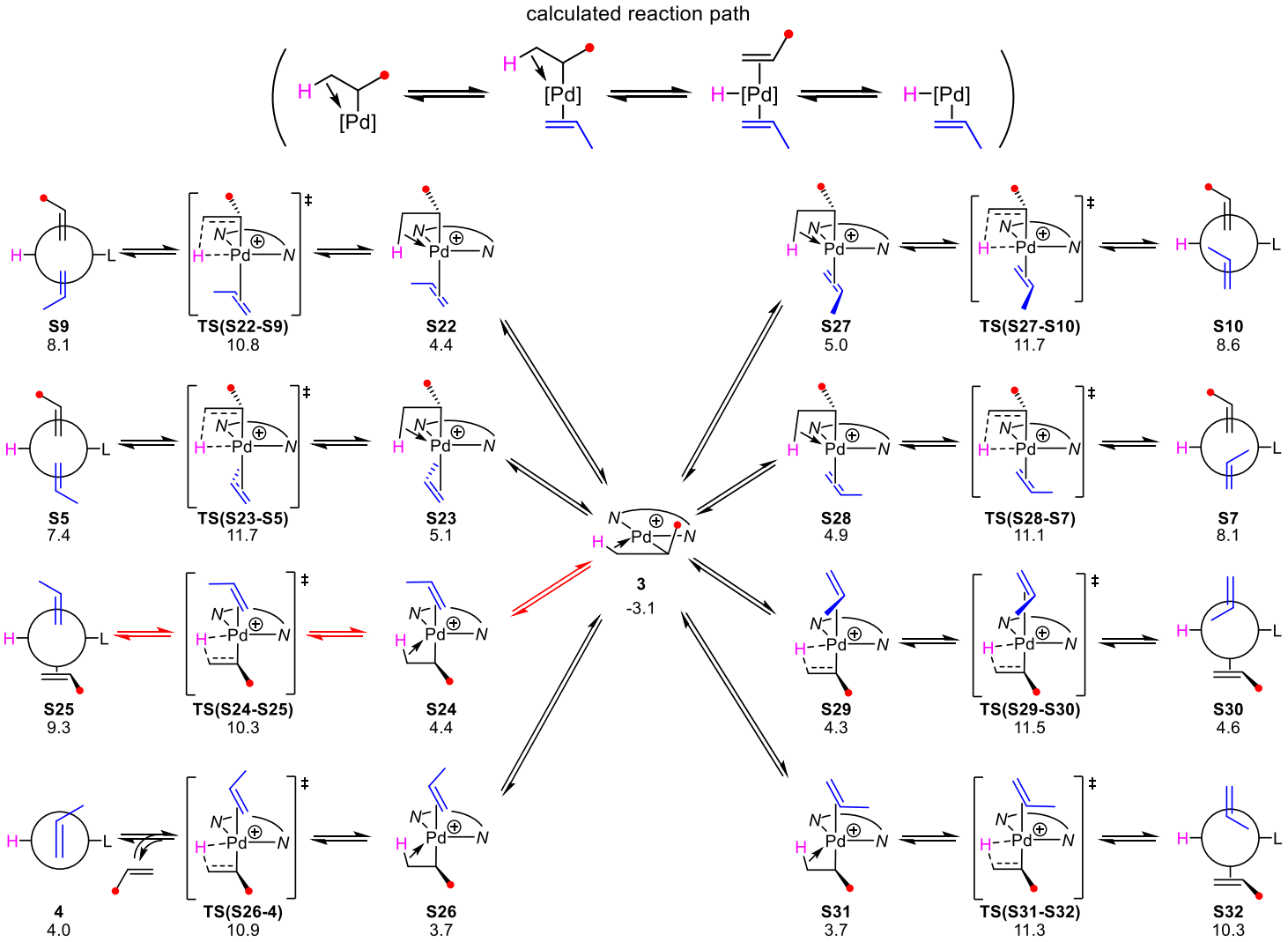

Figure S9. Examination of the associative alkene exchange pathways via direct association of the incoming propene with the (phen)Pd^{i}Pr complex. The number associated with each structure is the Gibbs free energy (ΔG, kcal/mol).

V. Structural and Electronic Parameters of Palladium Hydride Intermediates/TSs Containing 1,10-Phenanthroline and Cis-2-Butene Ligands.

Table S6. Energy Decomposition Analyses of Cis-2-Butene Hydride Palladium Intermediates/TSs (kcal/mol)[a]

	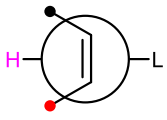 **9c**	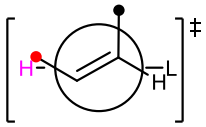 TS(**7c**-**9c**)	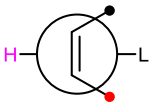 **9c'**	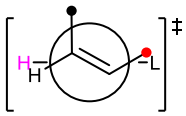 TS(**7c**-**9c'**)
Δ*G*	2.4	5.7	3.2	6.5
Δ*E*	7.6	9.2	6.6	10.6
INT[a]	-39.8	-39.5	-41.0	-40.9
DEF_{alkene}[a]	2.2	3.8	2.7	6.1
$DEF_{[Pd]}$[a]	1.2	0.9	1.0	1.5

a) For energy decomposition analysis (EDA), the optimized structure is divided into the catalyst fragment [Pd] and the alkene, whose energies are calculated without further structural optimization. Separately, the two fragments are structurally optimized and then their energies are calculated. The interaction energy, INT, is defined as the difference between the total electronic energy (ΔE_0) of the original palladium complex and the sum of ΔE_0 of the structurally-unoptimized fragments. The deformation energy, DEF, is defined as the difference between ΔE_0 of the structurally-optimized and -unoptimized fragment.

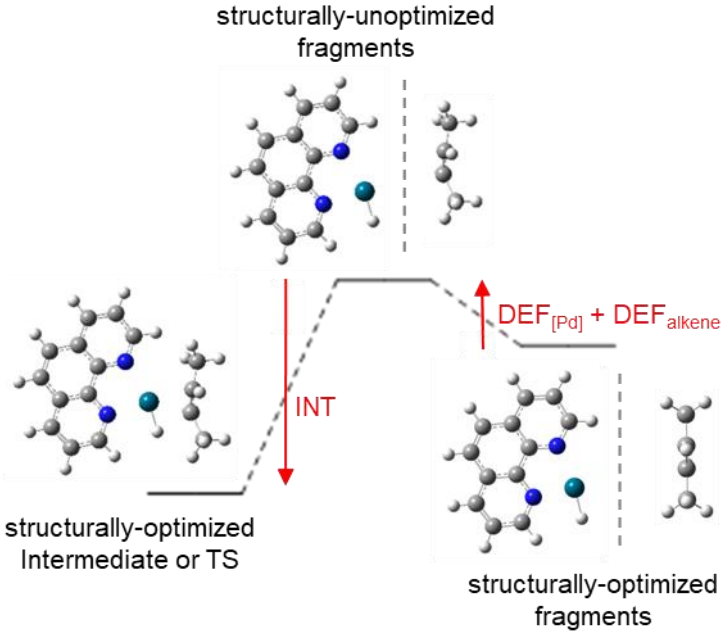

Table S7. Structural Parameters around the Cis-2-Butene Ligand of the Hydride Palladium Intermediates/TSs

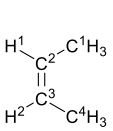
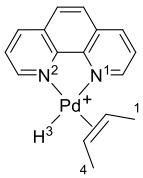

	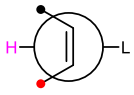 **9c**	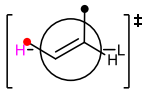 TS(**7c**-**9c**)	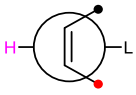 **9c'**	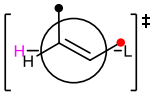 TS(**7c**-**9c'**)
$C^1–C^2=C^3–H^2$ 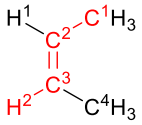	-163.3°	-155.4°	-164.7°	-150.1°
$H^1–C^2=C^3–C^4$ 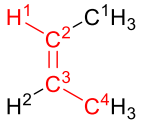	162.5°	166.8°	163.3°	165.7°
$C^2=C^3$ 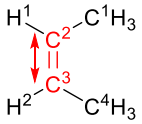	1.385 Å	1.387 Å	1.385 Å	1.390 Å
$C^1–C^2–H^1$ 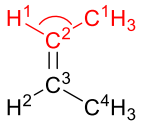	114.7°	115.7°	114.9°	115.7°
$C^4–C^3–H^2$ 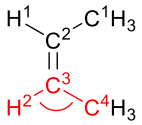	114.7°	115.2°	114.8°	115.3°
Pyramidalization angle (C^2HMe)[a]	13.5°	15.9°	12.3°	15.6°
Pyramidalization angle (C^3HMe)[a]	13.4°	14.4°	12.8°	20.2°

a) The pyramidalization angle is defined as the angle between the C=C bond and the plane formed by one of the alkene carbon, the hydrogen substituent, and the ligating atom of the R substituent (R = Me or H).

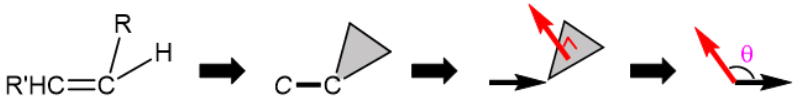

pyramidarization angle (CRH) = 180 – θ

Table S8. Structural Parameters Concerning the Relationship between the Cis-2-Butene and the Palladium Center

	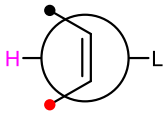 **9c**	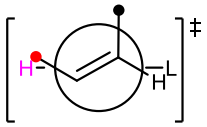 TS(**7c**-**9c**)	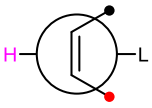 **9c'**	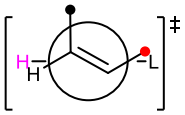 TS(**7c**-**9c'**)
Pd–C^2 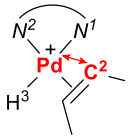	2.224 Å	2.205 Å	2.235 Å	2.261 Å
Pd–C^3 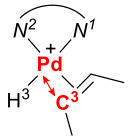	2.224 Å	2.275 Å	2.237 Å	2.218 Å
Pd–centroid 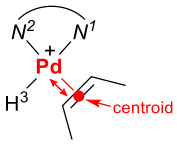	2.111 Å	2.130 Å	2.126 Å	2.129 Å
Pd–alkene distance 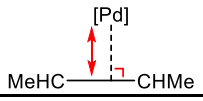	2.111 Å	2.127 Å	2.126 Å	2.128 Å
N^1–Pd–centroid 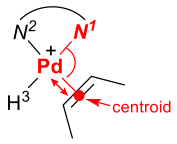	101.2°	107.5°	108.3°	116.9°
C^4–N^1–Pd–centroid 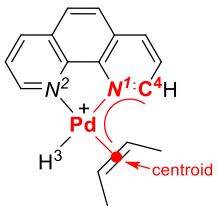	-2.0°	1.9°	-1.1°	-3.3°
Pd–centroid–C^1 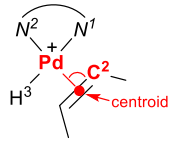	90.2°	93.1°	90.1°	91.9°

Table S9. Structural Parameters Concerning the Relationship between the Hydride/1,10-Phenanthroline Ligands and the Palladium Center of the Cis-2-Butene Complex

	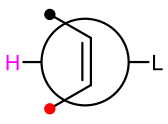 **9c**	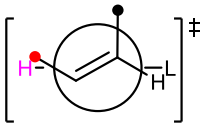 TS(**7c**-**9c**)	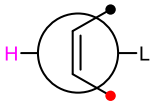 **9c'**	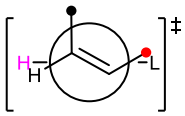 TS(**7c**-**9c'**)
Pd–H^3 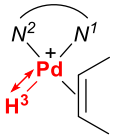	1.542 Å	1.534 Å	1.536 Å	1.532 Å
N^2–Pd–H^3 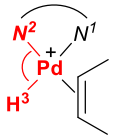	94.4°	91.5°	92.1°	90.0°
Pd–N^1 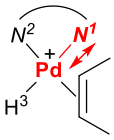	2.211 Å	2.230 Å	2.264 Å	2.264 Å
Pd–N^2 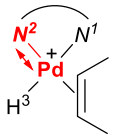	2.106 Å	2.102 Å	2.105 Å	2.119 Å

Table S10. NBO analyses of the Cis-2-Butene Hydride Palladium Intermediates/TSs

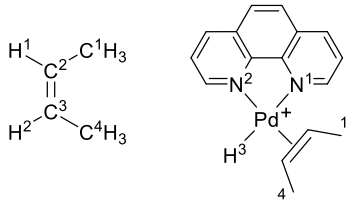

	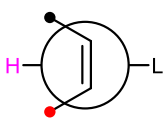	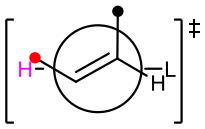	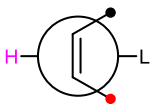	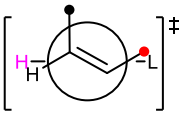
	9c	TS(**7c**-**9c**)	**9c'**	TS(**7c**-**9c'**)
σ(C^2=C^3) [a]	1.98	1.98	1.98	1.98
σ*(C^2=C^3) [a]	0.02	0.02	0.02	0.02
p(C^2) of σ(C^2=C^3) [b]	64.9%	64.8%	65.5%	65.4%
p(C) of σ(C^2=C^3) [b]	65.0%	65.7%	65.4%	65.3%
π(C^2=C^3) [a]	1.66	1.64	1.66	1.66
π*(C^2=C^3) [a]	0.20	0.21	0.19	0.24
p(C^2) of π(C^2=C^3) [b]	97.3%	97.8%	96.6%	96.8%
p(C^3) of π(C^2=C^3) [b]	97.2%	96.5%	96.6%	96.7%
bond index (Pd–C^2)	0.30	0.26	0.31	0.27
bond index (Pd–C^3)	0.30	0.36	0.31	0.33
bond index (C^2=C^3)	1.5444	1.496	1.5334	1.529
Mulliken Charge (alkene)	0.38	0.35	0.39	0.35
Mulliken Charge (Pd)	0.16	0.20	0.15	0.21
Natural Charge (alkene)	0.22	0.19	0.23	0.20
Natural Charge (Pd)	0.27	0.27	0.27	0.27

a) The occupancy of the natural bond orbital.

b) The p character of the orbitals of the corresponding atom in the natural bond orbital.

VI. Structural and Electronic Parameters of Palladium Hydride Intermediates/TSs Containing 1,10-Phenanthroline and Trans-2-Butene Ligands.

Table S11. Energy Decomposition Analyses of Trans-2-Butene Hydride Palladium Intermediates/TSs (kcal/mol)[a]

	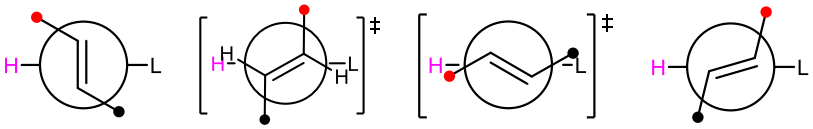			
	9t	TS(**9t-8't**)	TS(**8t-9t**)	**8't**
Δ*G*	2.0	3.1	10.1	1.7
Δ*E*	6.0	6.6	13.8	6.3
INT[a]	-40.8	-40.6	-40.1	-41.6
DEF_{alkene}[a]	4.5	5.0	10.8	5.8
$DEF_{[Pd]}$[a]	0.9	0.8	1.8	0.8

a) For energy decomposition analysis (EDA), the optimized structure is divided into the catalyst fragment [Pd] and the alkene, whose energies are calculated without further structural optimization. Separately, the two fragments are structurally optimized and then their energies are calculated. The interaction energy, INT, is defined as the difference between the total electronic energy (ΔE_0) of the original palladium complex and the sum of ΔE_0 of the structurally-unoptimized fragments. The deformation energy, DEF, is defined as the difference between ΔE_0 of the structurally-optimized and -unoptimized fragment.

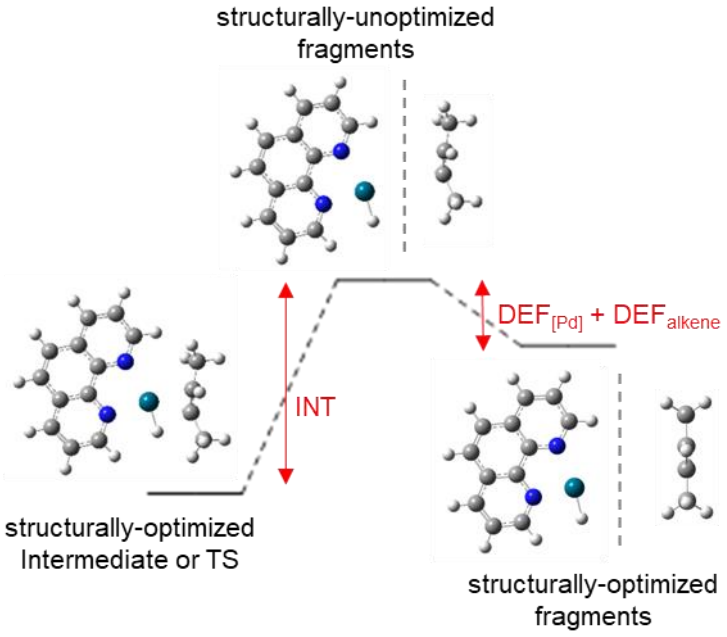

Table S12. Structural Parameters around the Trans-2-Butene Ligand of the Hydride Palladium Intermediates/TSs

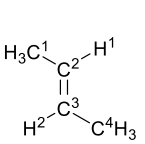
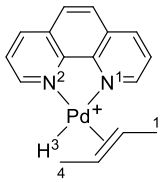

	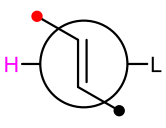 **9t**	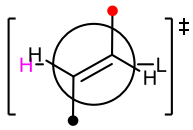 TS(**9t-8't**)	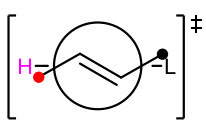 TS(**8t-9t**)	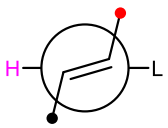 **8't**
$C^1–C^2=C^3–C^4$ 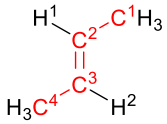	160.6°	160.8°	140.7°	158.4°
$H^1–C^2=C^3–H^2$ 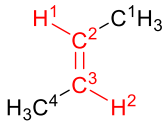	165.1°	161.9°	169.1°	161.5°
$C^2=C^3$ 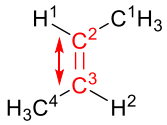	1.384 Å	1.384 Å	1.389 Å	1.388 Å
$C^1–C^2–H^1$ 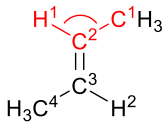	116.0°	116.5°	115.5°	116.4°
$C^4–C^3–H^2$ 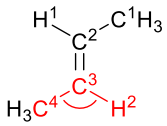	115.8°	116.5°	115.9°	117.1°
Pyramidalization angle (C^2H_2)[a]	13.4°	14.3°	19.4°	15.8°
Pyramidalization angle (C^3HMe)[a]	14.4°	15.5°	21.9°	16.8°

a) The pyramidalization angle is defined as the angle between the C=C bond and the plane formed by one of the alkene carbon, the hydrogen substituent, and the ligating atom of the R substituent (R = Me or H).

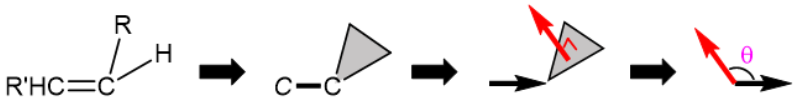

pyramidarization angle (CRH) = 180 – θ

Table S13. Structural Parameters Concerning the Relationship between the Trans-2-Butene and the Palladium Center

	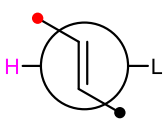 **9t**	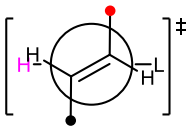 TS(**9t-8't**)	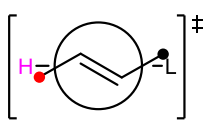 TS(**8t-9t**)	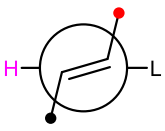 **8't**
Pd–C^2 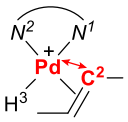	2.208 Å	2.254 Å	2.269 Å	2.265 Å
Pd–C^3 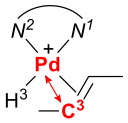	2.230 Å	2.196 Å	2.222 Å	2.182 Å
Pd–centroid 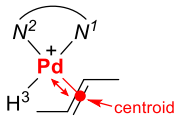	2.108 Å	2.115 Å	2.135 Å	2.113 Å
Pd–alkene distance 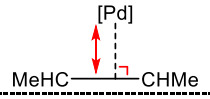	2.108 Å	2.113 Å	2.134 Å	2.109 Å
N^1–Pd–centroid 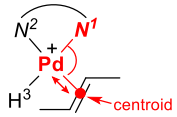	104.4°	108.1°	118.5°	110.1°
C^4–N^1–Pd–centroid 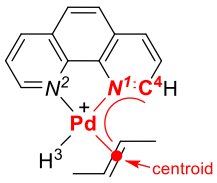	3.1°	2.3°	-7.3°	1.1°
Pd–centroid–C^1 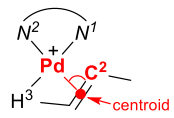	92.0°	91.0°	92.5°	93.6°

Table S14. Structural Parameters Concerning the Relationship between the Hydride/1,10-Phenanthroline Ligands and the Palladium Center of the Trans-2-Butene Complex

	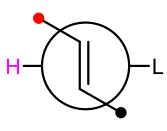 **9t**	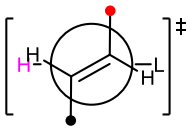 TS(**9t-8't**)	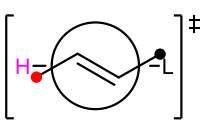 TS(**8t-9t**)	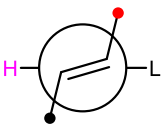 **8't**
Pd–H^3 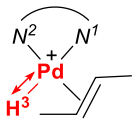	1.542 Å	1.542 Å	1.521 Å	1.546 Å
N^2–Pd–H^3 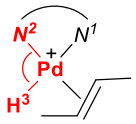	93.2°	91.9°	88.4°	91.9°
Pd–N^1 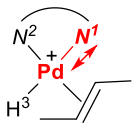	2.225 Å	2.223 Å	2.273 Å	2.212 Å
Pd–N^2 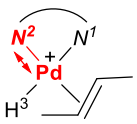	2.103 Å	2.101 Å	2.119 Å	2.104 Å

Table S15. NBO analyses of the Trans-2-Butene Hydride Palladium Intermediates/TSs

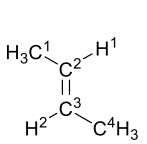

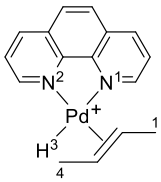

	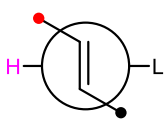 **9t**	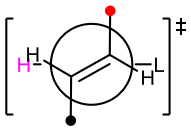 TS(**9t-8't**)	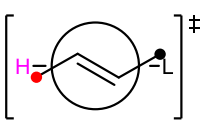 TS(**8t-9t**)	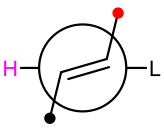 **8't**
σ(C^2=C^3) [a]	1.98	1.98	1.98	1.98
σ*(C^2=C^3) [a]	0.02	0.02	0.02	0.02
p(C^2) of σ(C^2=C^3) [b]	65.4%	65.4%	65.3%	65.5%
p(C) of σ(C^2=C^3) [b]	65.7%	65.6%	66.0%	65.7%
π(C^2=C^3) [a]	1.65	1.65	1.64	1.64
π*(C^2=C^3) [a]	0.20	0.22	0.23	0.24
p(C^2) of π(C^2=C^3) [b]	97.0%	97.3%	96.8%	97.2%
p(C^3) of π(C^2=C^3) [b]	96.4%	96.4%	96.1%	96.4%
bond index (Pd–C^2)	0.29	0.27	0.27	0.26
bond index (Pd–C^3)	0.33	0.35	0.36	0.37
bond index (C^2=C^3)	1.53	1.51	1.50	1.49
Mulliken Charge (alkene)	0.39	0.38	0.34	0.36
Mulliken Charge (Pd)	0.16	0.15	0.23	0.16
Natural Charge (alkene)	0.22	0.20	0.17	0.18
Natural Charge (Pd)	0.26	0.26	0.29	0.27

a) The occupancy of the natural bond orbital.

b) The p character of the orbitals of the corresponding atom in the natural bond orbital.

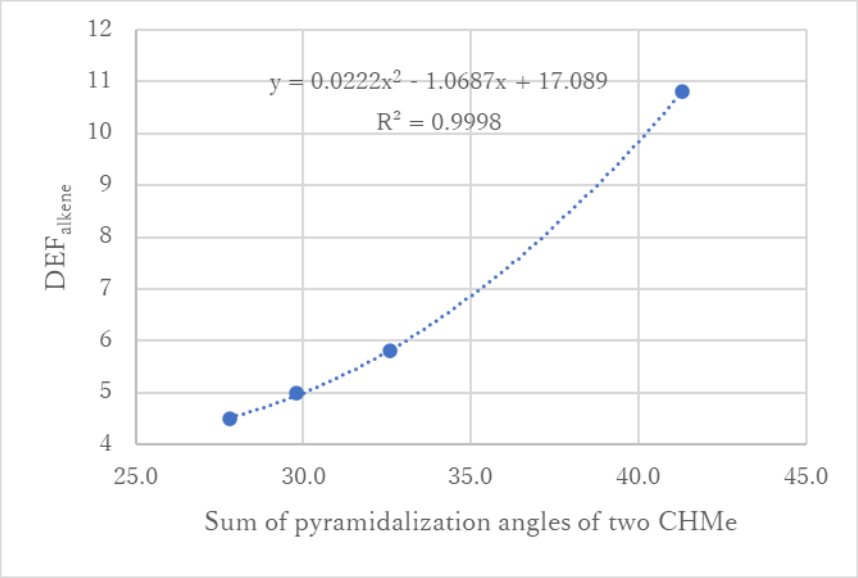

Figure S10. The quadratic regression of the strain energy of the trans-2-butene (DEF_{alkene}) on the sum of the propene pyramidalization angles of the intermediates/TSs.

VII. Calculated Reaction Pathways of the Palladium Chain Walking on the Four-Carbon Alkyl Chain and Alkene Exchange

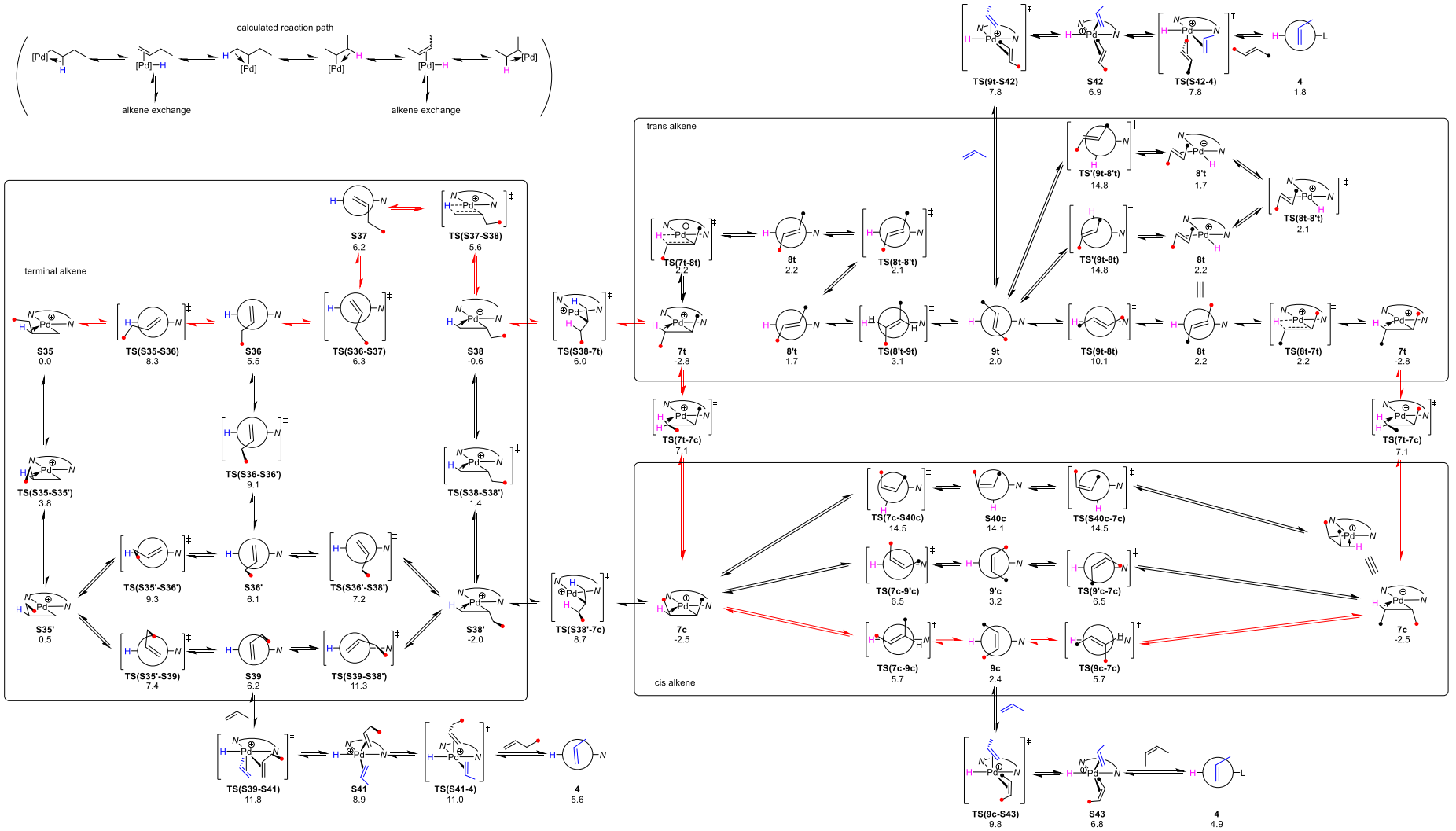

Figure S11. The calculated pathways in the (phen)Pd chain walking on the four carbon chain. The number associated with each structure is the Gibbs free energy (ΔG, kcal/mol).

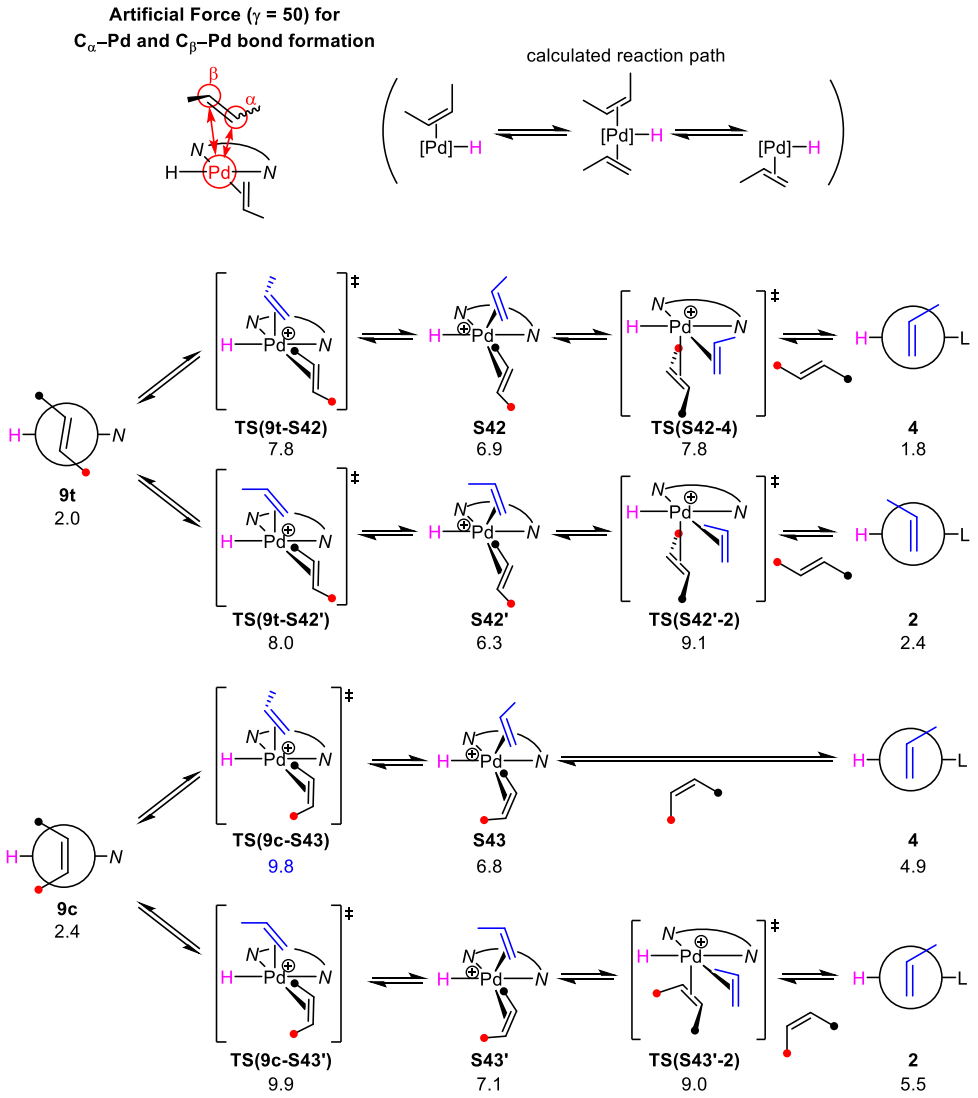

Figure S12. Comparison of the pathways for associative alkene exchange of the *trans*- or *cis*-2-butene complex with propene. The number associated with each structure is the Gibbs free energy (Δ*G*, kcal/mol).

VIII. Calculated Reaction Pathways of the Palladium Chain Walking on the Five-Carbon Alkyl Chain

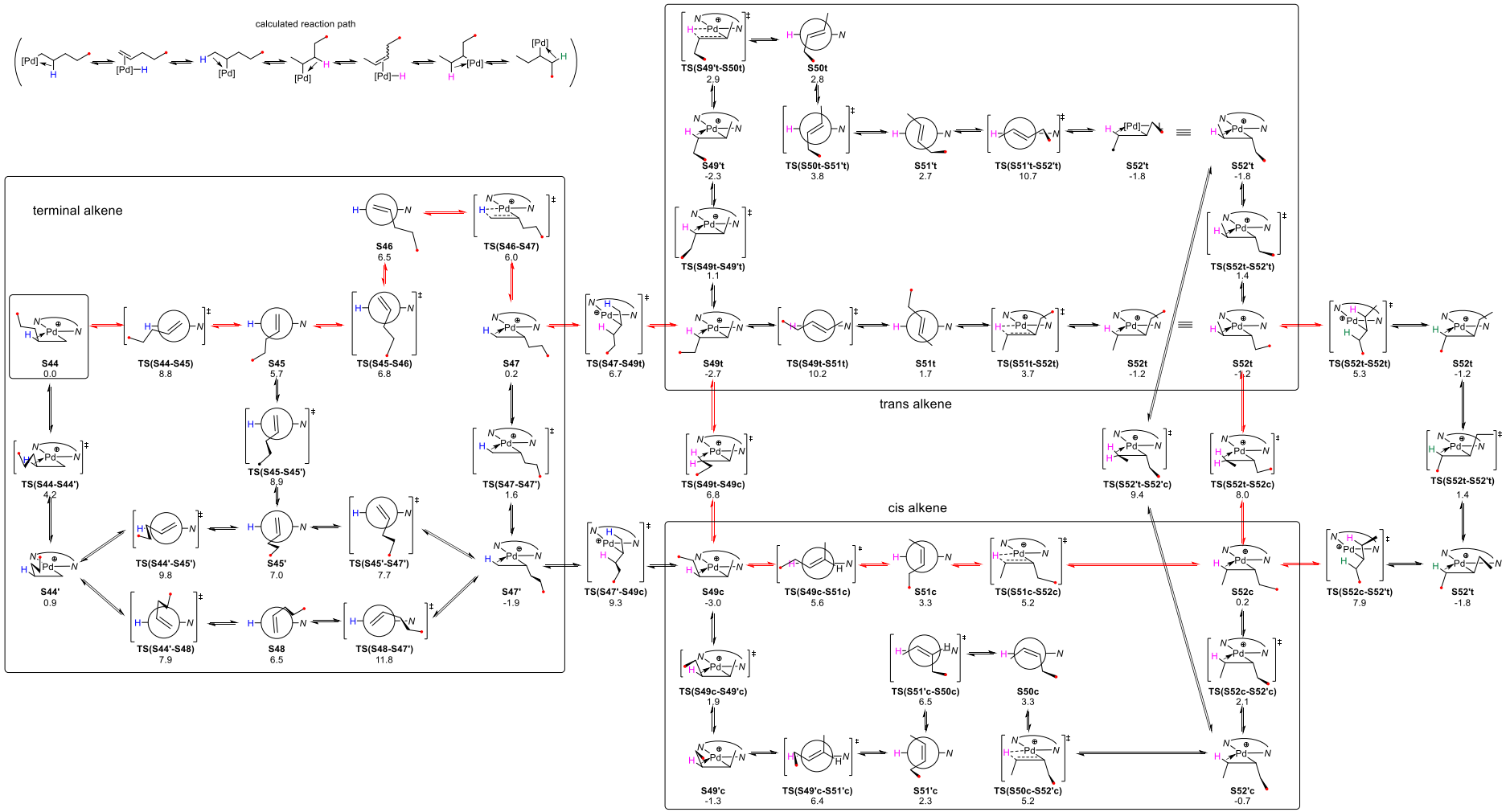

Figure S13. The calculated pathways in the (phen)Pd chain walking on the five carbon chain. The number associated with each structure is the Gibbs free energy (ΔG, kcal/mol).

IX. Calculated Reaction Pathways of the Palladium Chain Walking on the Six-Carbon Alkyl

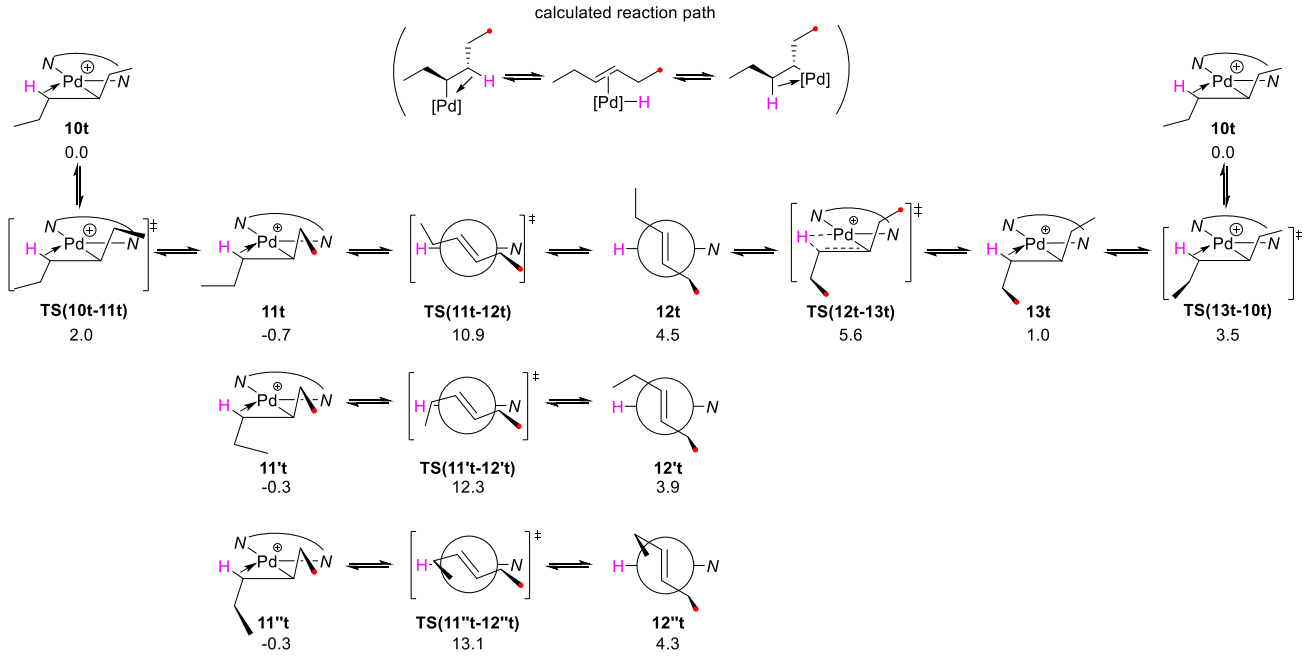

Figure S14. The Gibbs free energy diagram of the calculated pathways for the (phen)Pd chain walking between the 3- and 4- position of the six carbon chain via *trans*-3-hexene intermediates. The pathways differ by the orientation of the terminal methyl groups. The number associated with each structure is the Gibbs free energy (ΔG, kcal/mol).

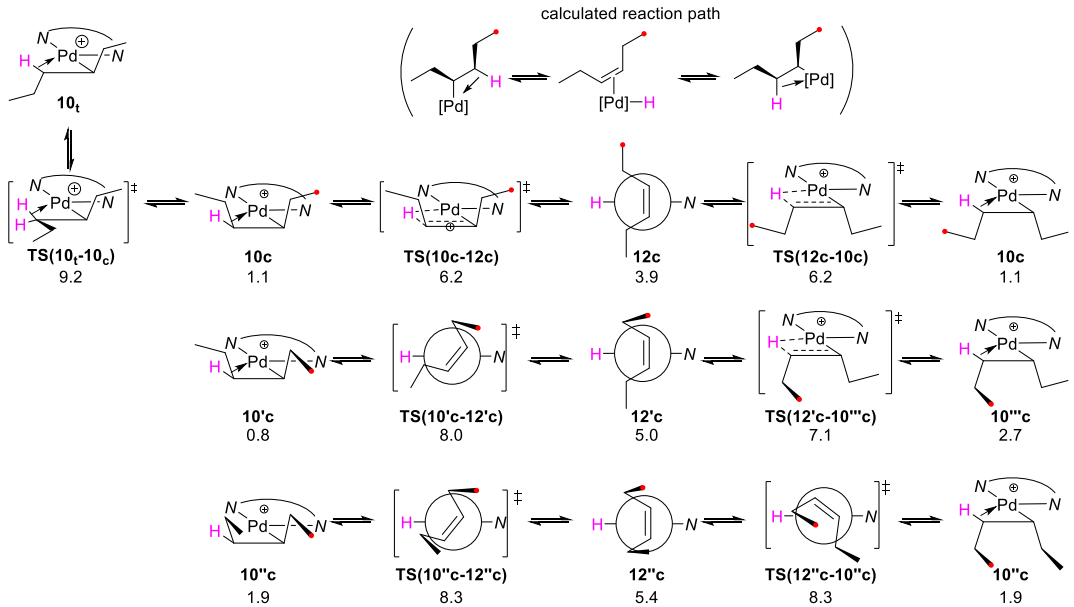

Figure S15. The calculated pathways for the (phen)Pd chain walking between the 3- and 4- position of the six carbon chain via *cis*-3-hexene intermediates. The pathways differ by the orientation of the terminal methyl groups. The number associated with each structure is the Gibbs free energy (ΔG, kcal/mol).

X. Deuterium Labeling Experiments

Preparation of Acetate 14

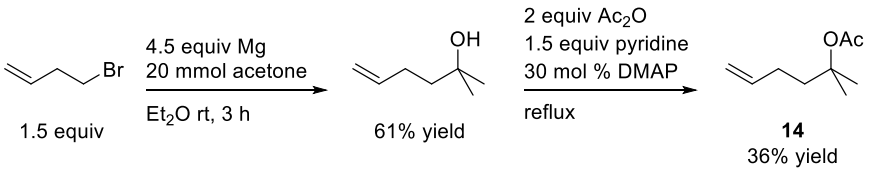

The Grignard reaction and acetylation of the alcohols were carried out by a procedure similar to that reported in literature.[17]

To a suspension of Mg (2.23 g, 92.4 mmol, 4.5 equiv) in 15 mL of Et_2O was slowly added the alkyl bromide (4.03 g, 29.9 mmol, 1.5 equiv) in 30 mL of Et_2O, and the mixture was refluxed for 10 min. After cooling to rt, a solution of acetone (1.17 g, 20.1 mmol, 1 equiv) in 15 mL of Et_2O was slowly added to the reaction mixture, which was then stirred at rt for 3 h. A saturated aqueous solution of NH_4Cl was then added to the resulting mixture, which was extracted three times with Et_2O. The combined organic extracts were washed with brine, dried over $MgSO_4$, filtered, and concentrated at 0 ˚C. Silica gel column chromatography (hexane: Et_2O = 3:1) of the crude material afforded 1.43 g of the corresponding alcohol (61% yield) that was used without further purification.

Acetic anhydride (2.04 g, 20.0 mmol, 2.0 equiv), pyridine (1.19 g, 15.0 mmol, 1.5 equiv), and 4-(dimethylamino)pyridine (372 mg, 3.04 mmol, 0.3 equiv) were added to a stirred solution of the aforementioned alcohol in 25 mL of CH_2Cl_2 at rt. The reaction mixture was stirred for 16 h. After dilution with diethyl ether, the mixture was washed with saturated aqueous solution of NH_4Cl, $NaHCO_3$, and brine. The organic layer was dried over MgSO4, filtered, and concentrated at 0 ˚C. Silica gel column chromatography (hexane:EtOAc = 50:1) of the crude material afforded 696 mg of the corresponding acetate **14** (36% yield): IR (neat): 3079 w, 2979 s, 2935 m, 1736 s, 1643 m, 1474 m, 1452 m, 1385 m, 1368 s, 1255 s, 1213 s, 1147 s, 1019 s, 997 m, 944 m, 911 m, 610 w cm^{-1}; ^1H NMR (400 MHz, $CDCl_3$): δ 5.82 (ddt, *J* = 16.8, 10.0, 6.3 Hz, 1H), 5.07-4.98 (m, 1H), 4.98-4.92 (m, 1H), 2.14-2.03 (m, 2H), 1.97 (s, 3H), 1.88-1.78 (m, 2H), 1.44 (s, 6H); ^{13}C NMR (100 MHz, $CDCl_3$): δ 170.5, 138.4, 114.4, 82.0, 39.9, 28.3, 26.0 (2C), 22.4; HRMS (DART-TOF) m/z: $[M+H]^+$ Calcd for $C_9H_{16}O_2$ 157.1229; Found 157.1272.

Preparation of 6.3.4-(1,3-dioxolan-2-yl)-2-methylbutan-2-yl acetate S1

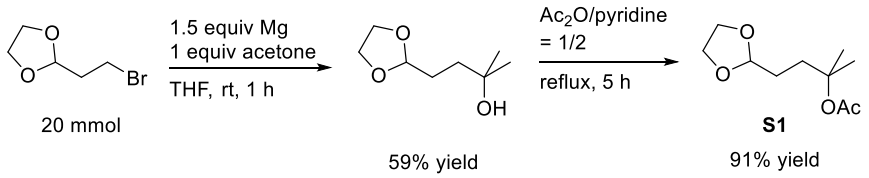

The Grignard reaction was carried out by a procedure similar to that reported in literature.[18] The acetylation of the alcohols was carried out by a procedure similar to that reported in literature.[17]

To a suspension of Mg (2.13 g, 88.3 mmol, 1.5 equiv) in 30 mL of THF was slowly added the alkyl bromide (10.6 g, 58.6 mmol, 1.0 equiv) in 40 mL of THF, and the mixture was stirred at rt for 2 h. A solution of acetone (3.36 g, 57.9 mmol) in 30 mL of THF was slowly added to the reaction mixture, which was then stirred at rt for 1h. A saturated aqueous solution of NH_4Cl was then added to the resulting mixture at 0 ˚C, which was extracted three times with Et_2O. The combined organic extracts were washed with brine, dried over $MgSO_4$, filtered, and

concentrated. Silica gel column chromatography (hexane:EtOAc = 2:1 to 1:1) of the crude material afforded 4.70 g of the corresponding alcohol (53% yield) that was used without further purification.

A solution of aforementioned alcohol in 40 mL of acetic anhydride and 20 mL of pyridine was stirred at 130 ˚C for 3 h under N_2. Excess acetic anhydride and pyridine were removed by distillation of the reaction mixture. Silica gel column chromatography (hexane:EtOAc = 4:1) of the resulting residue the crude material afforded 2.56 g of the corresponding acetate **S1** (43% yield) as colorless oil: IR (neat): 2979 m, 2939 m, 2887 m, 1809 w, 1734 s, 1454 m, 1370 s, 1256 s, 1212 s, 1171 s, 1129 s, 1022 s, 949 m, 884 w, 611 w cm^{-1}; ^1H NMR (400 MHz, $CDCl_3$): δ 4.85 (t, *J* = 4.5 Hz, 1H), (m, 2H), (m, 2H), 1.97 (s, 3H), (m, 2H), (m, 2H), 1.45 (s, 6H); ^{13}C NMR (100 MHz, $CDCl_3$): δ 170.6, 104.6, 81.7, 65.1 (2C), 35.2, 28.6, 26.0 (2C), 22.5; HRMS (DART-TOF) m/z: $[M+H]^+$ Calcd for $C_{10}H_{18}O_4$ 203.1283; Found 203.1333.

Preparation of Acetate 14-*d*$_4$

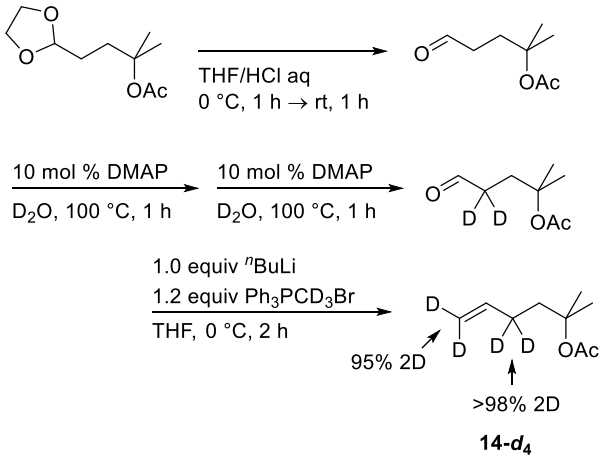

14-*d*$_4$

A solution of acetate **S1** (2.01 g, 10 mmol) in 100 mL of THF was added HCl aq. (3 M, 80 mL) at 0 ˚C. the reaction mixture was stirred for 1 h at 0 ˚C and then for 1 h at rt. The mixture was neutralized by the addition of a saturated aqueous solution of $NaHCO_3$. After volatile materials were removed by rotary evaporation, the mixture was extracted four times with Et_2O. The combined organic extracts were washed with brine, dried over Na_2SO_4, filtered, and concentrated. Silica gel column chromatography (hexane:EtOAc = 4:1) of the crude material afforded 1.32 g of the corresponding aldehyde that was used without further purification (84% yield, 94% purity including 6% of acetal **S1**).

The aforementioned aldehyde (1.32 g, 8 mmol), DMAP (98.4 mg, 0.81 mmol) and 2.3 mL of D_2O (99.8% D) were placed in oven-dried flask with reflux condenser. The reaction mixture was stirred for 1 h at 100 ˚C, and then cooled at 0 ˚C. The solution was added HCl aq. (0.5 M, 1 mL), and extracted three times with Et_2O. The combined organic extracts were washed with saturated aqueous solution of $NaHCO_3$, brine, dried over Na_2SO_4, filtered, and concentrated. Then, the deuteriation process was conducted again. Silica gel column chromatography (hexane:EtOAc = 1:1) of the crude material afforded 559 mg of the corresponding aldehyde (>98% D at the α position of aldehyde) that was used without further purification.

An oven-dried flack was charged with CD_3PPh_3Br (1.55 g, 4.30 mmol, 1.2 equiv) in 40 mL of THF and cooled at –78 ˚C. *n*-Butyllithium in Hexane (1.6 M, 2.2 mL, 1.0 equiv) was added dropwise to the solution, and then

stirred for 1 h at 0 ˚C. The aforementioned aldehyde (556 mg, 3.47 mmol) in 10 mL of THF was added slowly to the yellow solution at –78 ˚C and stirred for 2 h at 0 ˚C. The reaction mixture was quenched by addition of a saturated aqueous solution of NH_4Cl (5 mL) and extracted three times with Et_2O. The combined organic extracts were washed with brine, dried over $MgSO_4$, filtered, and concentrated. Silica gel column chromatography (hexane:EtOAc = 50:1) of the crude material afforded 143 mg of the corresponding alkene **14-*d*$_4$** as colorless oil (26% yield).

Remote Arylative Substitution of Alkenes Possessing a Remote Acetoxy Group

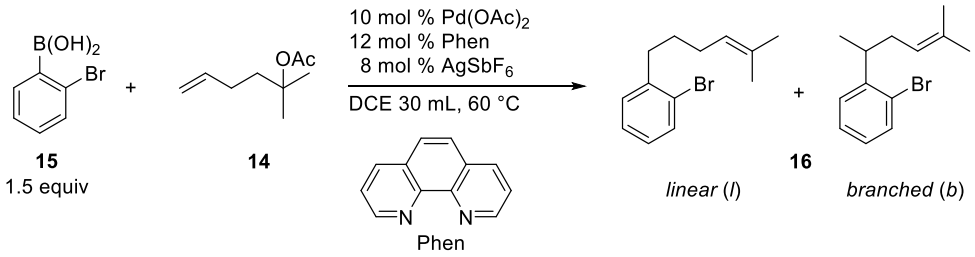

The remote arylative substitution was carried out by a procedure similar to that reported in literature.[17]

To an oven-dried flask containing $Pd(OAc)_2$ (8.98 mg, 0.040 mmol), 1,10-phenathroline (8.71 mg, 0.048 mmol), and $AgSbF_6$ (13.7 mg, 0.040 mmol) was added 1,2-dichloroethane (115 mL), and the mixture was stirred at 25 °C for 10 min to form a yellow suspension. Arylboronic acid **15** (120 mg, 0.60 mmol), acetate **14** (63.2 mg, 0.40 mmol), and 1,2-dichloroethane (5 mL) were added sequentially, and the resulting mixture was stirred at 60 °C for 48 h. Hexane (90 mL) was added to the resulting mixture, which was then passed through a short column of silica gel (hexane:EtOAc = 7:1) and concentrated. Silica gel column chromatography (hexane only) of the crude material afforded 39.7 mg of the arylation product **16** (39% yield, *l*/*b* = 3.9). IR (neat): 3057 w, 2964 s, 2927 s, 2858 m, 1592 w, 1567 w, 1470 s, 1439 m, 1376 m, 1099 w, 1022 m, 940 w, 832 w, 748 s, 659 m, 520 w cm^{-1}; ^{1}H NMR (400 MHz, $CDCl_3$): δ7.53 (dd, *J* = 8.1, 1,1 Hz, 1H, ***b***), 7.52 (dd, *J* = 8.1, 1.1 Hz, 1H, ***l***), 7.27-7.23 (m, 2H, ***b***), 7.23-7.18 (m, 2H, ***l***), 7.07-7.00 (m, 1H, ***l***+***b***), 5.16 (t, sept, *J* = 7.1, 1.4 Hz, 1H, ***l***), 5.14-5.07 (m, 1H, ***b***), 3.26 (sextet, *J* = 6.9 Hz, 1H, ***b***), 2.75-2.68 (m, 2H, ***l***), 2.30 (dt, *J* = 14.1, 6.9 Hz, 1H, ***b***), 2.19 (dt, *J* = 14.1, 6.9 Hz, 1H, ***b***), 2.06 (q *J* = 7.4 Hz, 2H, ***l***), 1.70 (d, *J* = 1.1 Hz, 3H, ***l***), 1.674 (br, 3H, ***b***), 1.65 (tt, *J* = 7.4, 2.2 Hz, 2H, ***l***), 1.61 (br, 3H, ***l***), 1.57 (br, 3H, ***b***), 1.21 (d, *J* = 6.9 Hz, 3H, ***b***); ^{13}C NMR (***l***, 100 MHz, $CDCl_3$): δ 141.9, 132.7, 132.0, 130.3, 127.33, 127.26, 124.5, 124.1, 35.8, 35.5, 30.0, 27.7, 25.73, 17.7; ^{13}C NMR (***b***, 100 MHz, $CDCl_3$): δ 146.1, 132.9, 127.42, 127.37, 127.22, 124.7, 124.1, 122.2, 38.5, 25.78, 20.1, 17.8; HRMS (DART-TOF) m/z: $[M+H]^+$ Calcd for $C_{12}H_{18}{}^{79}Br$ 253.0592; Found 253.05961.

Derivatization to 2-(1,2,3,4-tetrahydronaphthalen-1-yl)propan-2-ol 18

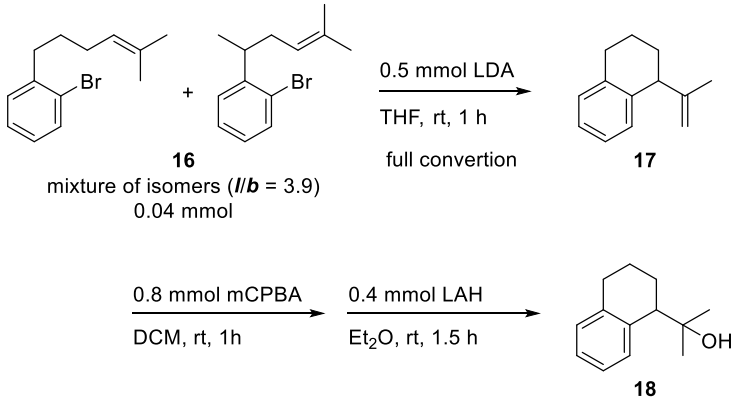

The cyclization reaction using LDA was carried out by a procedure similar to that reported in literature.[20] The epoxidation and ring opening reaction with LAH were carried out by a procedure similar to that reported in literature.[21]

An oven-dried flask was charged with diisopropylamine (86.9 mg 0.86 mmol) in 2 mL of THF. After the solution was cooled at 0 ˚C, a solution of ^{n}BuLi in hexane (1.6 M, 0.33 mL, 0.53 mmol) was slowly added. The reaction mixture was stirred at 0 ˚C for 30 min. To a separate flask charged with the aryl bromide **16** (39.7 mg, 0.15 mmol) in 0.7 mL of THF at rt, the aforementioned LDA solution (0 ˚C) was added rapidly via a cannula. The orange reaction mixture was stirred at rt for 3 h. After the reaction was quenched by addition of NH_4Cl(sat.), brine was added, and the solution extracted three times with hexane. The extracts were dried over $MgSO_4$, filtered and concentrated at 0 ˚C. the crude material was purified by silica gel column chromatography (Hexane:EtOAc = 50:1), and GPC ($CHCl_3$), and product **17** was used without further purification.

To a solution of aforementioned alkene **17** in CH_2Cl_2 (2 mL) *m*-chloroperbenzoic acid (143 mg, 0.83 mmol) was added. The resulting mixture was stirred for 1 h at room temperature. After the reaction mixture was diluted with ether, the organic layer was washed with a 10% aqueous solution of $Na_2S_2O_3$ and then with a saturated aqueous solution of $NaHCO_3$, and dried over $MgSO_4$. Evaporation of the organic solvent gave a residue, which was directly used in the next step. $LiAlH_4$ (15.2 mg, 0.40 mmol) was added to a suspension of the crude material in 1 mL of Et_2O at 0 ºC. After the mixture was stirred for 1.5 h at room temperature, the reaction mixture was carefully quenched with a saturated aqueous solution of NH_4Cl at 0 ˚C. The solution was extracted three times with Et_2O, and the combined organic extracts were washed with brine, dried over $MgSO_4$, filtered, and concentrated. The crude material was purified by silica gel column chromatography (hexane:EtOAc = 10:1 to 4:1) and GPC ($CHCl_3$) to afford 22.3 mg of alcohol **18** as a colorless oil (78% yield based on the mixture of linear and branched **16**): IR (neat): 3445 m, 3060 w, 3017 m, 2933 s, 2865 m, 1677 m, 1601 w, 1489 m, 1451 m, 1371 m, 1288 m, 1144 s, 939 m, 894 m, 774 m, 746 s cm^{-1}; ^{1}H NMR (400 MHz, C_6D_6): δ 7.57-7.51 (m, 1H), 7.12-7.05 (m, 2H), 7.03-6.98 (m, 1H), 2.75 (t, J = 7.0 Hz, 1H), 2.56 (ddd, J = 15.8, 8.4, 5.4 Hz, 1H), 2.50 (dt, J = 15.8, 5.6 Hz, 1H), 1.86 (ddddd, J = 12.7, 6.0, 5.6, 5.4, 4.3 Hz, 1H), 1.68 (ddddd, J = 13.8, 7.0, 6.0, 4.3, 1.1 Hz, 1H), 1.50 (dddd, J = 13.8, 10.0, 7.0, 4.3 Hz, 1H), 1.34 (ddddd, J = 12.7, 10.0, 8.4, 5.6, 4.3 Hz, 1H), 1.08 (s, 3H), 0.93 (s, 3H); ^{13}C NMR (100 MHz, C_6D_6): δ 140.0, 137.5, 131.6, 129.1, 126.2, 125.4, 74.0, 48.3, 30.4, 29.6, 26.3, 26.0, 22.2; HRMS (DART-TOF) m/z: $[M+O_2]^-$ Calcd for $C_{13}H_{18}O$ 222.1256; Found 222.1257.

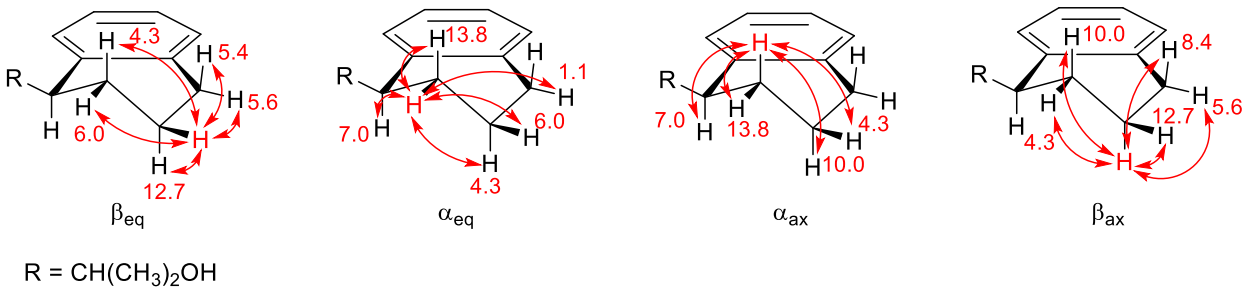

Figure S16. The coupling constants (Hz) of ^{1}H NMR signals of methylene protons at the α- and β-positions of **18**.

Remote Arylative Substitution of Alkenes Possessing a Remote Acetoxy Group

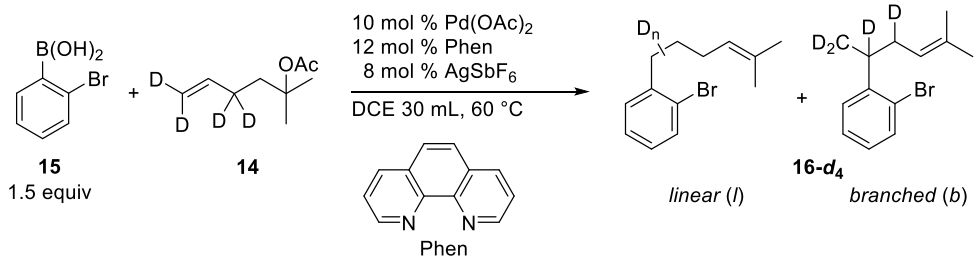

To an oven-dried flask containing $Pd(OAc)_2$ (8.90 mg, 0.040 mmol), 1,10-phenathroline (8.47 mg, 0.047 mmol), and $AgSbF_6$ (13.3 mg, 0.039 mmol) was added 1,2-dichloroethane (115 mL), and the mixture was stirred at 25 °C for 10 min to form a yellow suspension. Arylboronic acid **15** (118 mg, 0.59 mmol), acetate **14-*d*$_4$** (55.7 mg, 0.35 mmol), and 1,2-dichloroethane (5 mL) were added sequentially, and the resulting mixture was stirred at 60 °C for 48 h. Hexane (90 mL) was added to the resulting mixture, which was then passed through a short column of silica gel (hexane:EtOAc = 7:1) and concentrated. Silica gel column chromatography (hexane only) of the crude material afforded 41.0 mg of the arylation product **16-*d*$_4$** (46% yield, *l*/*b* = 3.9).

Derivatization to 2-(1,2,3,4-tetrahydronaphthalen-1-yl)propan-2-ol 18-*d*$_4$

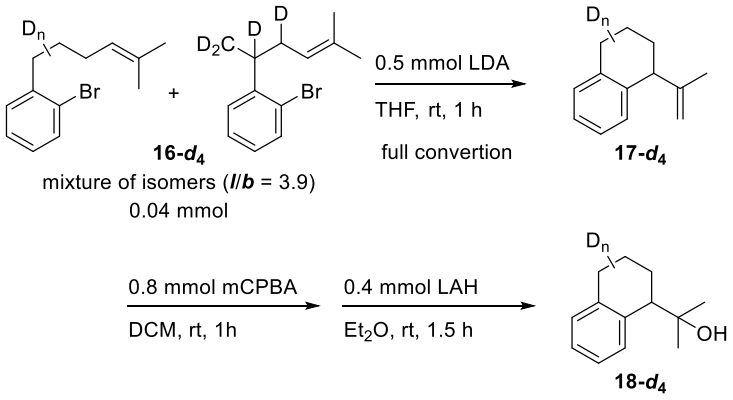

An oven-dried flask was charged with diisopropylamine (85.4 mg 0.84 mmol) in 1 mL of THF. After the solution was cooled at 0 ˚C, a solution of ^{n}BuLi in hexane (1.6 M, 0.33 mL, 0.53 mmol) was slowly added. The reaction mixture was stirred at 0 ˚C for 30 min. To a separate flask charged with the aryl bromide **16-*d*$_4$** (41.0 mg, 0.16 mmol) in 0.7 mL of THF at rt, the aforementioned LDA solution (0 ˚C) was added rapidly via a cannula. The

orange reaction mixture was stirred at rt for 3 h. After the reaction was quenched by addition of NH_4Cl(sat.), brine was added, and the solution extracted three times with hexane. The extracts were dried over $MgSO_4$, filtered and concentrated at 0 ˚C. the crude material was purified by silica gel column chromatography (Hexane:EtOAc = 50:1), and GPC ($CHCl_3$), and product **3** was used without further purification.

To a solution of aforementioned alkene **17-*d*$_4$** in CH_2Cl_2 (2 mL) *m*-chloroperbenzoic acid (146 mg, 0.85 mmol) was added. The resulting mixture was stirred for 1 h at room temperature. After the reaction mixture was diluted with ether, the organic layer was washed with a 10% aqueous solution of $Na_2S_2O_3$ and then with a saturated aqueous solution of $NaHCO_3$, and dried over $MgSO_4$. Evaporation of the organic solvent gave a residue, which was directly used in the next step. $LiAlH_4$ (16.8 mg, 0.44 mmol) was added to a suspension of the crude material in 1 mL of Et_2O at 0 ºC. After the mixture was stirred for 1.5 h at room temperature, the reaction mixture was carefully quenched with a saturated aqueous solution of NH_4Cl at 0 ˚C. The solution was extracted three times with Et_2O, and the combined organic extracts were washed with brine, dried over $MgSO_4$, filtered, and concentrated. The crude material was purified by silica gel column chromatography (hexane:EtOAc = 10:1 to 4:1) and GPC ($CHCl_3$) to afford 15.6 mg of alcohol **18-*d*$_4$** as a colorless oil (56% yield based on the mixtures of liner and branched **16-*d*$_4$**)

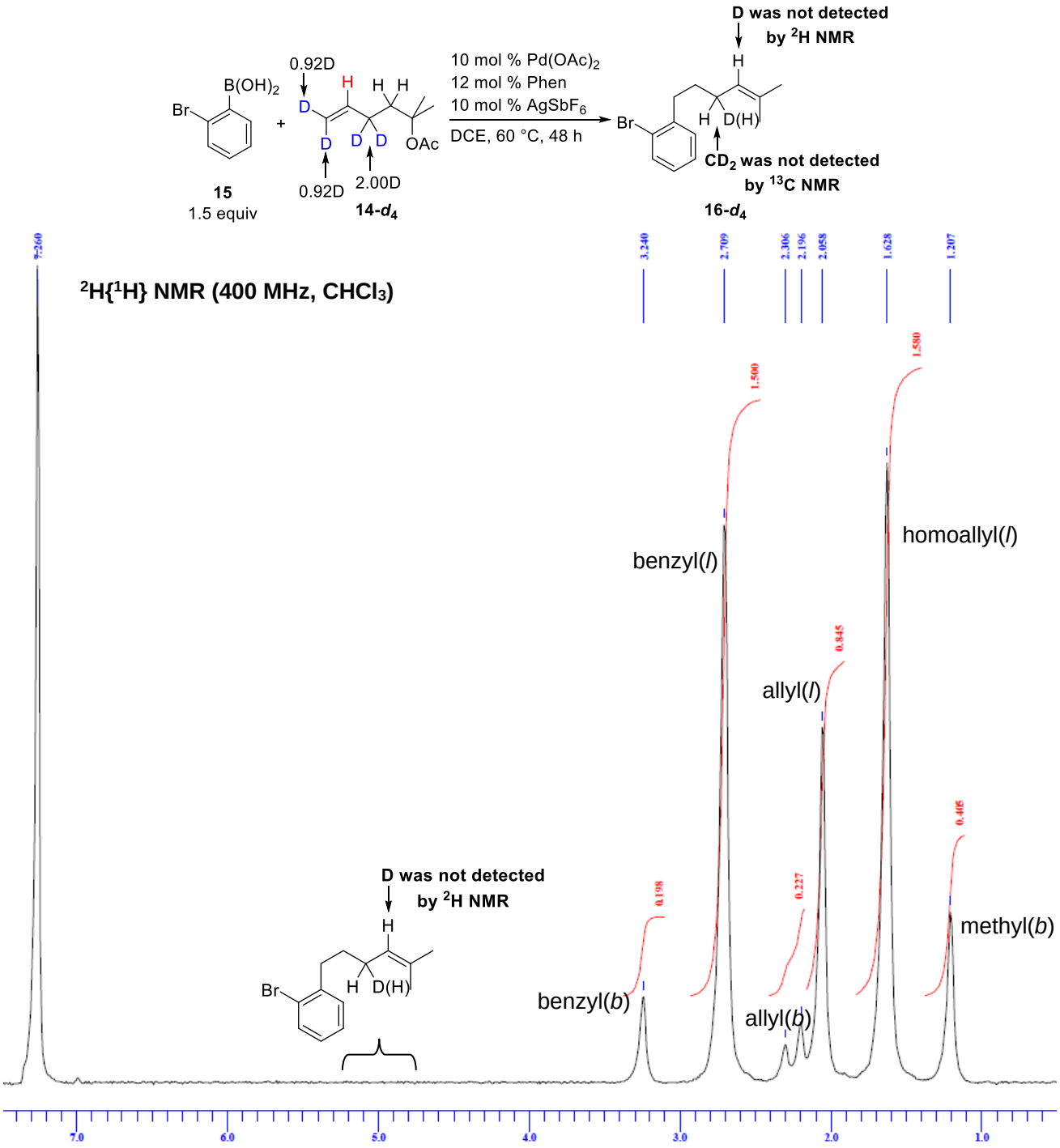

Figure S17. $^{2}H\{^{1}H\}$ NMR spectrum of **16-*d*$_4$.**

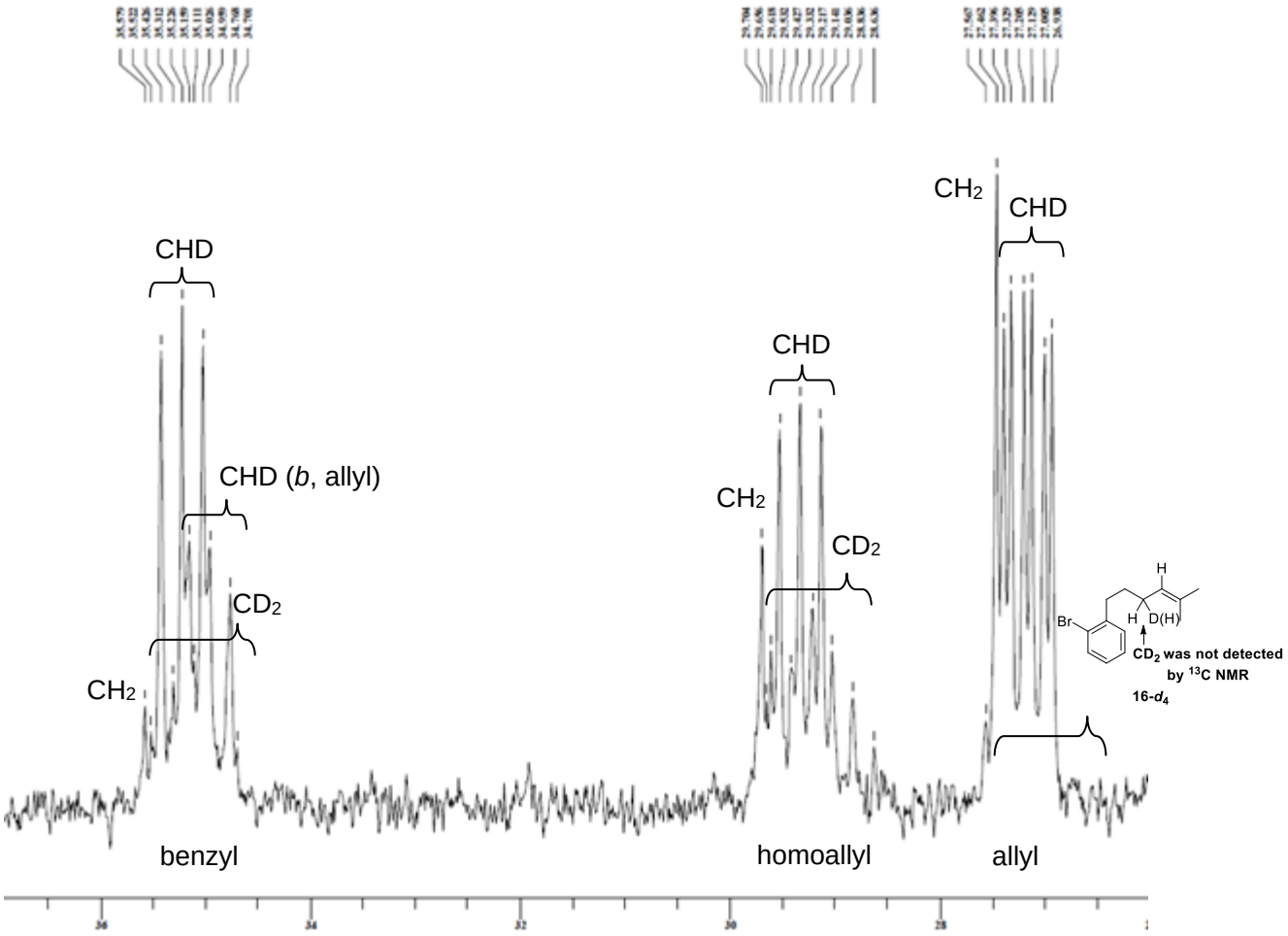

Figure S18. $^{13}C\{^{1}H\}$ NMR signals of three methylene carbons of **16-*d*$_4$.**

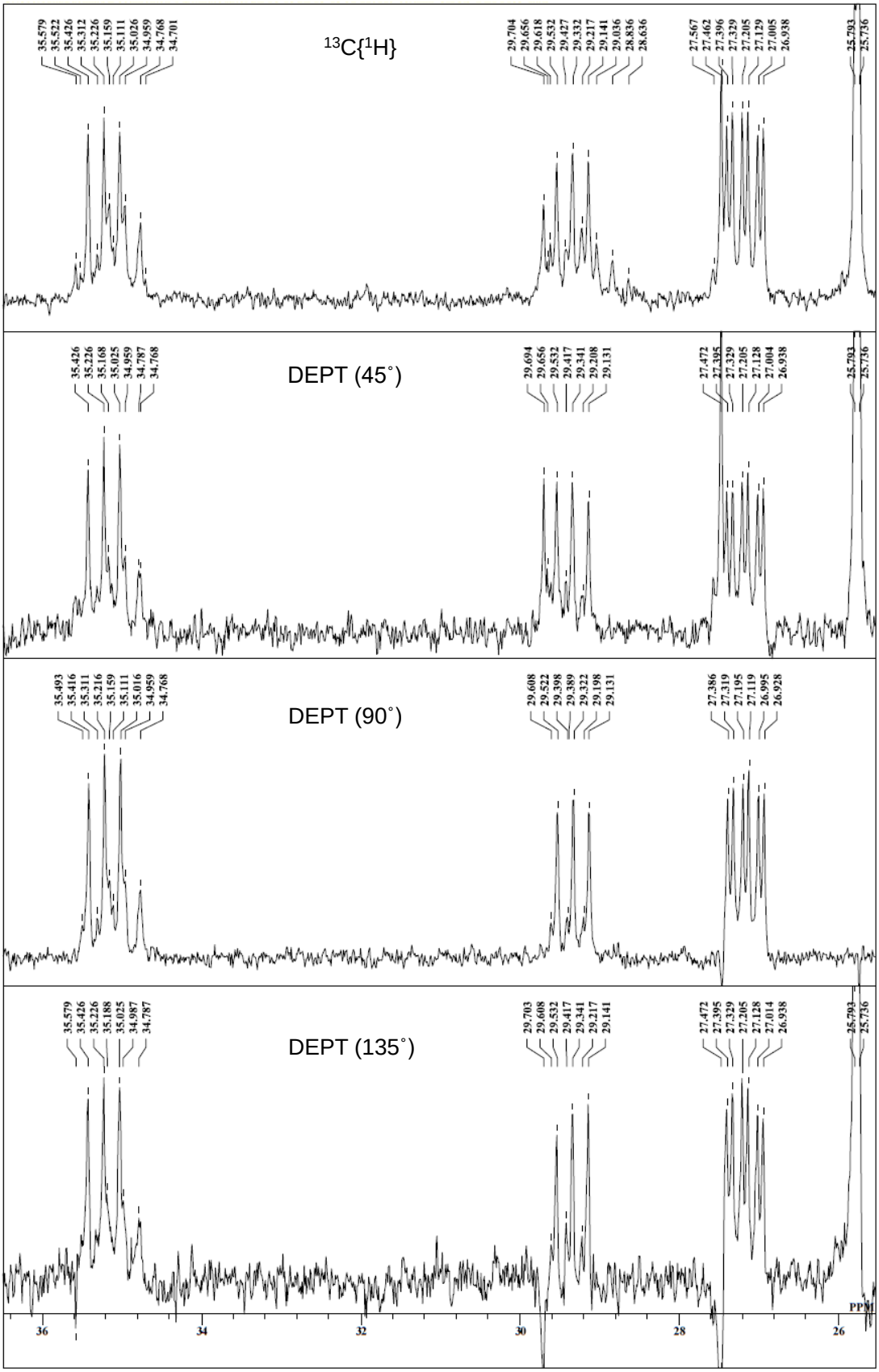

Figure S19. $^{13}C\{^{1}H\}$ and DEPT NMR spectrums of **16-*d*$_4$.**

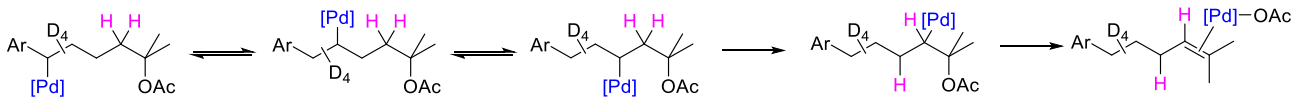

Figure S20. A plausible reaction mechanism from the (phen)Pd chain walking and the reversibility of each steps in the remote arylative substitution, supported by the deuterium-labeling experiment and the DFT calculation.

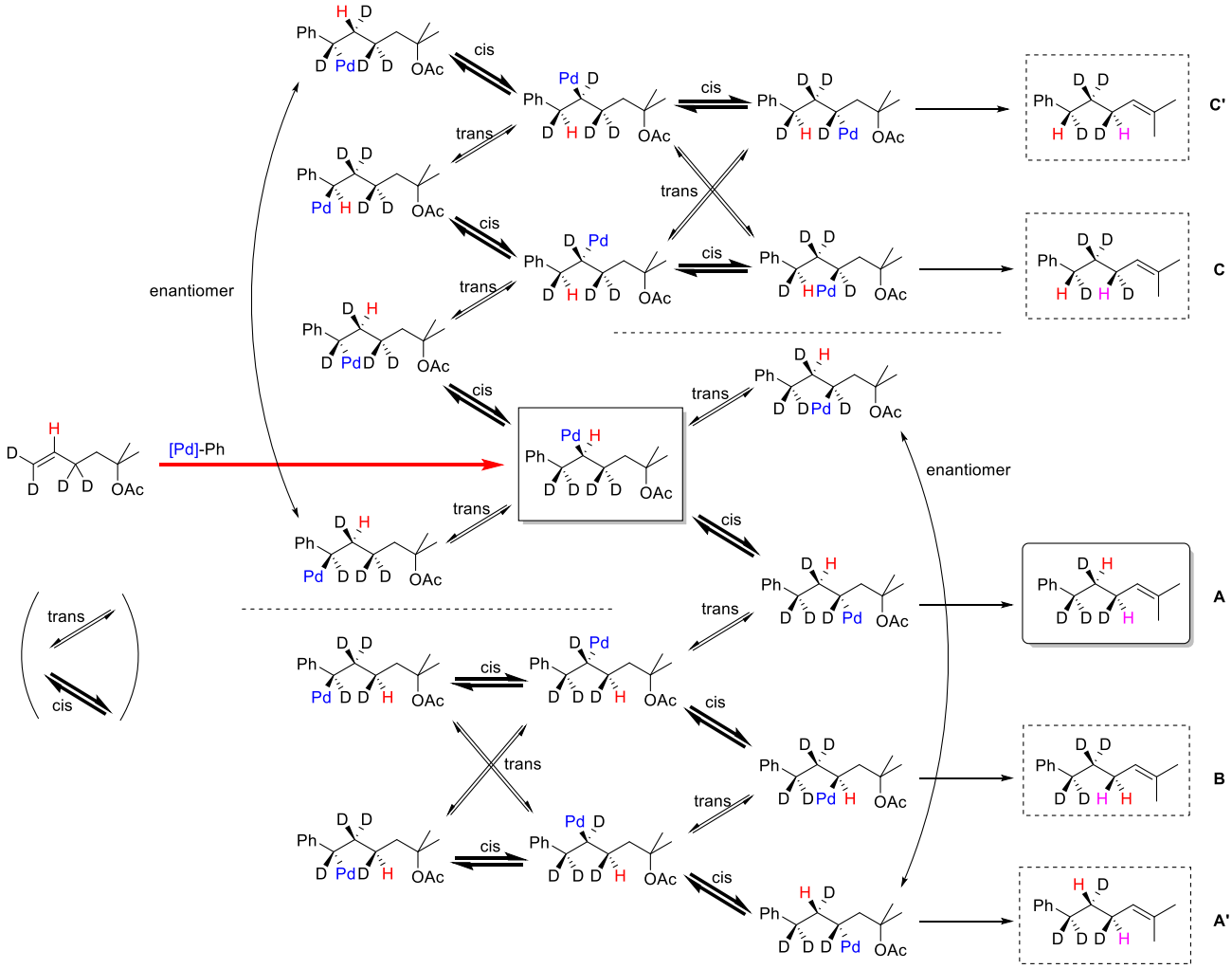

Figure S21. Possible pathways for deuterium migration in the remote arylative substitution.

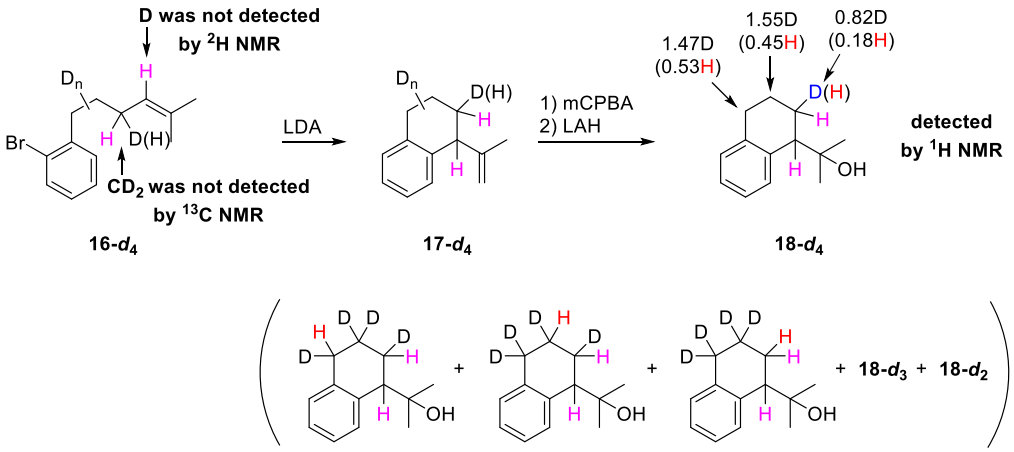

Figure S22. A deuterium-labeling experiment of **18-*d*$_4$.**

XI. Calculated Reaction Pathways of the Palladium Chain Walking on the Six-Carbon Alkyl Chain with 6-Phenyl, 2-OAc and 2-Me Groups

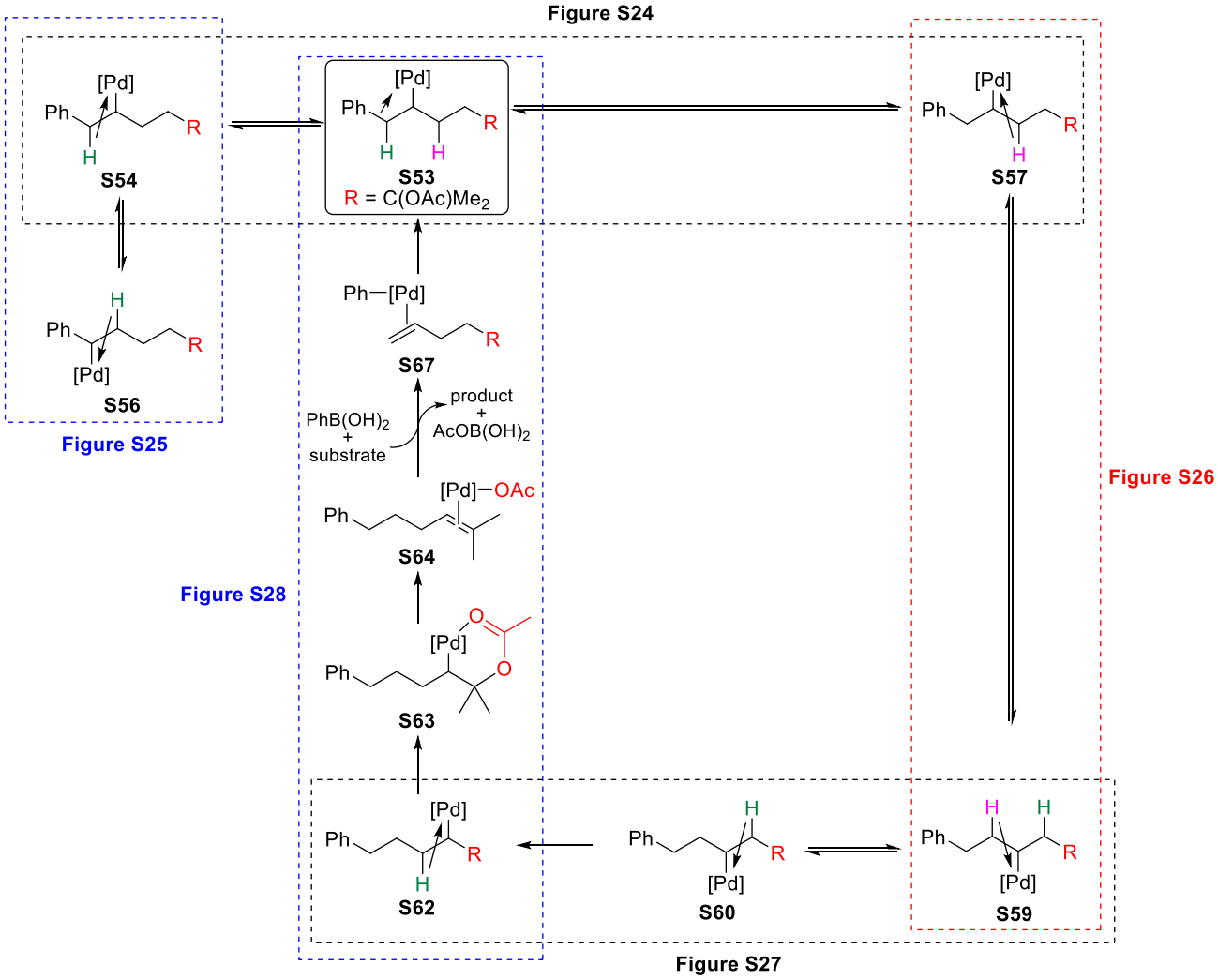

Figure S23. Reaction pathways of remote arylative substitution with phenylboronic acid, which was used instead of **15** for the DFT calculation for simplicity.

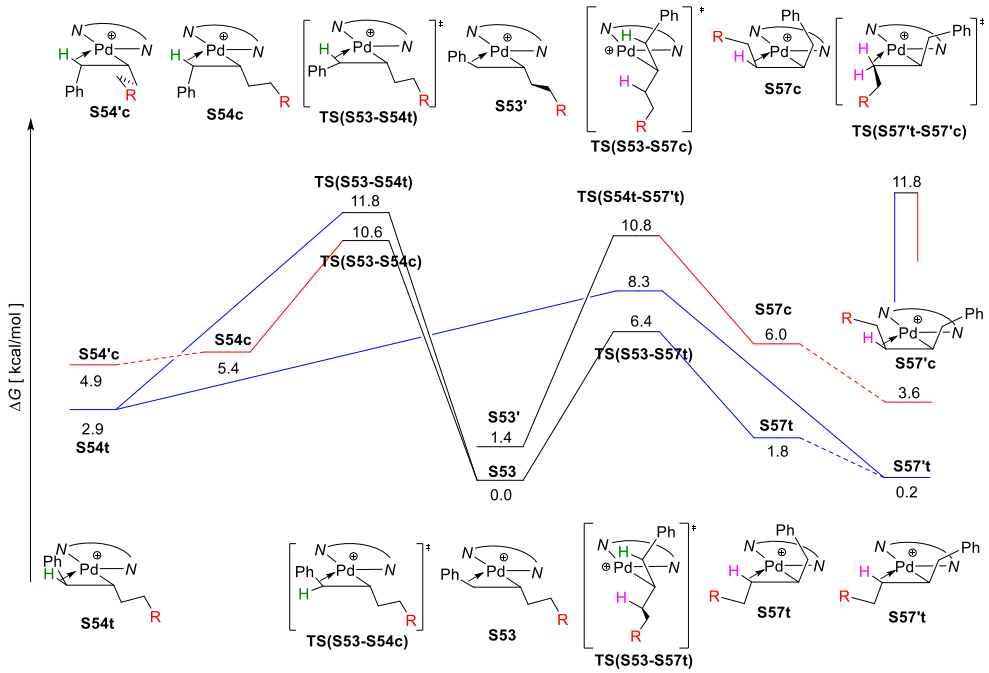

Figure S24. Energy diagram of agostic β-H exchange of the homobenzylpalladium complexes.

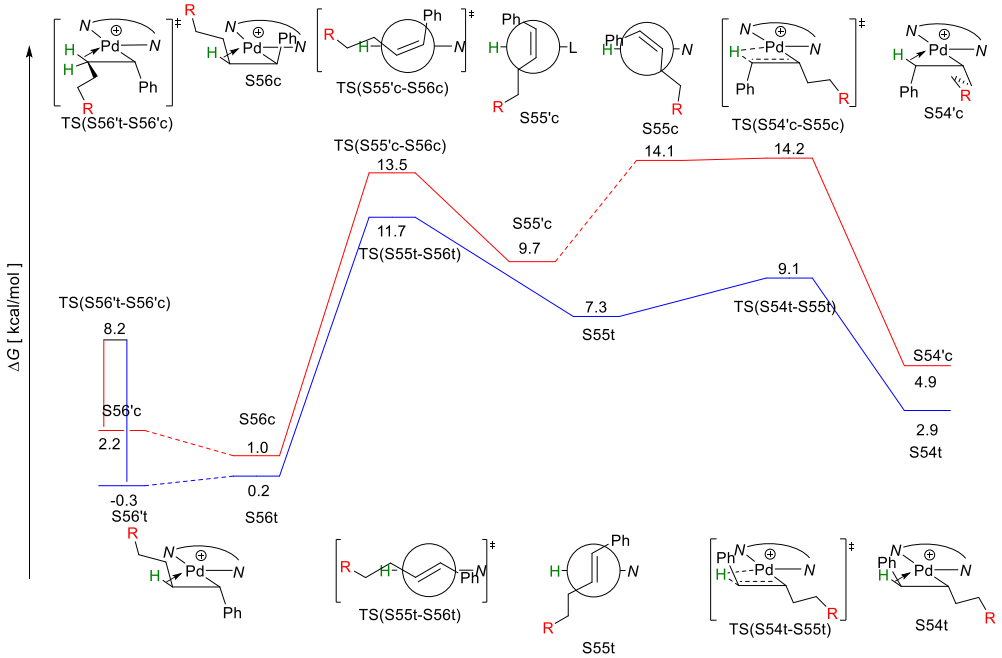

Figure S25. Energy diagram of chain walking of the palladium center from the homobenzylic position to the benzylic position.

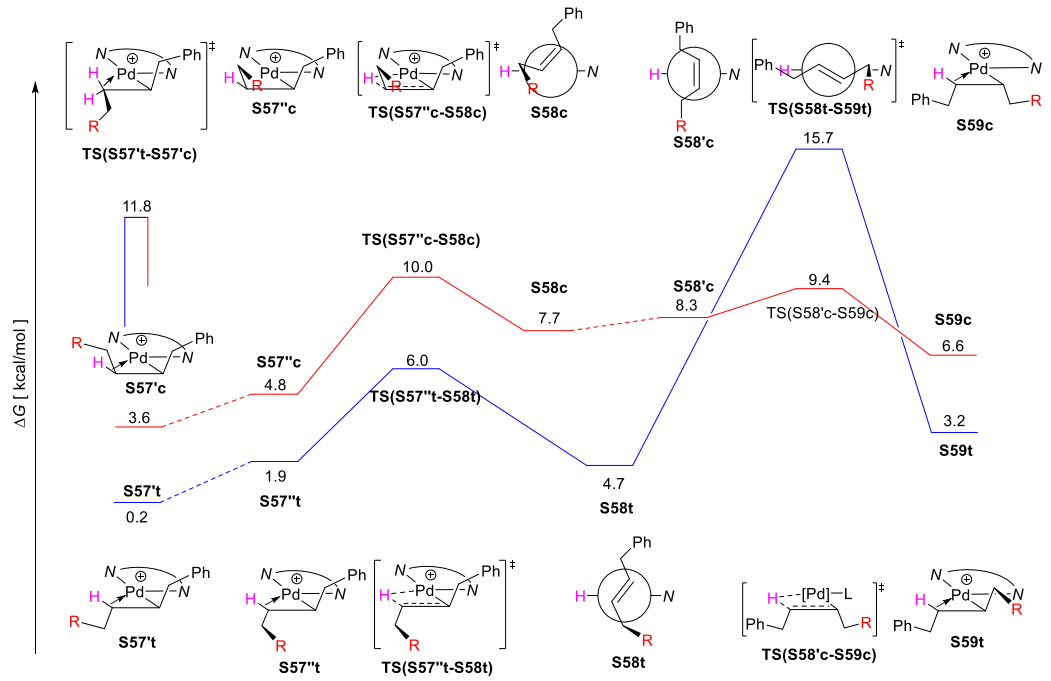

Figure S26. Energy diagram of chain walking of the palladium center from the homobenzylic position to the γ-position of the acetoxy group.

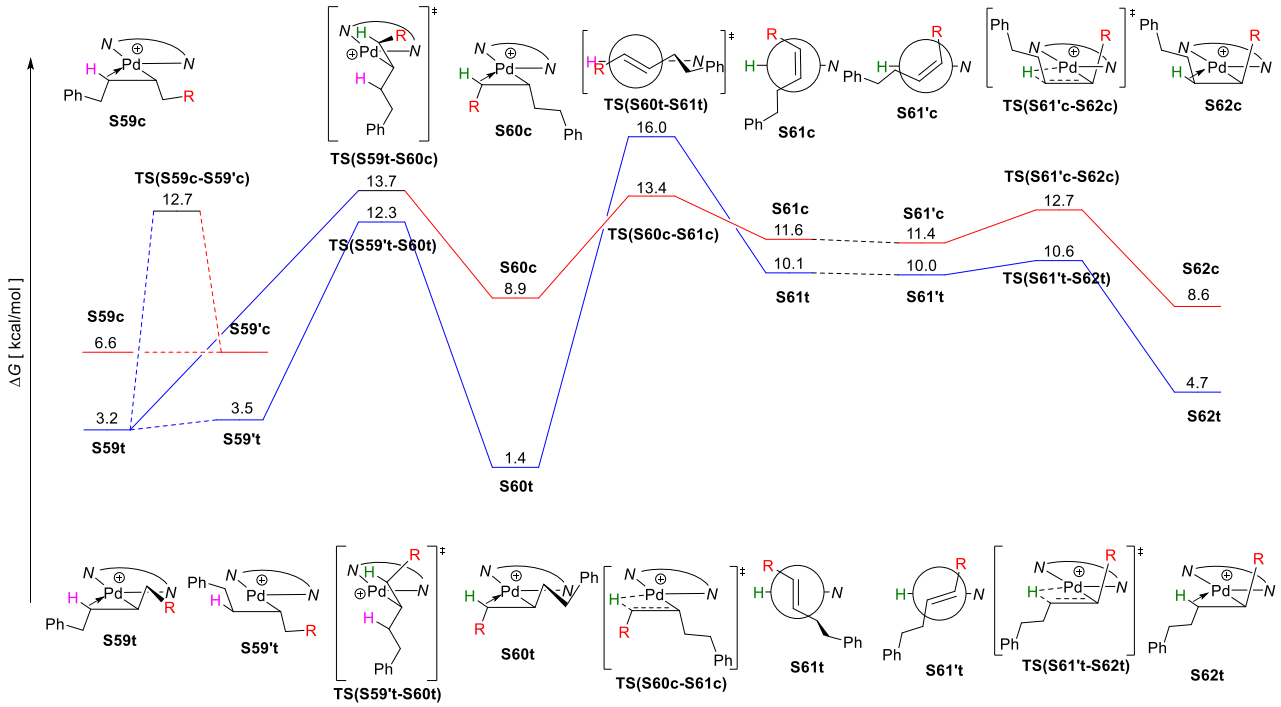

Figure S27. Energy diagram of agostic β-H exchange of 1-alkyl-3-phenylpropylpalladium complexes and chain walking of the palladium center from the γ-position to the β-position of the acetoxy group.

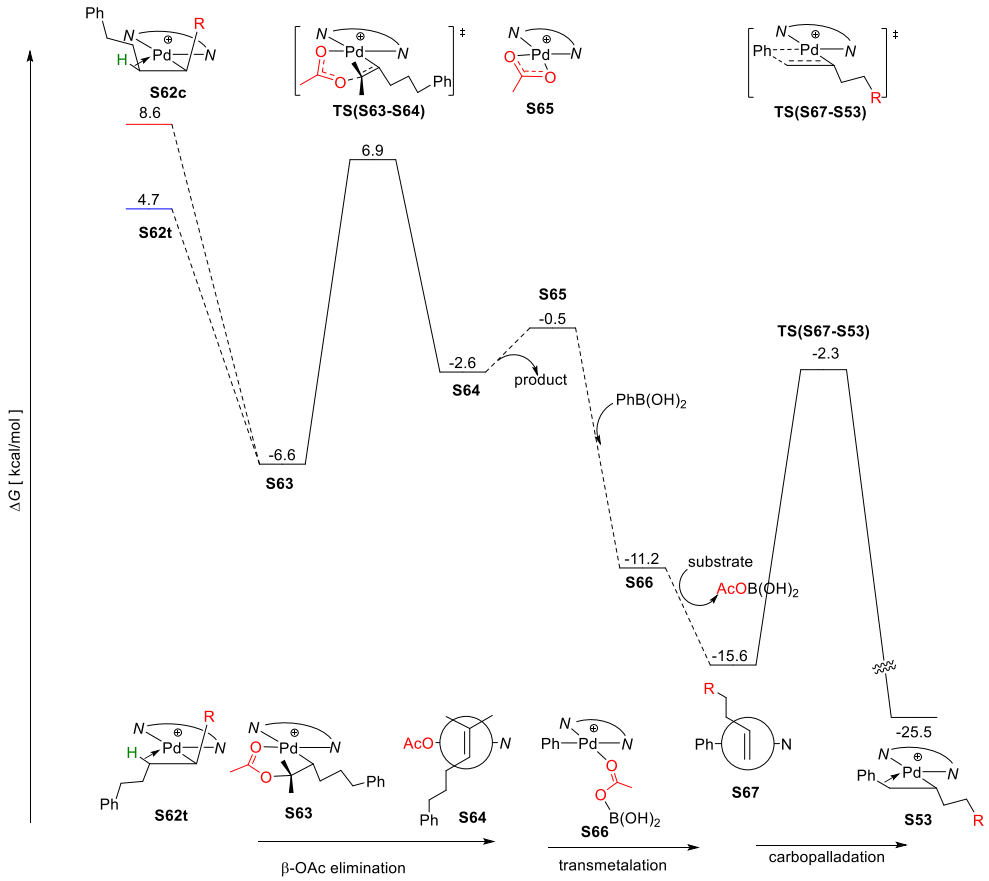

Figure S28. Energy diagram of β-OAc elimination, transmetalation and carbopalladation of the terminal alkene.

XII. Geometries of the Optimized Structures

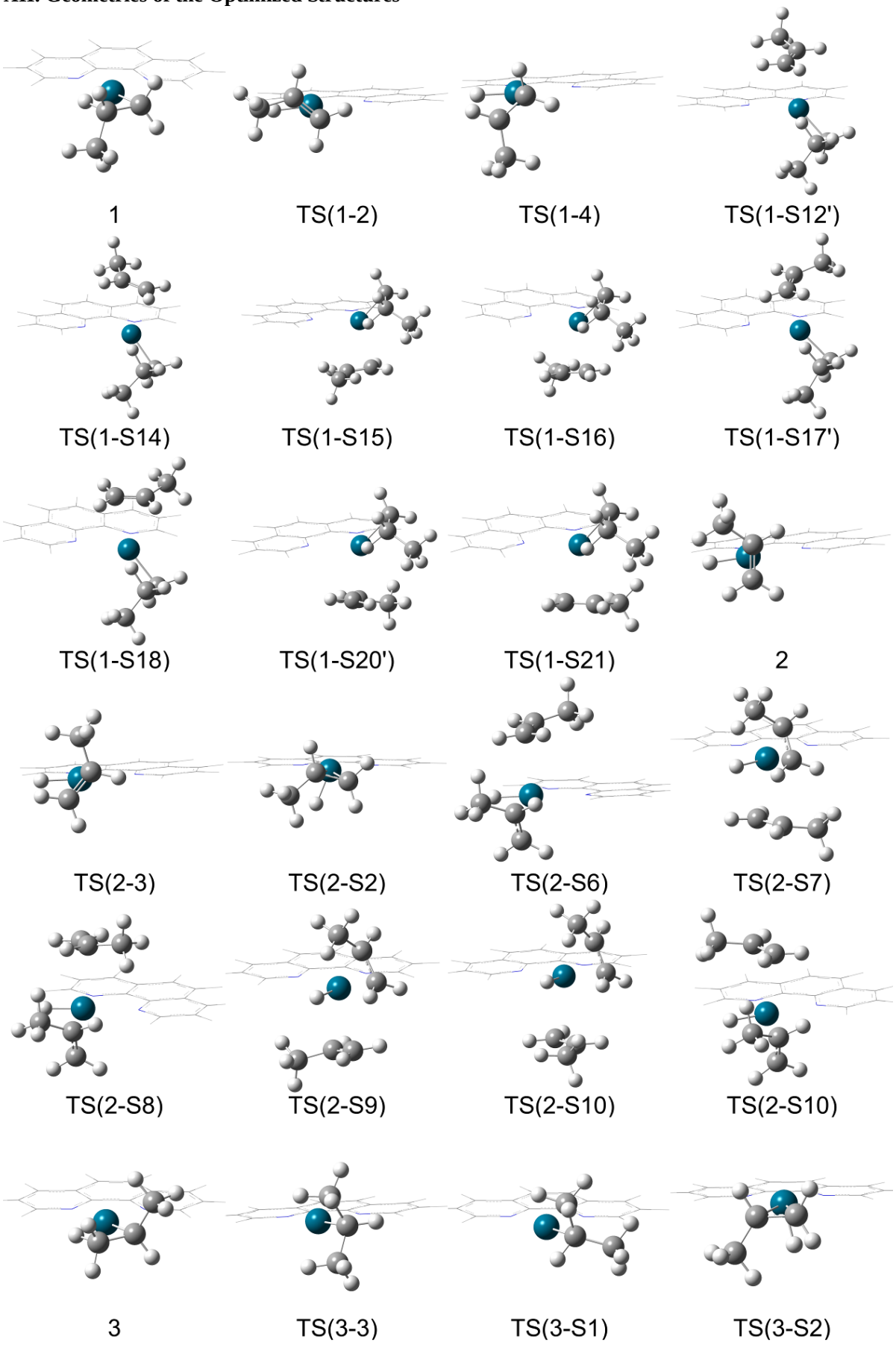

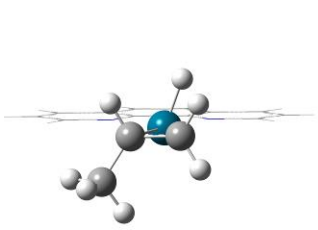

TS(3-S2')

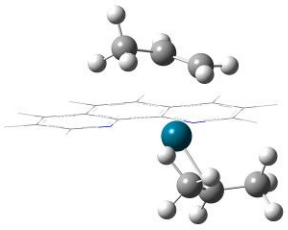

TS(3-S24)

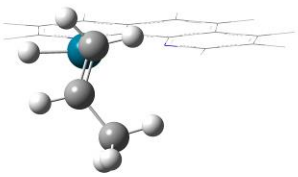

4

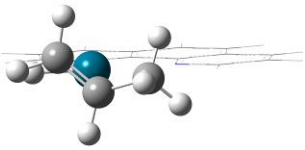

TS(4-3)

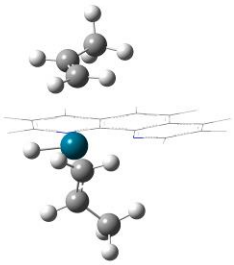

TS(4-5)

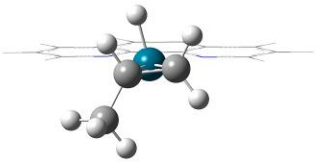

TS(4-S2')

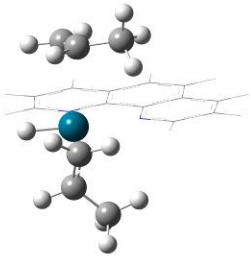

TS(4-S3)

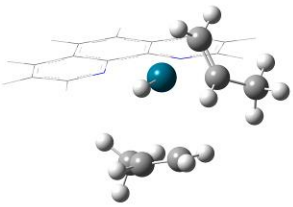

TS(4-S3)

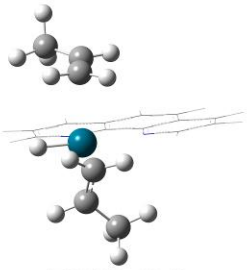

TS(4-S5)

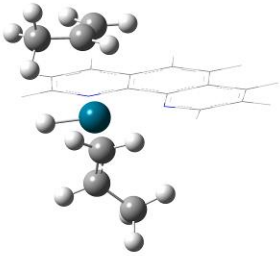

TS(4-S6)

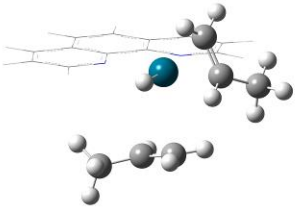

TS(4-S7)

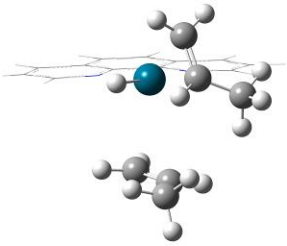

TS(4-S8)

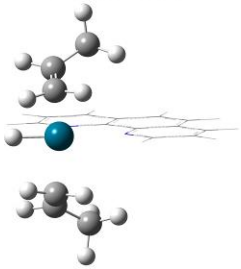

5

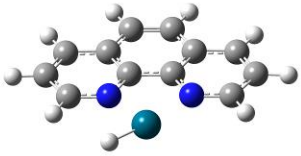

6

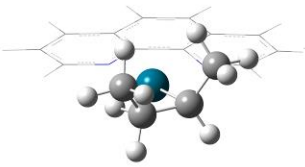

7c

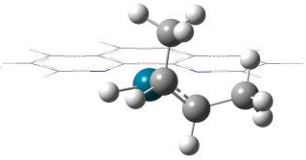

TS(7c-9'c)

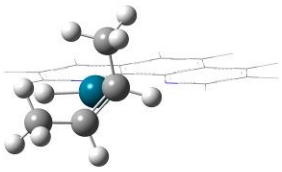

TS(7c-9c)

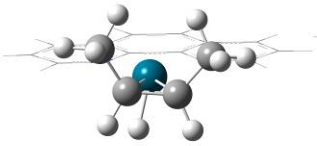

TS(7c-S40c)

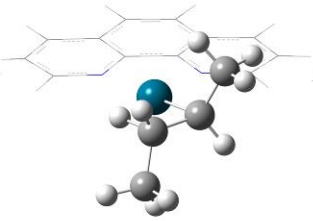

7t

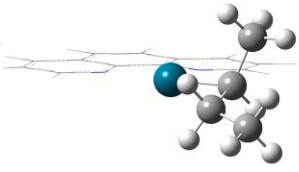

TS(7t-7c)

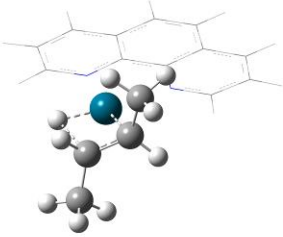

TS(7t-8t)

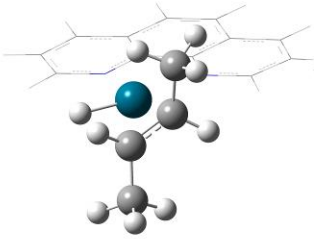

8't

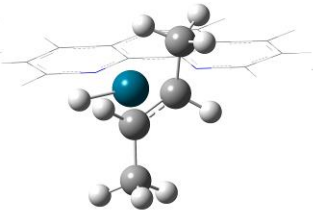

TS(8't-8t)

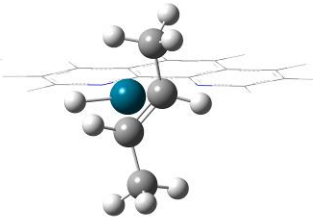

TS(8't-9t)

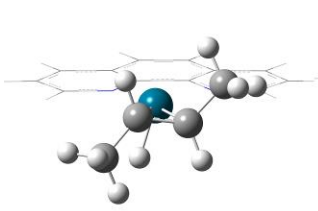

TS(8't-9t)

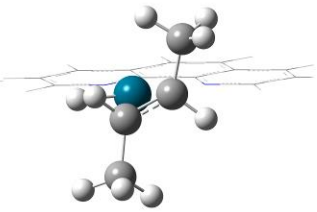

8t

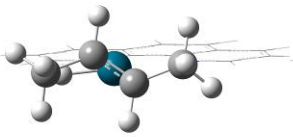

TS(8t-9t)

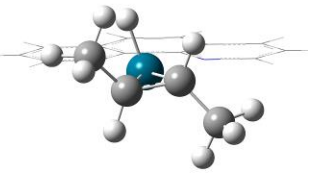

TS(8t-9t)

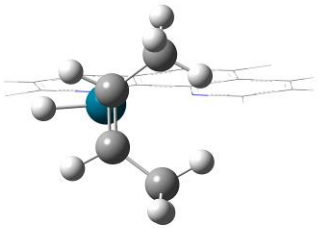

9'c

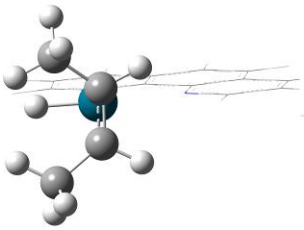

9c

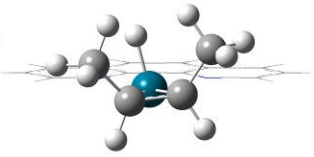

TS(9c-S40'c)

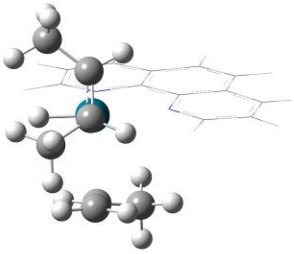

TS(9c-S43)

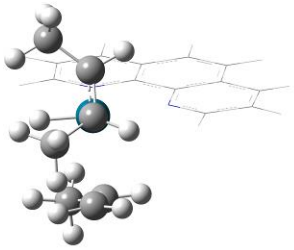

TS(9c-S43')

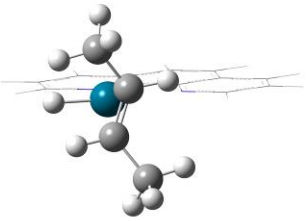

9t

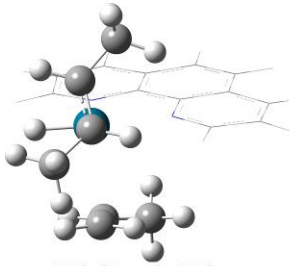

TS(9t-S42)

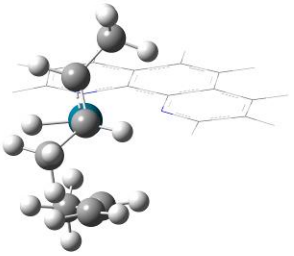

TS(9t-S42')

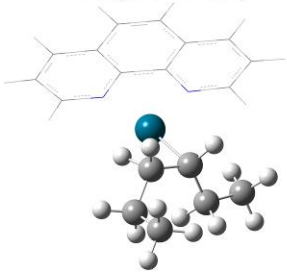

10'''c

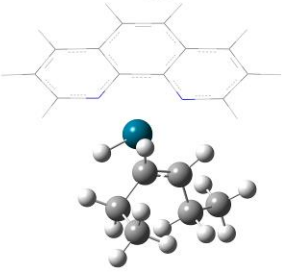

TS(10'''c-12'c)

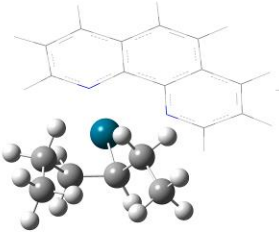

10''c

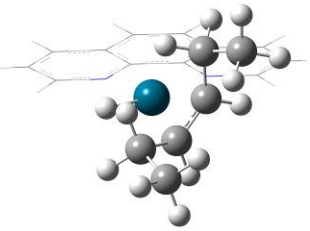

TS(10''c-12''c)

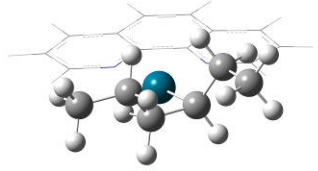

10'c

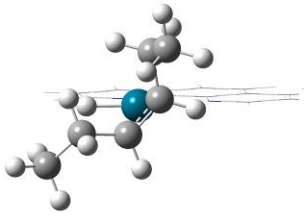

TS(10'c-12'c)

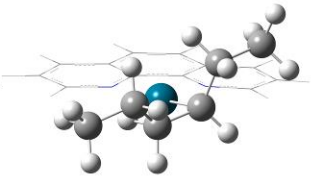

10c

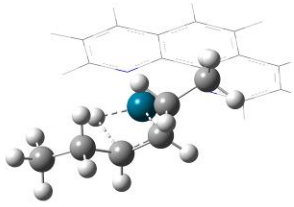

TS(10c-12c)

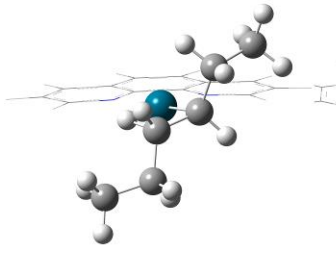

10t

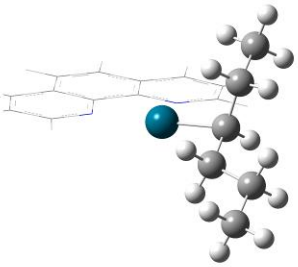

TS(10t-10c)

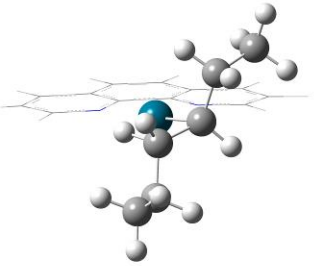

TS(10t-11t)

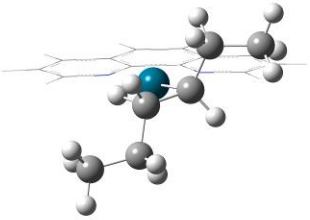

TS(10t-13t)

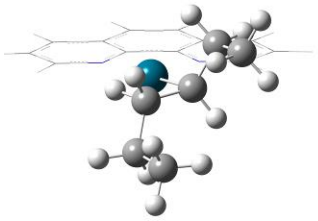

11"t

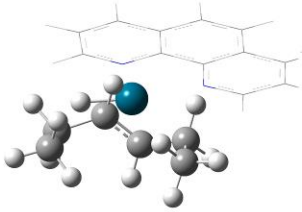

TS(11"t-12"t)

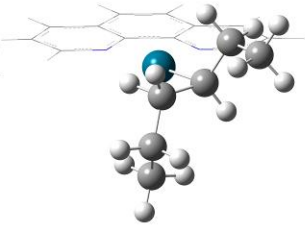

11't

TS(11't-12't)

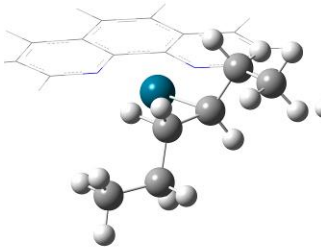

11t

TS(11t-12t)

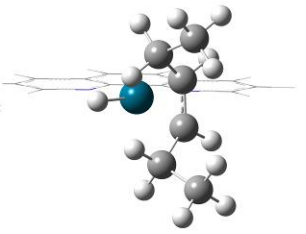

12"c

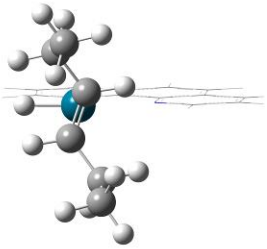

12"t

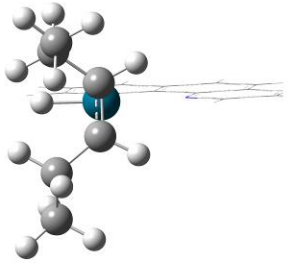

12'c

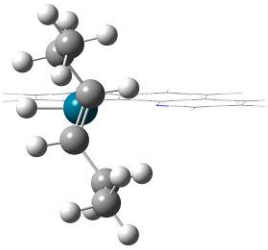

12't

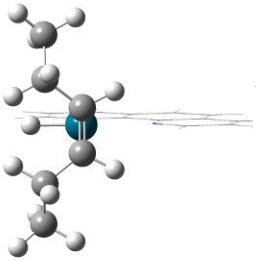

12c

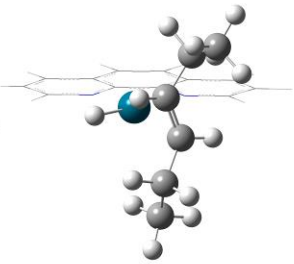

12t

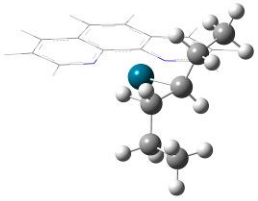

13t

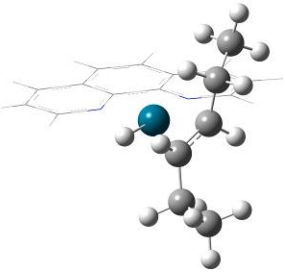

TS(13t-12t)

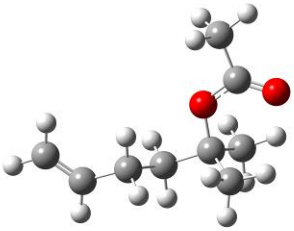

14

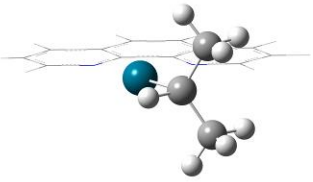

S1

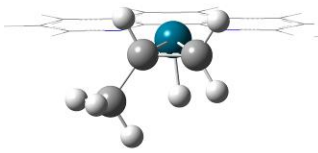

S2

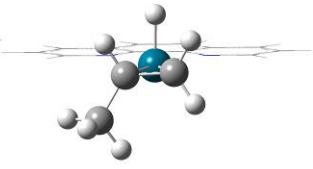

S2'

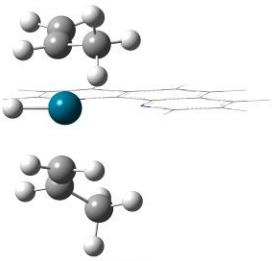

S3

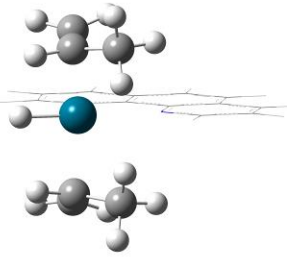

S4

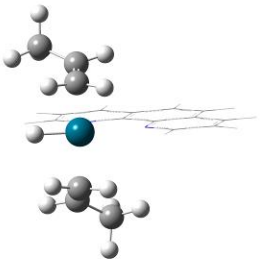

S5

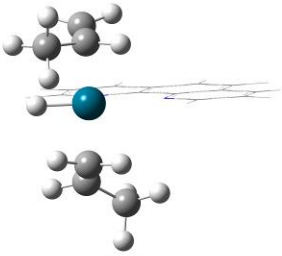

S6

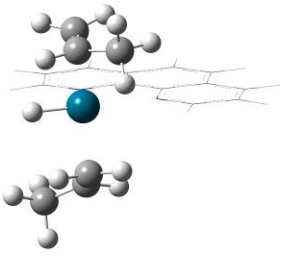

S7

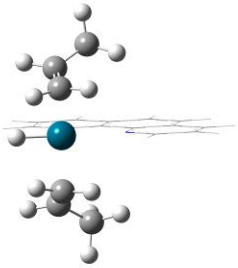

S8

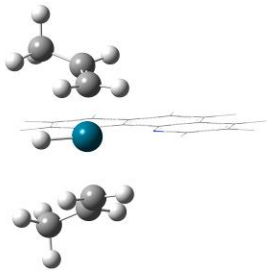

S9

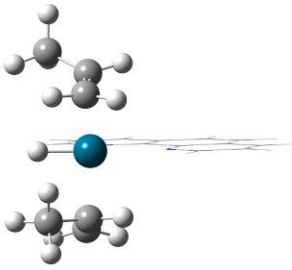

S10

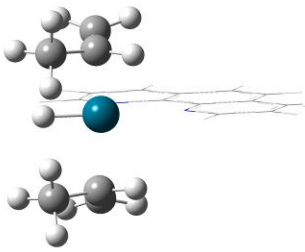

S11

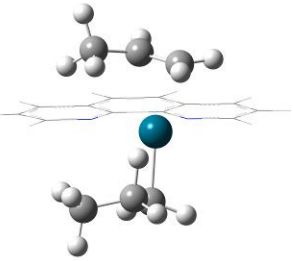

S12

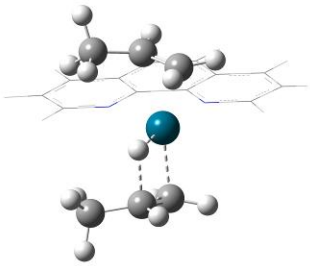

TS(S12-S13)

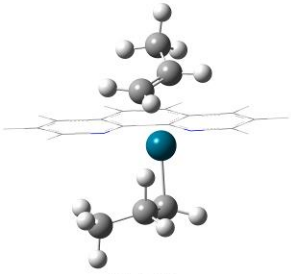

S12'

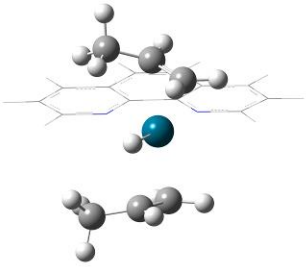

S13

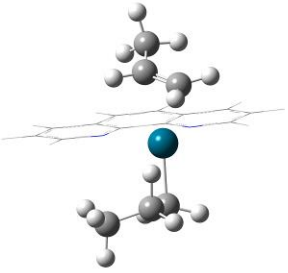

S14

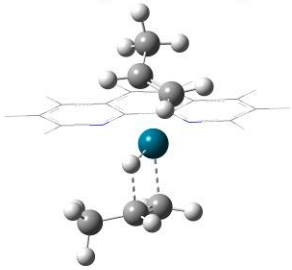

TS(S14-4)

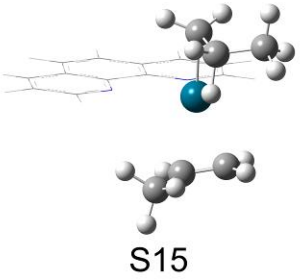

S15

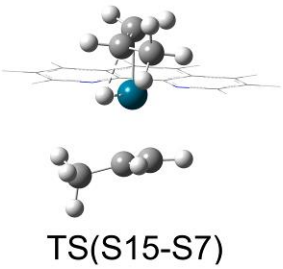

TS(S15-S7)

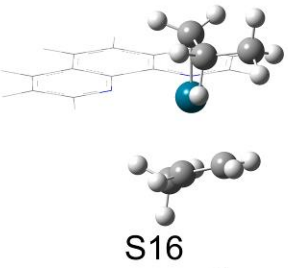

S16

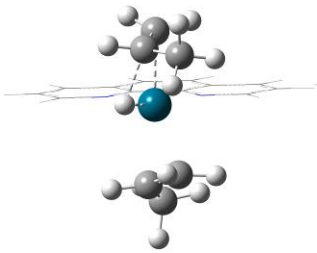

TS(S16-S3)

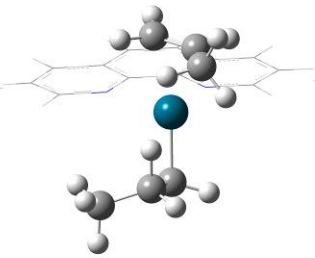

S17

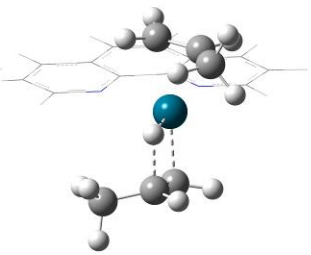

TS(S17-2)

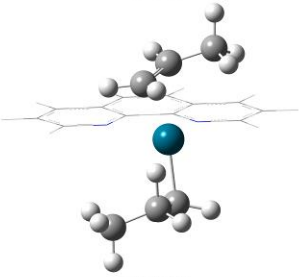

S17'

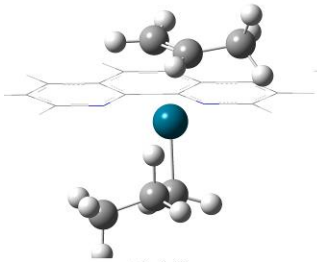

S18

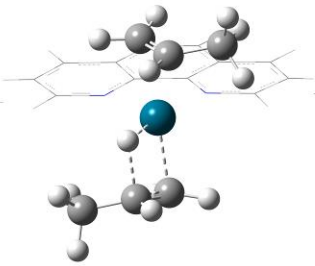

TS(S18-S19)

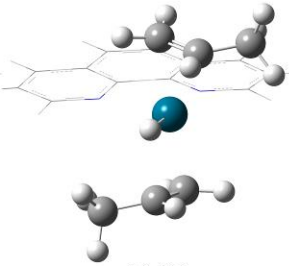

S19

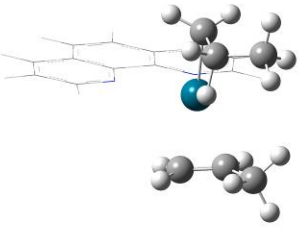

S20

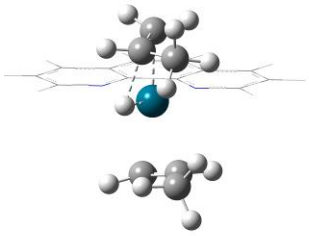

TS(S20-S8)

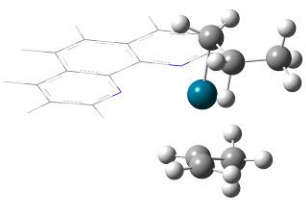

S20'

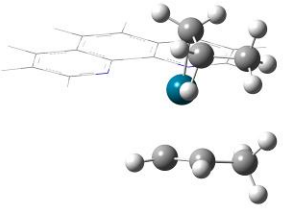

S21

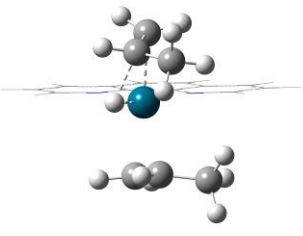

TS(S21-S4)

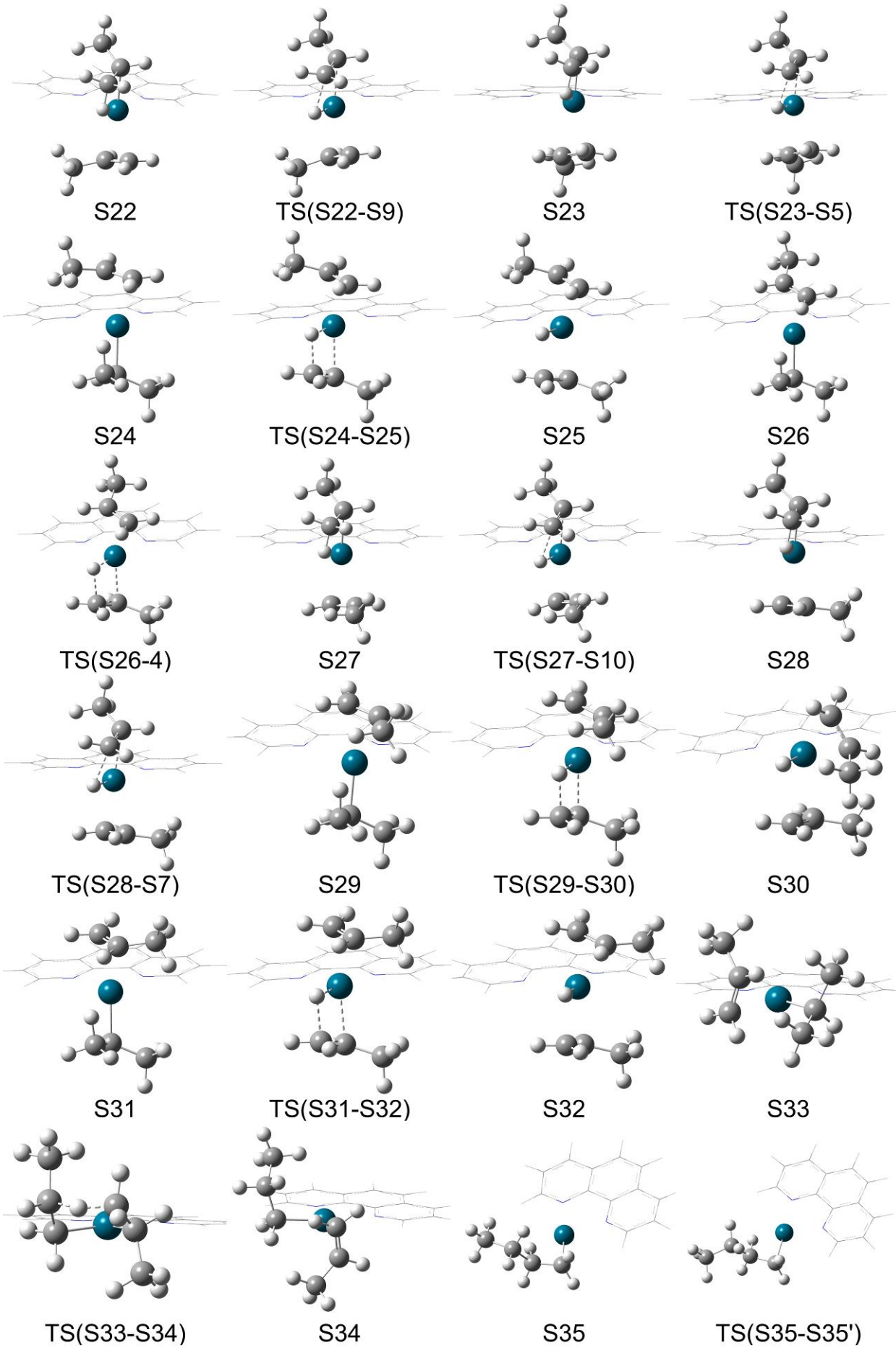
S22
TS(S22-S9)
S23
TS(S23-S5)
S24
TS(S24-S25)
S25
S26
TS(S26-4)
S27
TS(S27-S10)
S28
TS(S28-S7)
S29
TS(S29-S30)
S30
S31
TS(S31-S32)
S32
S33
TS(S33-S34)
S34
S35
TS(S35-S35')

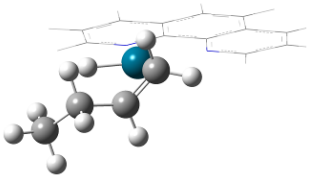

TS(S35-S36)

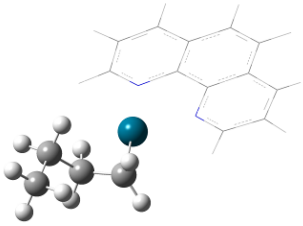

S35'

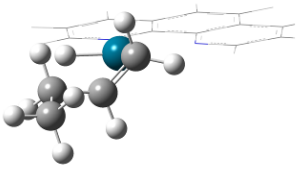

TS(S35'-S36')

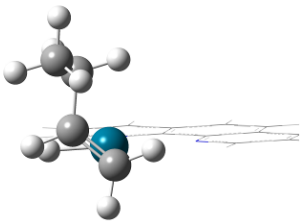

TS(S35'-S39)

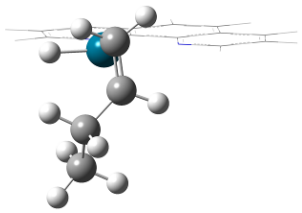

S36

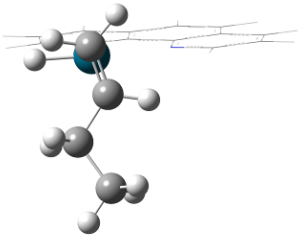

TS(S36-S36')

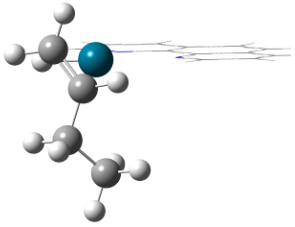

TS(S36-S37)

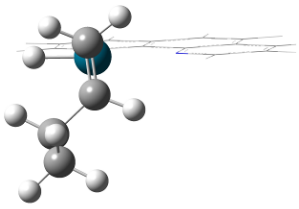

S36'

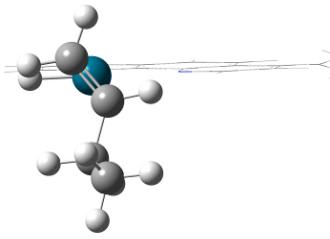

TS(S36'-S38')

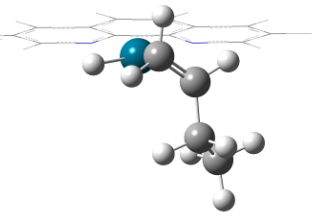

S37

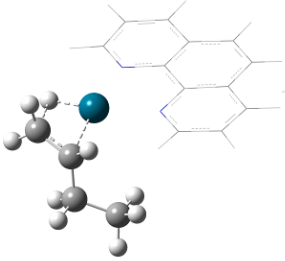

TS(S37-S38)

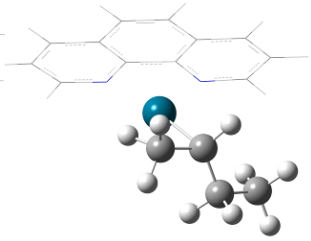

S38

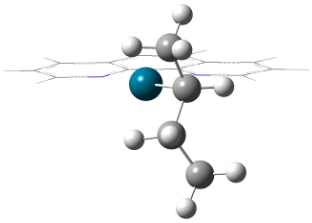

TS(S38-7t)

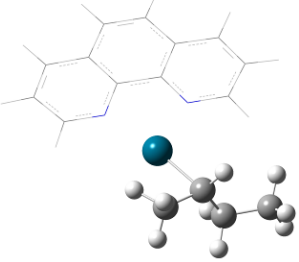

TS(S38-S38')

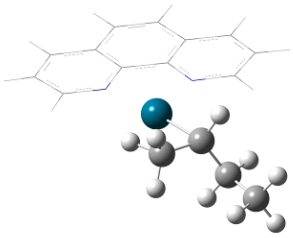

S38'

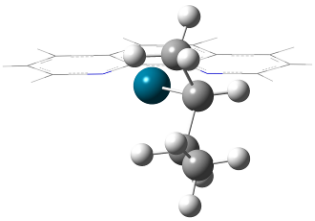

TS(S38'-7c)

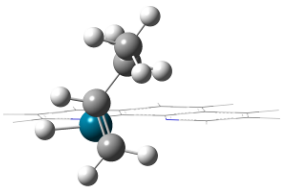

S39

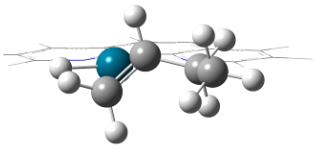

TS(S39-S38')

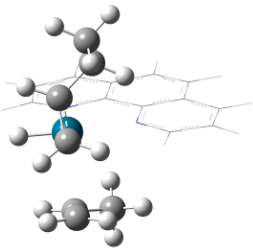

TS(S39-S41)

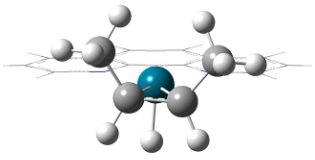

S40c

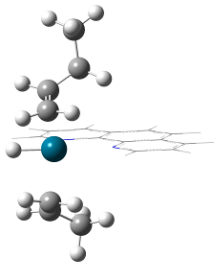

S41

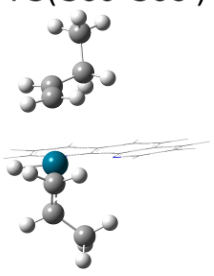

TS(S41-4)

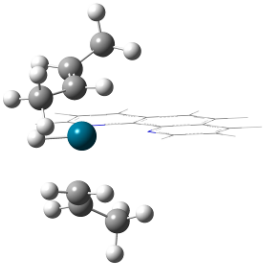

S42

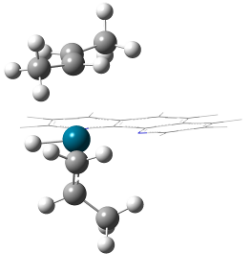

TS(S42-4)

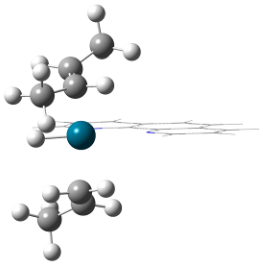

S42'

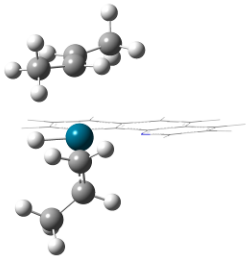

TS(S42'-2)

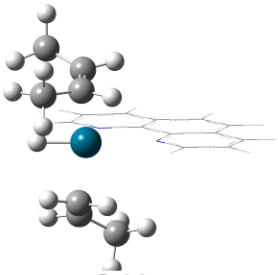

S43

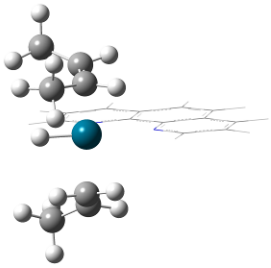

S43'

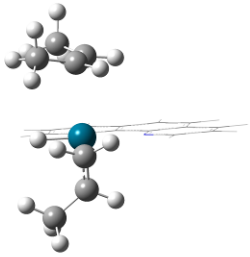

TS(S43'-2)

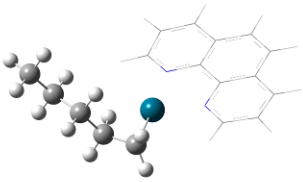

S44

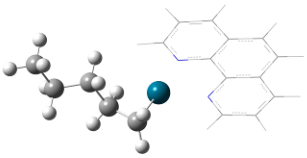

TS(S44-S44')

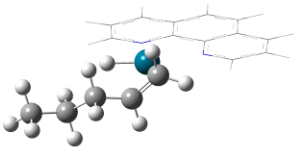

TS(S44-S45)

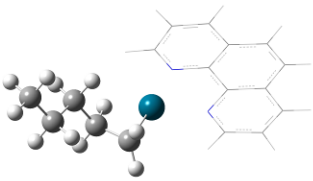

S44'

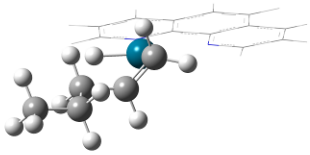

TS(S44'-S45')

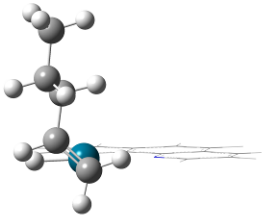

TS(S44'-S48)

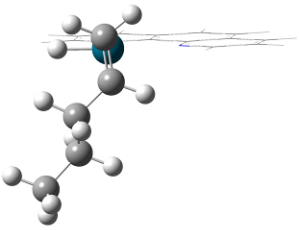

S45

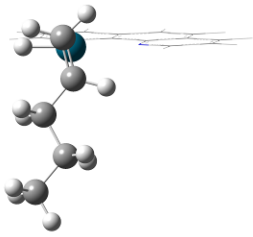

TS(S45-S45')

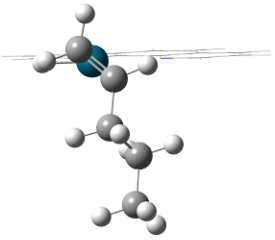

TS(S45-S46)

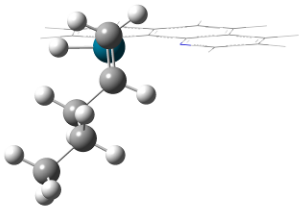

S45'

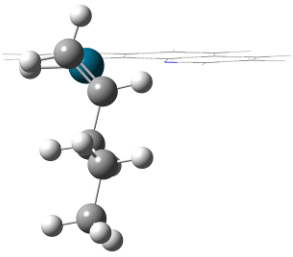

TS(S45'-S47')

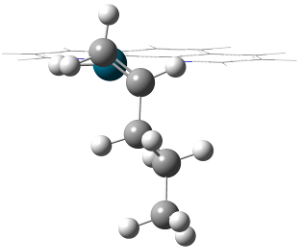

S46

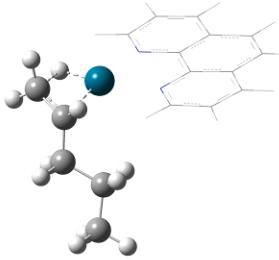

TS(S46-S47)

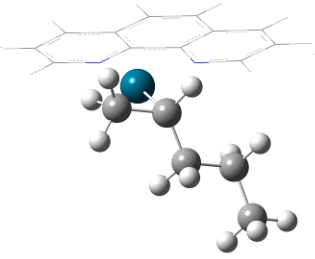

S47

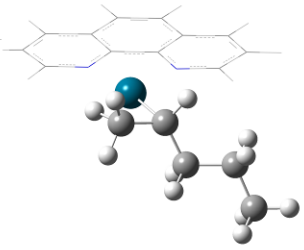

TS(S47-S47')

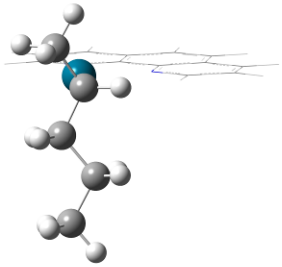

TS(S47-S49t)

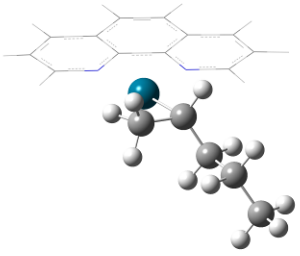

S47'

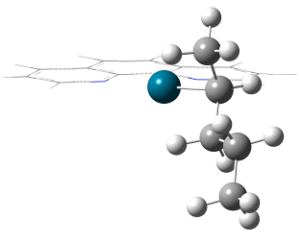

TS(S47'-S49c)

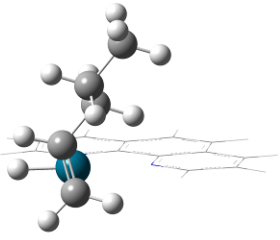

S48

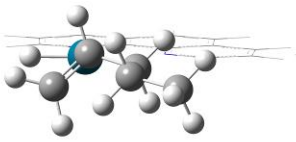

TS(S48-S47')

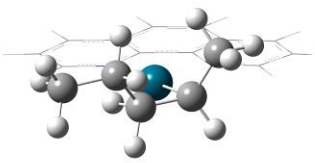

S49'c

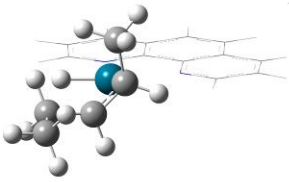

TS(S49'c-S51'c)

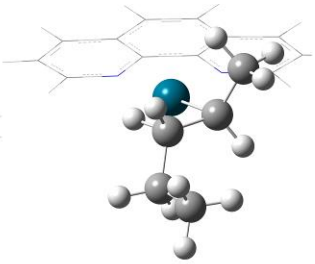

S49't

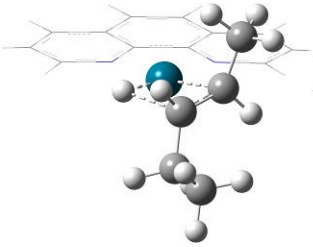

TS(S49't-S50t)

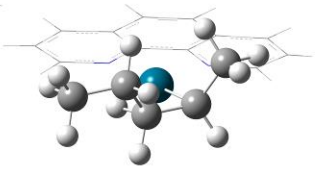

S49c

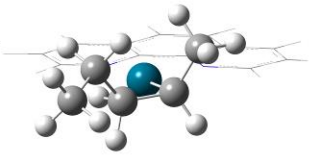

TS(S49c-S49'c)

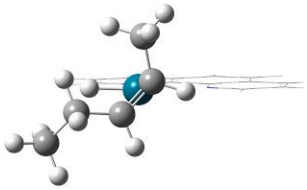

TS(S49c-S51c)

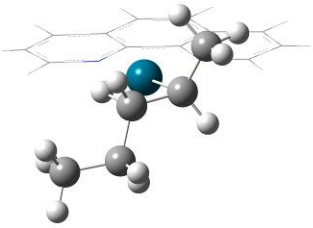

S49t

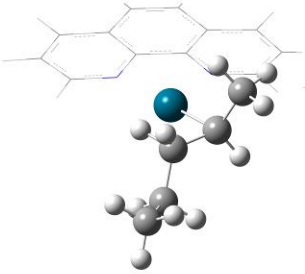

TS(S49t-S49't)

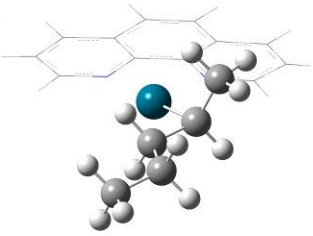

TS(S49t-S49c)

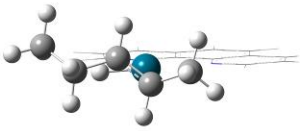

TS(S49t-S51t)

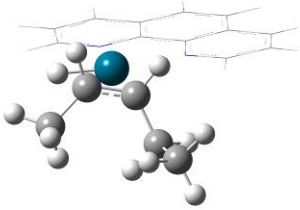

S50c

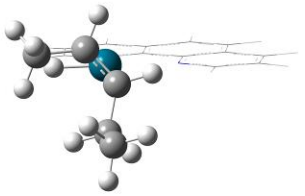

TS(S50c-S51'c)

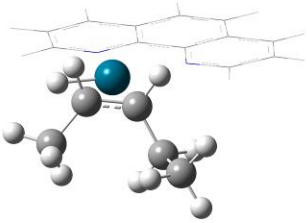

TS(S50c-S52'c)

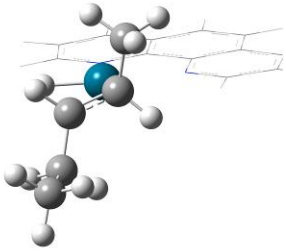

S50t

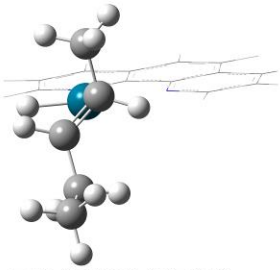

TS(S50t-S51't)

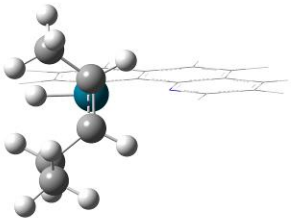

S51'c

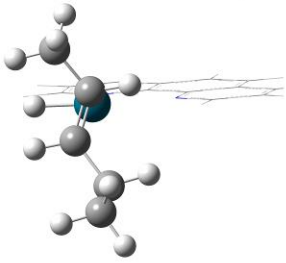

S51't

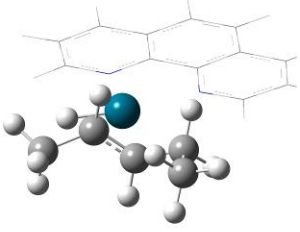

TS(S51't-S52't)

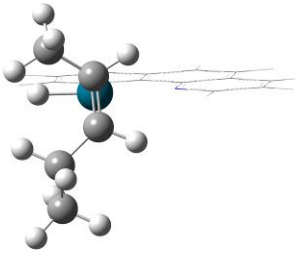

S51c

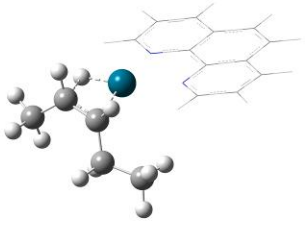

TS(S51c-S52c)

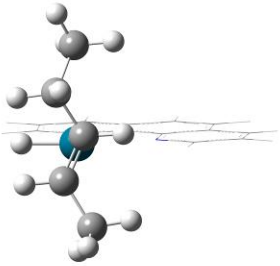

S51t

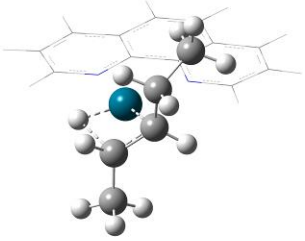

TS(S51t-S52t)

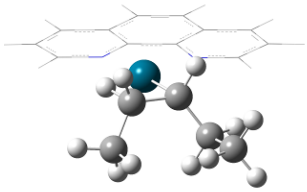

S52'c

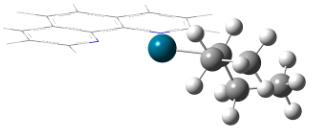

TS(S52'c-S52't)

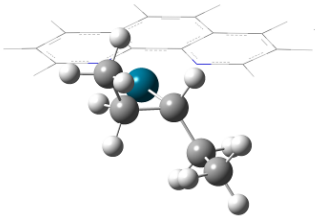

S52't

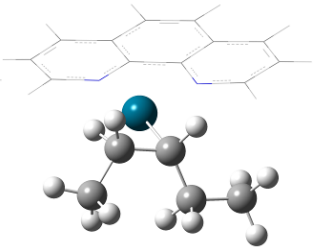

S52c

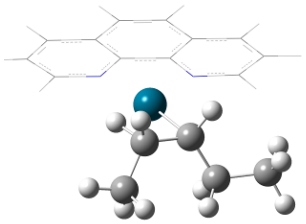

TS(S52c-S52'c)

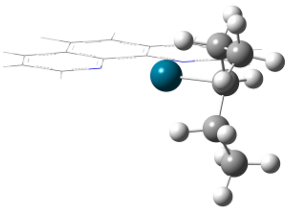

TS(S52c-S52't)

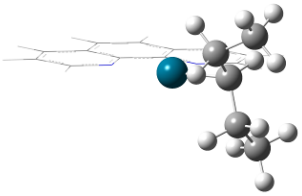

TS(S52c-S52t)

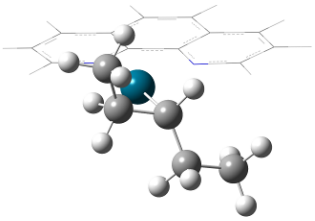

S52t

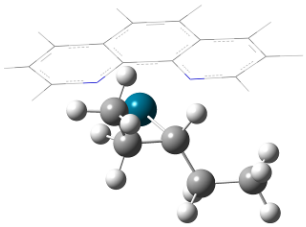

TS(S52t-S52't)

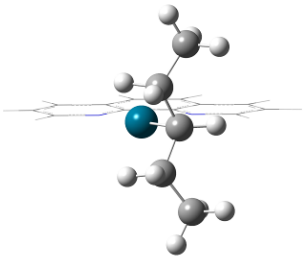

TS(S52t-S52t)

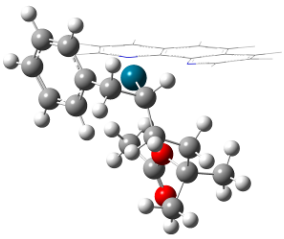

S53

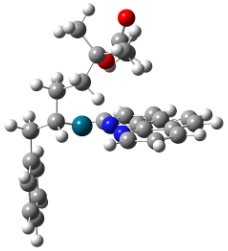

TS(S53-S54')

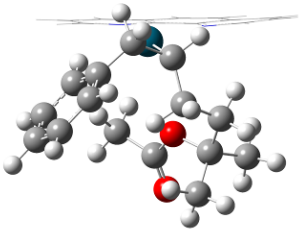

TS(S53-S54c)

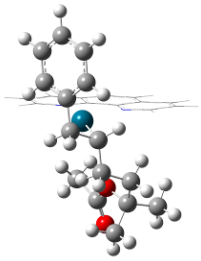

TS(S53-S54t)

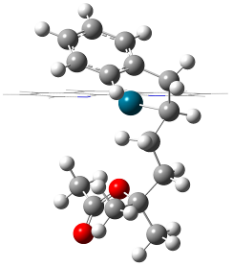

TS(S53-S57t)

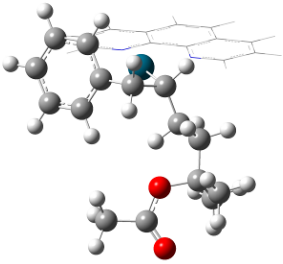

S53'

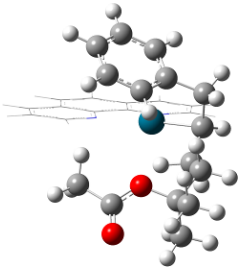

TS(S53'-S57c)

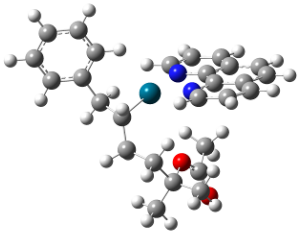

S54'

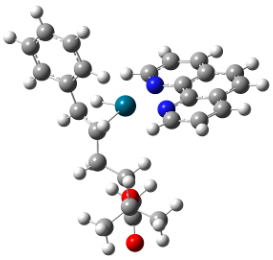

TS(S54'-S55t)

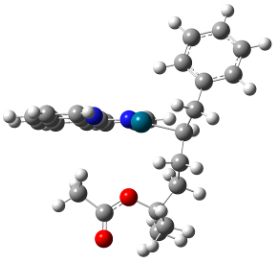

TS(S54'-S57't)

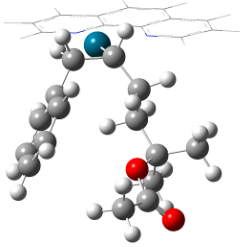

S54'c

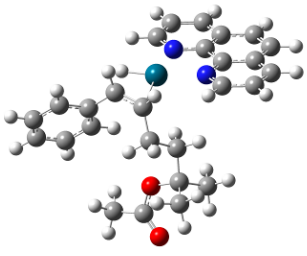

TS(S54'c-S55'c)

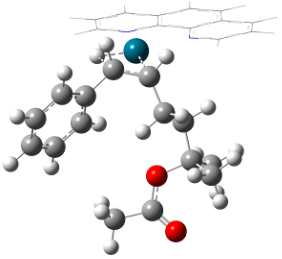

TS(S54'c-S55c)

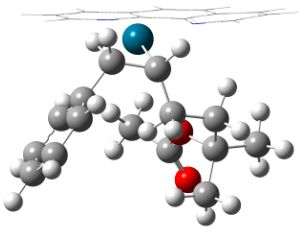

S54c

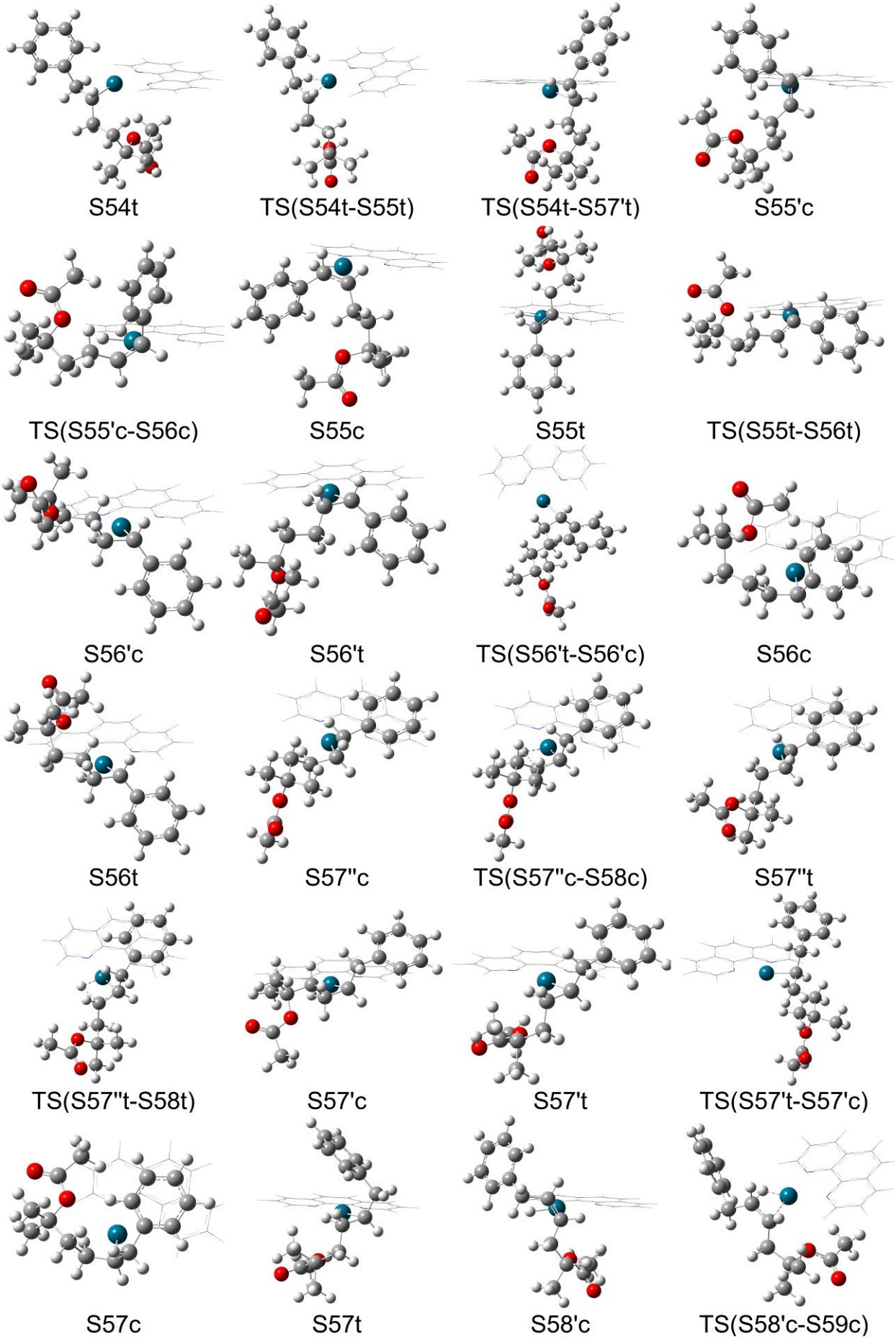
S54t
TS(S54t-S55t)
TS(S54t-S57't)
S55'c
TS(S55'c-S56c)
S55c
S55t
TS(S55t-S56t)
S56'c
S56't
TS(S56't-S56'c)
S56c
S56t
S57"c
TS(S57"c-S58c)
S57"t
TS(S57"t-S58t)
S57'c
S57't
TS(S57't-S57'c)
S57c
S57t
S58'c
TS(S58'c-S59c)

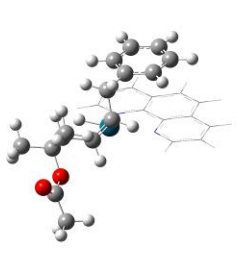

S58c

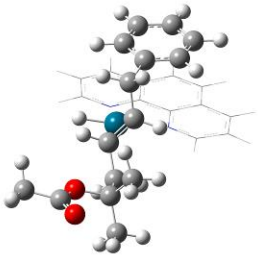

S58t

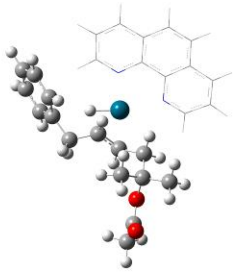

TS(S58t-S59t)

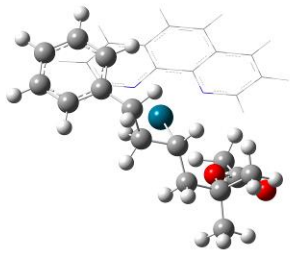

S59't

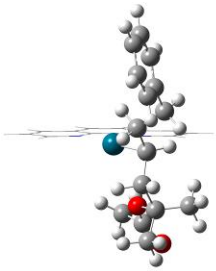

TS(S59't-S60t)

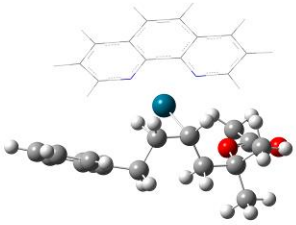

S59c

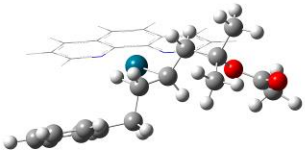

S59t

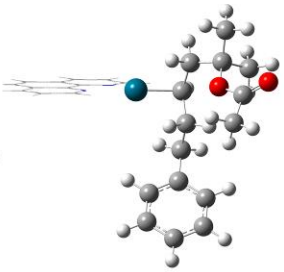

TS(S59t-S60c)

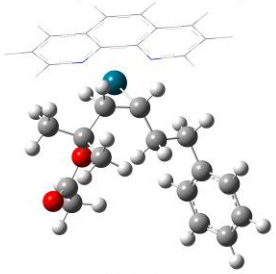

S60c

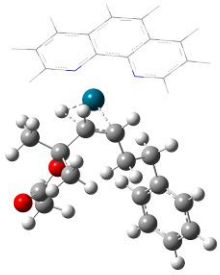

TS(S60c-S61c)

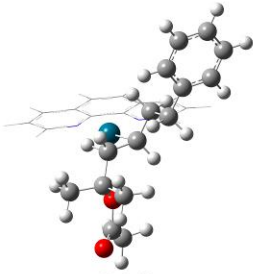

S60t

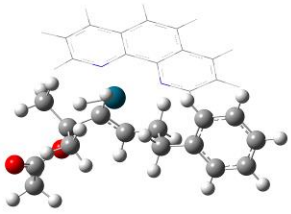

TS(S60t-S61t)

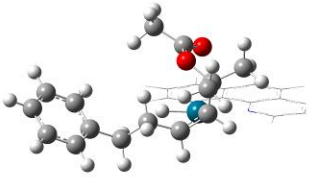

S61'c

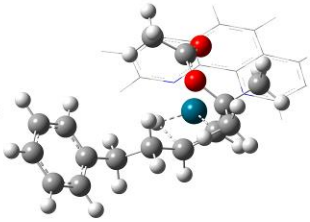

TS(S61'c-S62c)

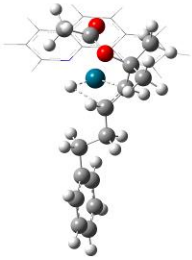

S61't

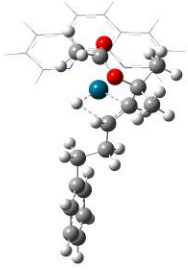

TS(S61't-S62t)

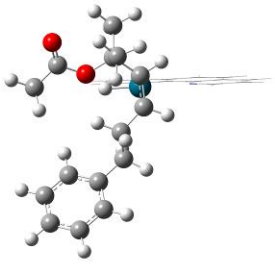

S61c

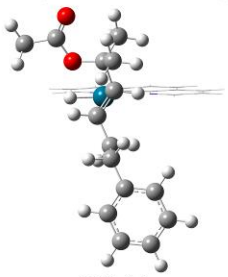

S61t

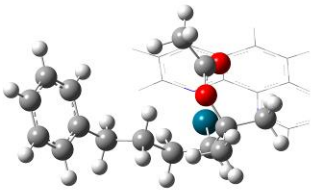

S62c

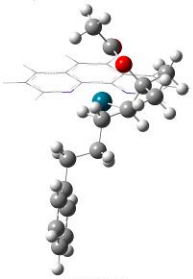

S62t

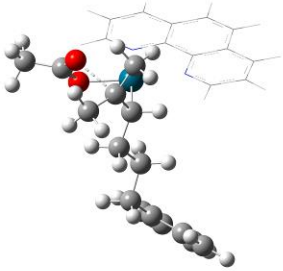

TS(S63-S64)

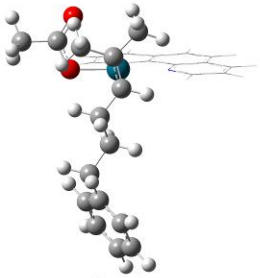

S64

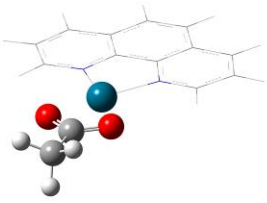

S65

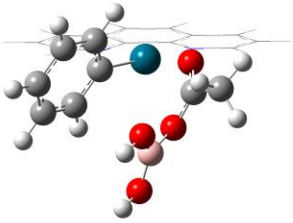

S66

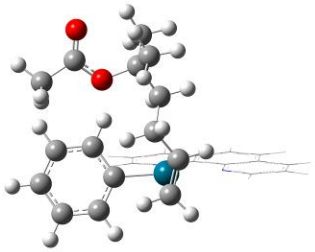

S67

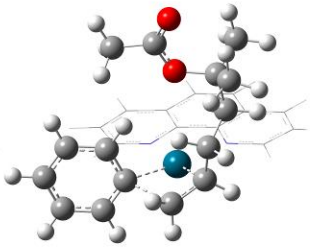

TS(S67-S53)

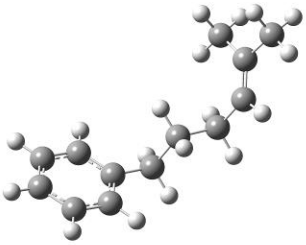

S68

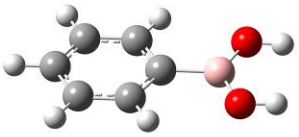

S69

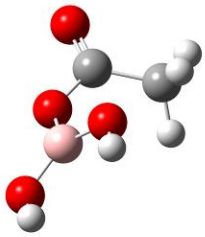

S70

XIII. Energies and eigenfrequencies of Optimized Structures

Structure number	Imaginary frequency (cm^{-1})	E_0 (Hartree)	G (Hartree)
1		-817.43962	-817.21846
1-2	-62.5358	-817.42486	-817.20496
1-4	-46.0546	-817.42846	-817.20882
1-S12'	-124.2352	-935.24003	-934.94601
1-S14	-118.3428	-935.23915	-934.94548
1-S15	-98.1267	-935.23853	-934.94443
1-S16	-100.5426	-935.24000	-934.94485
1-S17'	-124.4792	-935.23942	-934.94739
1-S18	-118.6946	-935.23860	-934.94478
1-S20'	-94.2601	-935.24100	-934.94739
1-S21	-114.8863	-935.23965	-934.94498
2		-817.43019	-817.21113
2-3	-56.3655	-817.42826	-817.20899
2-S2	-148.0837	-817.40742	-817.19026
2-S6	-56.6210	-935.24270	-934.94945
2-S7	-48.1673	-935.24311	-934.94958
2-S8	-43.7050	-935.24179	-934.94745
2-S9	-34.0718	-935.24282	-934.94876
2-S10-ts	-24.7174	-935.24125	-934.94859
2-S10-ts'	-56.4031	-935.24138	-934.94890
3		-817.44408	-817.22338
3-3	-75.9545	-817.42958	-817.20889
3-S1	-97.4526	-817.42549	-817.20497
3-S2	-136.5302	-817.40848	-817.19160
3-S2'	-311.6408	-817.40882	-817.19248
3-S24	-81.3202	-935.24333	-934.94989
4		-817.42984	-817.21216
4-3	-71.6846	-817.42208	-817.20294
4-5	-39.3870	-935.24419	-934.95107
4-S2'	-191.0779	-817.40910	-817.19243
4-S3-ts	-30.4910	-935.24350	-934.94883
4-S3-ts'	-40.8585	-935.24084	-934.94893

Structure number	Imaginary frequency (cm^{-1})	E_0 (Hartree)	G (Hartree)
4-S5	-36.8417	-935.24377	-934.94980
4-S6	-26.8522	-935.24165	-934.94897
4-S7	-42.2736	-935.23943	-934.94745
4-S8	-61.6671	-935.23803	-934.94689
5		-935.24676	-934.95265
6		-699.57362	-699.43081
7c		-856.72520	-856.47883
7c-9'c	-63.3249	-856.70897	-856.46451
7c-9c	-55.8981	-856.71127	-856.46579
7c-S40c	-113.7941	-856.69432	-856.45171
7t		-856.72586	-856.47928
7t-7c	-64.7422	-856.71079	-856.46361
7t-8t	-273.8366	-856.71557	-856.47136
8't		-856.71583	-856.47210
8't-8t	-71.3529	-856.71583	-856.47141
8't-9t-ts	-54.7073	-856.71536	-856.46996
8't-9t-ts'	-181.5623	-856.69271	-856.45122
8t		-856.71591	-856.47133
8t-9t-ts	-63.2898	-856.70387	-856.45882
8t-9t-ts'	-182.0290	-856.69271	-856.45125
9'c		-856.71374	-856.46976
9c		-856.71530	-856.47101
9c-S40'c	-181.9623	-856.69196	-856.45012
9c-S43	-37.6608	-974.52794	-974.20679
9c-S43'	-39.6064	-974.52750	-974.20661
9t		-856.71637	-856.47166
9t-S42	-47.2221	-974.52916	-974.21009
9t-S42'	-57.5057	-974.52879	-974.20973
10'''c		-935.28485	-934.98383
10'''c-12'c	-279.9236	-935.27353	-934.97685
10''c		-935.28493	-934.98522
10''c-12''c	-48.5426	-935.27287	-934.97493
10'c		-935.28669	-934.98690

Structure number	Imaginary frequency (cm^{-1})	E_0 (Hartree)	G (Hartree)
10'c-12'c	-45.0257	-935.27378	-934.97547
10c		-935.28583	-934.98651
10c-12c	-181.9451	-935.27467	-934.97827
10t		-935.28782	-934.98821
10t-10c	-104.4420	-935.27210	-934.97359
10t-11t	-101.8628	-935.28259	-934.98267
10t-13t	-95.4275	-935.28379	-934.98496
11''t		-935.28989	-934.98866
11''t-12''t	-27.1278	-935.26740	-934.96732
11't		-935.28936	-934.98874
11't-12't	-47.4078	-935.26689	-934.96868
11t		-935.28882	-934.98937
11t-12t	-83.2082	-935.26691	-934.97085
12''c		-935.27660	-934.97959
12''t		-935.27757	-934.98132
12'c		-935.27795	-934.98022
12't		-935.27712	-934.98195
12c		-935.27878	-934.98342
12t		-935.27870	-934.98110
13t		-935.28782	-934.98657
13t-12t	-227.5347	-935.27685	-934.97926
14		-502.70990	-502.51709
S1		-817.42784	-817.20828
S2		-817.40861	-817.19148
S2'		-817.40926	-817.19194
S3		-935.24662	-934.95236
S4		-935.24525	-934.95117
S5		-935.24662	-934.95431
S6		-935.24595	-934.95155
S7		-935.24644	-934.95317
S8		-935.24569	-934.95089
S9		-935.24675	-934.95319
S10		-935.24571	-934.95232

Structure number	Imaginary frequency (cm^{-1})	E_0 (Hartree)	G (Hartree)
S11		-935.24380	-934.94997
S12		-935.24737	-934.95390
S12-S13	-440.3122	-935.23960	-934.94797
S12'		-935.24774	-934.95420
S13		-935.24139	-934.95054
S14		-935.24722	-934.95676
S14		-935.24722	-934.95676
S14-4	-331.2889	-935.23896	-934.94734
S15		-935.24639	-934.95411
S15-S7	-385.5098	-935.23949	-934.94842
S16		-935.24660	-934.95430
S16-S3	-592.8082	-935.23894	-934.94754
S17		-935.24557	-934.95237
S17-2	-457.9591	-935.23731	-934.94552
S17'		-935.24784	-934.95418
S18		-935.24685	-934.95191
S18-S19	-425.1760	-935.23865	-934.94638
S19		-935.24020	-934.95027
S20		-935.24575	-934.95258
S20-S8	-506.4311	-935.23772	-934.94747
S20'		-935.24682	-934.95262
S21		-935.24629	-934.95354
S21-S4	-560.4182	-935.23949	-934.94810
S22		-935.25276	-934.95906
S22-S9	-352.3713	-935.24107	-934.94890
S23		-935.25278	-934.95795
S23-S5	-412.2389	-935.24031	-934.94807
S24		-935.25287	-934.95908
S24-S25	-342.5087	-935.24090	-934.94964
S25		-935.24203	-934.95118
S26		-935.25309	-934.96021
S26-4	-376.5303	-935.24009	-934.94866
S27		-935.25178	-934.95815

Structure number	Imaginary frequency (cm^{-1})	E_0 (Hartree)	G (Hartree)
S27-S10	-493.2291	-935.23980	-934.94741
S28		-935.25254	-934.95824
S28-S7	-347.6856	-935.24061	-934.94841
S29		-935.25136	-934.95928
S29-S30	-377.1530	-935.23844	-934.94773
S30		-935.24319	-934.94883
S31		-935.25210	-934.96022
S31-S32	-301.7656	-935.23972	-934.94803
S32		-935.24061	-934.94973
S33		-935.27438	-934.97647
S33-S34	-728.9914	-935.19358	-934.89938
S34		-935.27311	-934.97322
S35		-856.72129	-856.47485
S35-S35'	-102.0844	-856.71592	-856.46874
S35-S36	-67.0016	-856.70624	-856.46157
S35'		-856.72108	-856.47402
S35'-S36'	-64.0716	-856.70547	-856.46002
S35'-S39	-27.7455	-856.70873	-856.46309
S36		-856.71190	-856.46604
S36-S36'	-89.7779	-856.70534	-856.46031
S36-S37	-33.8367	-856.71050	-856.46488
S36'		-856.71016	-856.46512
S36'-S38'	-41.5326	-856.70849	-856.46331
S37		-856.71071	-856.46496
S37-S38	-236.9990	-856.71020	-856.46593
S38		-856.72407	-856.47585
S38-7t	-75.3186	-856.71158	-856.46533
S38-S38'	-93.1566	-856.72026	-856.47255
S38'		-856.72515	-856.47806
S38'-7c	-17.4498	-856.70883	-856.46105
S39		-856.71034	-856.46500
S39-S38'	-48.9016	-856.70252	-856.45681
S39-S41	-27.5716	-974.52477	-974.20368

Structure number	Imaginary frequency (cm^{-1})	E_0 (Hartree)	G (Hartree)
S40c		-856.69450	-856.45233
S41		-974.52703	-974.20825
S41-4	-34.1854	-974.52442	-974.20493
S42		-974.53240	-974.21139
S42-4	-44.3682	-974.52924	-974.21006
S42'		-974.53246	-974.21235
S42'-2	-26.4058	-974.52851	-974.20788
S43		-974.53184	-974.21160
S43'		-974.53159	-974.21111
S43'-2	-35.8646	-974.52824	-974.20814
S44		-896.00204	-895.73035
S44-S44'	-73.6558	-895.99682	-895.72365
S44-S45	-54.7223	-895.98727	-895.71637
S44'		-896.00188	-895.72892
S44'-S45'	-56.2004	-895.98641	-895.71470
S44'-S48	-38.9528	-895.98961	-895.71770
S45		-895.99269	-895.72121
S45-S45'	-88.4861	-895.98658	-895.71615
S45-S46	-57.8853	-895.99162	-895.71950
S45'		-895.99112	-895.71925
S45'-S47'	-35.6428	-895.98941	-895.71810
S46		-895.99158	-895.71995
S46-S47	-285.9443	-895.99085	-895.72075
S47		-896.00474	-895.73007
S47-S47'	-72.5041	-896.00133	-895.72781
S47-S49t	-36.4023	-895.99254	-895.71963
S47'		-896.00589	-895.73341
S47'-S49c	-13.9206	-895.99002	-895.71559
S48		-895.99096	-895.71994
S48-S47'	-25.6915	-895.98414	-895.71159
S49'c		-896.00555	-895.73244
S49'c-S51'c	-40.3488	-895.99228	-895.72017
S49't		-896.00752	-895.73398

Structure number	Imaginary frequency (cm^{-1})	E_0 (Hartree)	G (Hartree)
S49't-S50t	-190.9441	-895.99624	-895.72569
S49c		-896.00660	-895.73517
S49c-S49'c	-108.2200	-896.00106	-895.72739
S49c-S51c	-45.7850	-895.99308	-895.72145
S49t		-896.00777	-895.73458
S49t-S49't	-95.4440	-896.00234	-895.72853
S49t-S49c	-102.2316	-895.99212	-895.71956
S49t-S51t	-64.0319	-895.98619	-895.71415
S50c		-895.99413	-895.72211
S50c-S51'c	-45.4939	-895.99202	-895.71992
S50c-S52'c	-73.0642	-895.99408	-895.72334
S50t		-895.99642	-895.72585
S50t-S51't	-34.7197	-895.99572	-895.72426
S51'c		-895.99596	-895.72676
S51't		-895.99681	-895.72598
S51't-S52't	-57.8555	-895.98496	-895.71324
S51c		-895.99706	-895.72505
S51c-S52c	-215.6141	-895.99267	-895.72210
S51t		-895.99831	-895.72772
S51t-S52t	-252.2593	-895.99575	-895.72452
S52'c		-896.00512	-895.73146
S52'c-S52't	-117.3489	-895.99054	-895.71539
S52't		-896.00691	-895.73328
S52c		-896.00428	-895.73004
S52c-S52'c	-69.6435	-896.00133	-895.72701
S52c-S52't	-72.9289	-895.99056	-895.71783
S52c-S52t	-88.2335	-895.99106	-895.71768
S52t		-896.00582	-895.73248
S52t-S52't	-89.6192	-896.00178	-895.72818
S52t-S52t	-150.4494	-895.99357	-895.72198
S53		-1433.24935	-1432.80809
S53-S54'	-94.4336	-1433.22912	-1432.78934
S53-S54c	-152.6141	-1433.22875	-1432.79120

Structure number	Imaginary frequency (cm^{-1})	E_0 (Hartree)	G (Hartree)
S53-S54t	-94.4336	-1433.22912	-1432.78934
S53-S57t	-50.3510	-1433.23703	-1432.79789
S53'		-1433.24393	-1432.80581
S53'-S57c	-39.8882	-1433.23181	-1432.79082
S54'		-1433.24002	-1432.80339
S54'-S55t	-420.8125	-1433.22679	-1432.79356
S54'-S57't	-84.0133	-1433.23059	-1432.79492
S54'c		-1433.23899	-1432.80028
S54'c-S55'c	-398.8726	-1433.22296	-1432.78543
S54'c-S55c	-398.8726	-1433.22296	-1432.78543
S54c		-1433.23992	-1432.79948
S54t		-1433.24002	-1432.80339
S54t-S55t	-420.8125	-1433.22679	-1432.79356
S54t-S57't	-84.0133	-1433.23059	-1432.79492
S55'c		-1433.22363	-1432.78558
S55'c		-1433.22363	-1432.78558
S55'c-S56c	-32.1846	-1433.22349	-1432.78660
S55c		-1433.22363	-1432.78558
S55t		-1433.23308	-1432.79651
S55t-S56t	-15.9375	-1433.22655	-1432.78937
S56'c		-1433.24091	-1432.80464
S56't		-1433.24306	-1432.80860
S56't-S56'c	-112.2240	-1433.22944	-1432.79500
S56c		-1433.24732	-1432.80649
S56t		-1433.24798	-1432.80778
S57''c		-1433.23740	-1432.80037
S57''c-S58c	-298.3015	-1433.22742	-1432.79217
S57''t		-1433.24156	-1432.80505
S57''t-S58t	-417.1989	-1433.23209	-1432.79857
S57'c		-1433.23994	-1432.80229
S57't		-1433.24647	-1432.80906
S57't-S57'c	-12.8204	-1433.22656	-1432.78923
S57c		-1433.24325	-1432.79859

Structure number	Imaginary frequency (cm^{-1})	E_0 (Hartree)	G (Hartree)
S57t		-1433.24437	-1432.80526
S58'c		-1433.23192	-1432.79492
S58'c-S59c	-405.7151	-1433.22672	-1432.79306
S58c		-1433.23219	-1432.79580
S58t		-1433.23506	-1432.80064
S58t-S59t	-26.4833	-1433.21818	-1432.78303
S59't		-1433.24050	-1432.80252
S59't-S60t	-48.4445	-1433.22588	-1432.78842
S59c		-1433.23651	-1432.79759
S59t		-1433.24171	-1432.80399
S59t-S60c	-39.9038	-1433.22193	-1432.78632
S60c		-1433.23179	-1432.79396
S60c-S61c	-236.1747	-1433.21947	-1432.78674
S60t		-1433.23873	-1432.80580
S60t-S61t	-48.8266	-1433.21484	-1432.78254
S61'c		-1433.22227	-1432.78988
S61'c-S62c	-156.0690	-1433.22187	-1432.78786
S61't		-1433.22613	-1432.79221
S61't-S62t	-62.9086	-1433.22595	-1432.79118
S61c		-1433.22332	-1432.78957
S61t		-1433.22517	-1432.79193
S62c		-1433.23223	-1432.79435
S62t		-1433.23705	-1432.80067
S63		-1433.25658	-1432.81862
S63-S64	-150.4043	-1433.23182	-1432.79704
S64		-1433.24892	-1432.81230
S65		-927.40625	-927.22643
S66		-1335.47619	-1335.18133
S67		-1433.22665	-1432.79234
S67-S53	-298.8120	-1433.21088	-1432.77110
S68		-505.81240	-505.58245
S69		-408.02978	-407.93778
S70		-404.96649	-404.91303

XIV. References

[1] (CD3PPh3) Yin, G., Wu, Y. & Liu, G. Scope and Mechanism of Allylic C-H Amination of Terminal Alkenes by the Palladium/PhI(OPiv)$_2$ Catalyst System: Insights into the Effect of Naphthoquinone. *J. Am. Chem. Soc.* **132**, 11978–11987 (2010).

[2] (Gaussian 09, Revision D.01) Frisch, M. J., Trucks, G. W., Schlegel, H. B., Scuseria, G. E., Robb, M. A., Cheeseman, J. R., Scalmani, G., Barone, V., Mennucci, B., Petersson, G. A., Nakatsuji, H., Caricato, M., Li, X., Hratchian, H. P., Izmaylov, A. F., Bloino, J., Zheng, G., Sonnenberg, J. L., Hada, M., Ehara, M., Toyota, K., Fukuda, R., Hasegawa, J., Ishida, M., Nakajima, T., Honda, Y., Kitao, O., Nakai, H., Vreven, T., Montgomery, Jr., J. A., Peralta, J. E., Ogliaro, F., Bearpark, M., Heyd, J. J., Brothers, E., Kudin, K. N., Staroverov, V. N., Kobayashi, R., Normand, J., Raghavachari, K., Rendell, A., Burant, J. C., Iyengar, S. S., Tomasi, J., Cossi, M., Rega, N., Millam, N. J., Klene, M., Knox, J. E., Cross, J. B., Bakken, V., Adamo, C., Jaramillo, J., Gomperts, R., Stratmann, R. E., Yazyev, O., Austin, A. J., Cammi, R., Pomelli, C., Ochterski, J. W., Martin, R. L., Morokuma, K., Zakrzewski, V. G., Voth, G. A., Salvador, P., Dannenberg, J. J., Dapprich, S., Daniels, A. D., Farkas, Ö., Foresman, J. B., Ortiz, J. V., Cioslowski, J. & Fox, D. J. Gaussian, Inc., Wallingford CT, 2009.

[3] (M06) Zhao, Y. Truhlar, D. G. "The M06 suite of density functionals for main group thermochemistry, thermochemical kinetics, noncovalent interactions, excited states, and transition elements: two new functionals and systematic testing of four M06-class functionals and 12 other functionals," *Theor. Chem. Acc.* **120**, 215-241 (2008).

[4] (SDD) Dunning Jr. T. H. & Hay, P. J., in Modern Theoretical Chemistry, Ed. H. F. Schaefer III, Vol. 3 (Plenum, New York, 1977) 1-28.

[5] (cc-pVDZ) Dunning Jr., T. H. "Gaussian basis sets for use in correlated molecular calculations. I. The atoms boron through neon and hydrogen" *J. Chem. Phys.* **90**, 1007-1023 (1989).

[6] (GD3) Grimme, S., Antony, J., Ehrlich, S. & Krieg, H. "A consistent and accurate ab initio parameterization of density functional dispersion correction (DFT-D) for the 94 elements H-Pu," *J. Chem. Phys.* **132**, 154104 (2010).

[7] (PCM) Zhao, Y. & Truhlar, D. G. Density Functionals with Broad Applicability in Chemistry. *Acc. Chem. Res.* **41**, 157 (2008).

[8] (PCM) Kulkarni, A. D. & Truhlar, D. G. Performance of Density Functional Theory and Møller–Plesset Second-Order Perturbation Theory for Structural Parameters in Complexes of Ru. *J. Chem. Theory Comput.* **7**, 2325 (2011).

[9] (PCM) Zhao, Y. & Truhlar, D. G. Benchmark Energetic Data in a Model System for Grubbs II Metathesis Catalysis and Their Use for the Development, Assessment, and Validation of Electronic Structure Methods. *J. Chem. Theory Comput.* **5**, 324 (2009).

[10] (AFIR) Maeda, S., Harabuchi, Y., Takagi, M., Saita, K., Suzuki, K., Ichino, T., Sumiya, Y., Sugiyama, K. & Ono, Y. "Implementation and Performance of the Artificial Force Induced Reaction Method in the GRRM17 Program", *J. Comput. Chem.* **39**, 233–251 (2018).

[11] (MIN) Banerjee, A., Adams, N., Simons, J. & Shepard, R. "Search for Stationary Points on Surfaces", *J. Phys. Chem.* **89**, 52–57 (1985).

[12] (MIN) Culot, P., Dive, G., Nguyen, V. H. & Ghuysen, J. M. "A Quasi-Newton Algorithm for First-order Saddle-point Location", *Theor. Chim. Acta* **82**, 189–205 (1992).

[13] (LUP) Choi, C. & Elber, R. "Reaction Path Study of Helix Formation in Tetrapeptides: Effect of Side Chains", *J. Chem. Phys.* **94**, 751–760 (1991).

[14] (LUP) Ayala, P. Y. & Schlegel, H. B. "A Combined Method for Determining Reaction Paths, Minima, and Transition State Geometries", *J. Chem. Phys.* **107**, 375–384 (1997).

[15] (GRRM17) Maeda, S., Harabuchi, Y., Sumiya, Y., Takagi, M., Suzuki, K., Hatanaka, M., Osada, Y., Taketsugu, T., Morokuma, K. & Ohno, K. **GRRM17**, see http://iqce.jp/GRRM/index_e.shtml (accessed date 13 January, 2023).

[16] (GRRM17) Maeda, S., Ohno, K. & Morokuma, K. "Systematic Exploration of the Mechanism of Chemical Reactions: The Global Reaction Route Mapping (GRRM) Strategy by the ADDF and AFIR Methods", *Phys. Chem. Chem. Phys.* **15**, 3683–3701 (2013).

[17] (CW) Muto, K., Kumagai, T., Kakiuchi, F. & Kochi, T. Remote Arylative Substitution of Alkenes Possessing an Acetoxy Group via b-Acetoxy Elimination, *Angew. Chem., Int. Ed.* **60**, 24500-24504 (2021).

[18] (Grignard THF) Chen, G., Wang, Z., Wu, J. & Ding, K. Facile Preparation of α-Aryl Nitriles by Direct Cyanation of Alcohols with TMSCN Under the Catalysis of InX_3, *Org. Lett.* **10**, 4573–4576 (2008).

[19] (hydrogenation) Krawczyk, H. & Albrecht, Ł. A Novel and Convenient Synthesis of Cyclopent-1-enecarboxylates by an -Intramolecular Horner-Wadsworth-Emmons Reaction, *Synthesis* **2008**, 3951–3956 (2008).

[20] (LDA) Candito, D. A., Dobrovolsky, D. & Lautens, M. Development of an Intramolecular Aryne Ene Reaction and Application to the Formal Synthesis of (±)-Crinine, *J. Am. Chem. Soc.* **134**, 15572–15580 (2012).

[21] (mCPBA LAH) Domingo, V., Silva, L., Diéguez, H. R., Arteaga, J. F., del Moral, J. F. Q. & Barrero, A. F. Enantioselective Total Synthesis of the Potent Anti-inflammatory (+)-Myrrhanol A, *J. Org. Chem.* **74**, 6151–6156 (2009).

XV. NMR Spectra

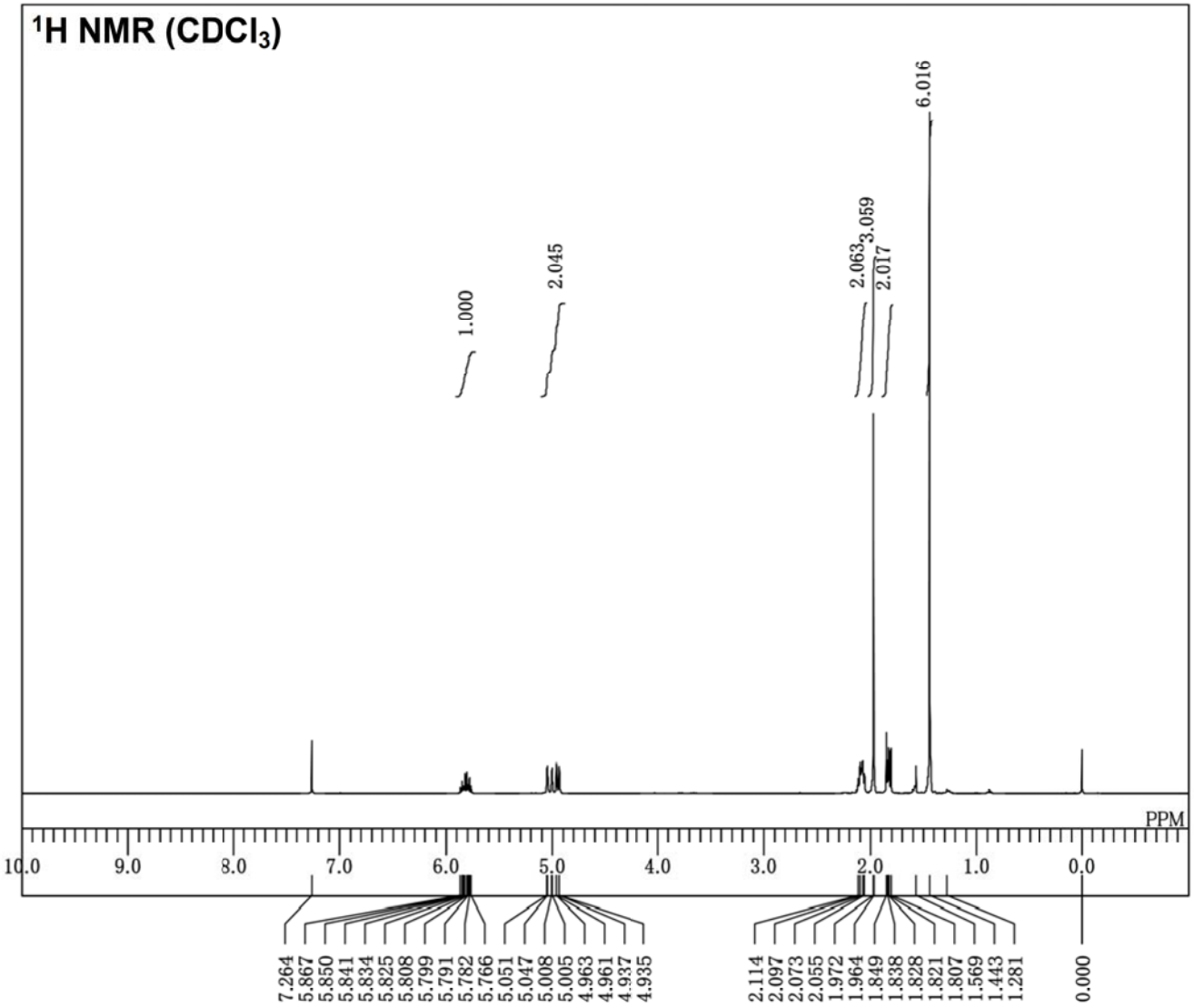

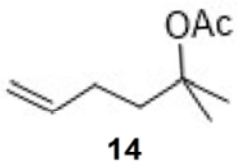

14

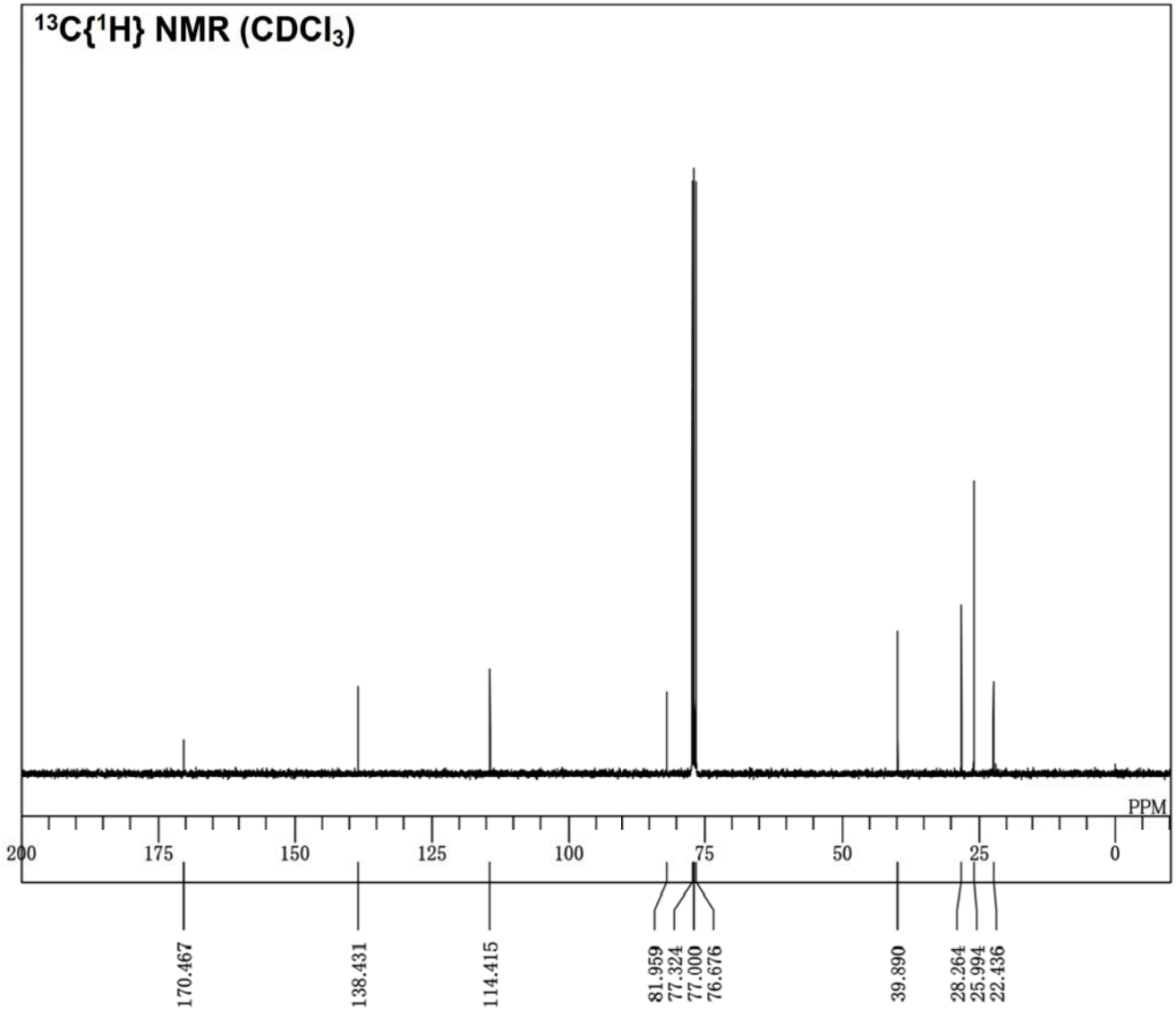
13C{1H} NMR (CDCl3)
PPM
200
175
150
125
100
75
50
25
0
170.467
138.431
114.415
81.959
77.324
77.000
76.676
39.890
28.264
25.994
22.436

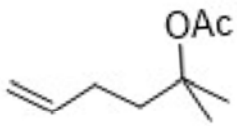
OAc

14

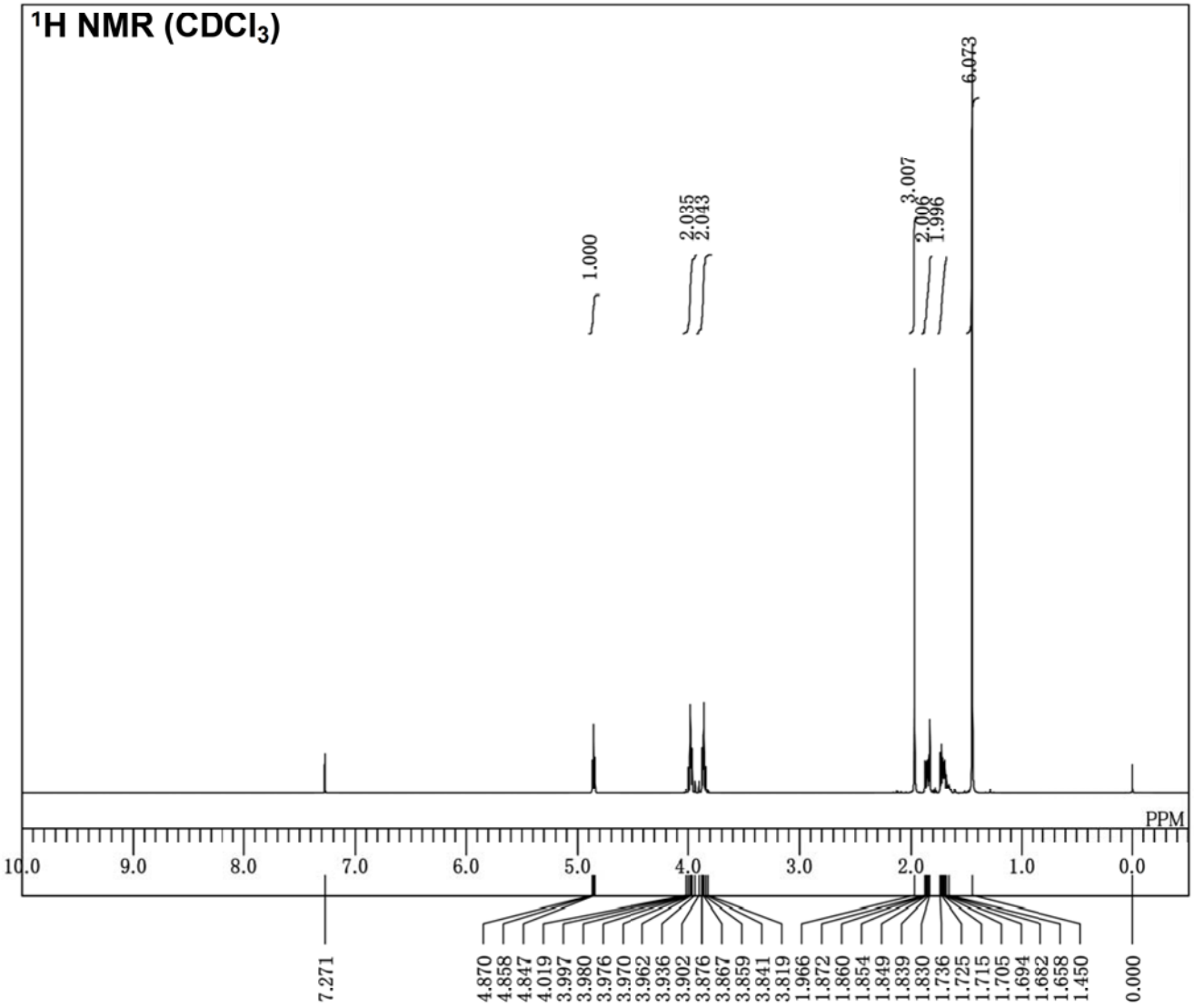
1H NMR (CDCl3)
1.000
2.035
2.043
3.007
2.006
1.996
6.073
PPM
10.0
9.0
8.0
7.0
6.0
5.0
4.0
3.0
2.0
1.0
0.0
7.271
4.870
4.858
4.847
4.019
3.997
3.980
3.976
3.970
3.962
3.936
3.902
3.876
3.867
3.859
3.841
3.819
1.966
1.872
1.860
1.854
1.849
1.839
1.830
1.736
1.725
1.715
1.705
1.694
1.682
1.658
1.450
0.000

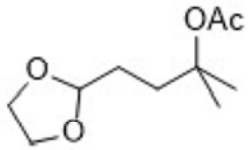
OAc
O
O

S1

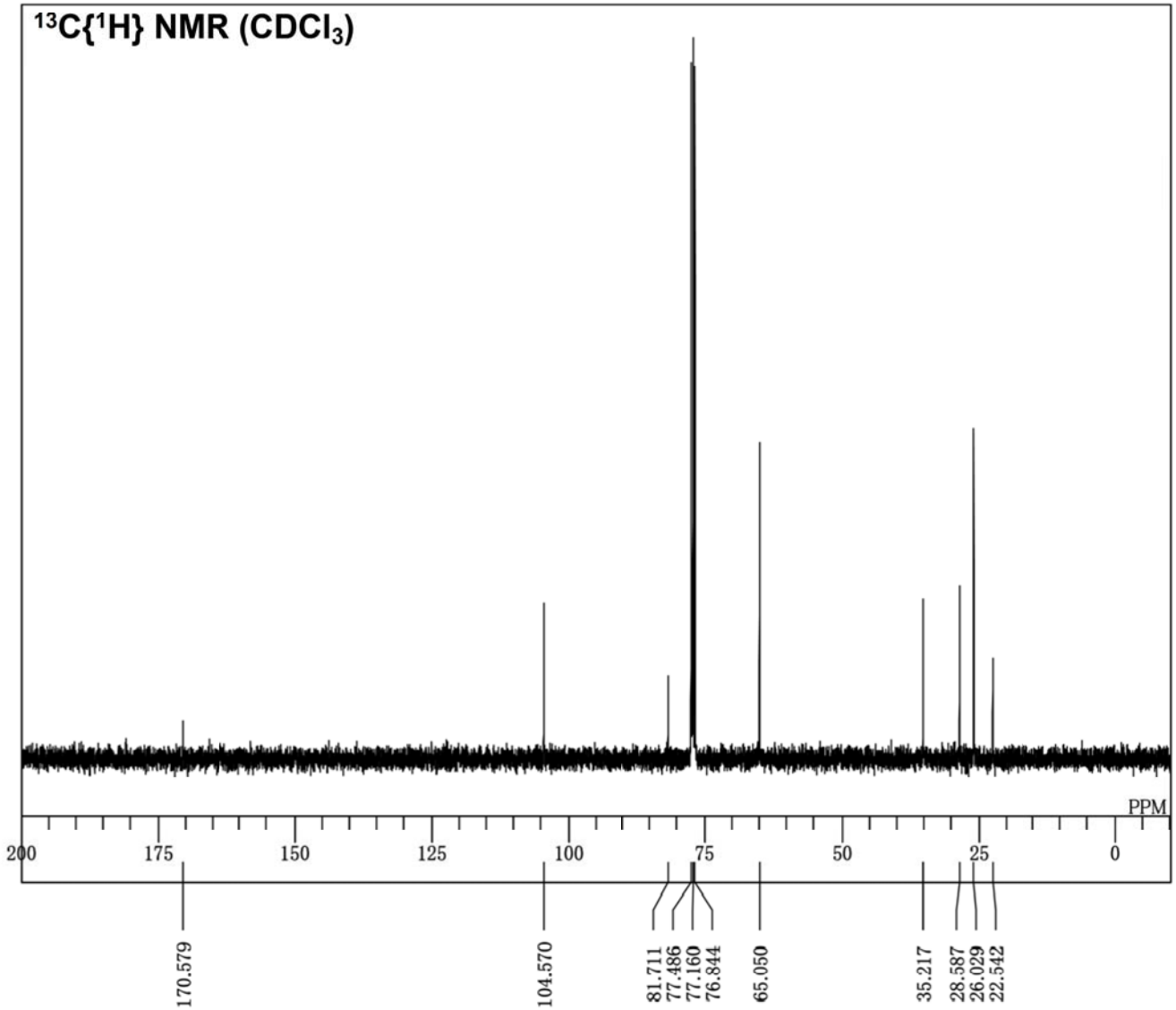
13C{1H} NMR (CDCl3)
PPM
200
175
150
125
100
75
50
25
0
170.579
104.570
81.711
77.486
77.160
76.844
65.050
35.217
28.587
26.029
22.542

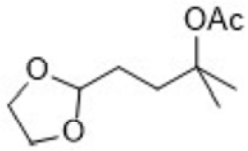
OAc
O
O

S1

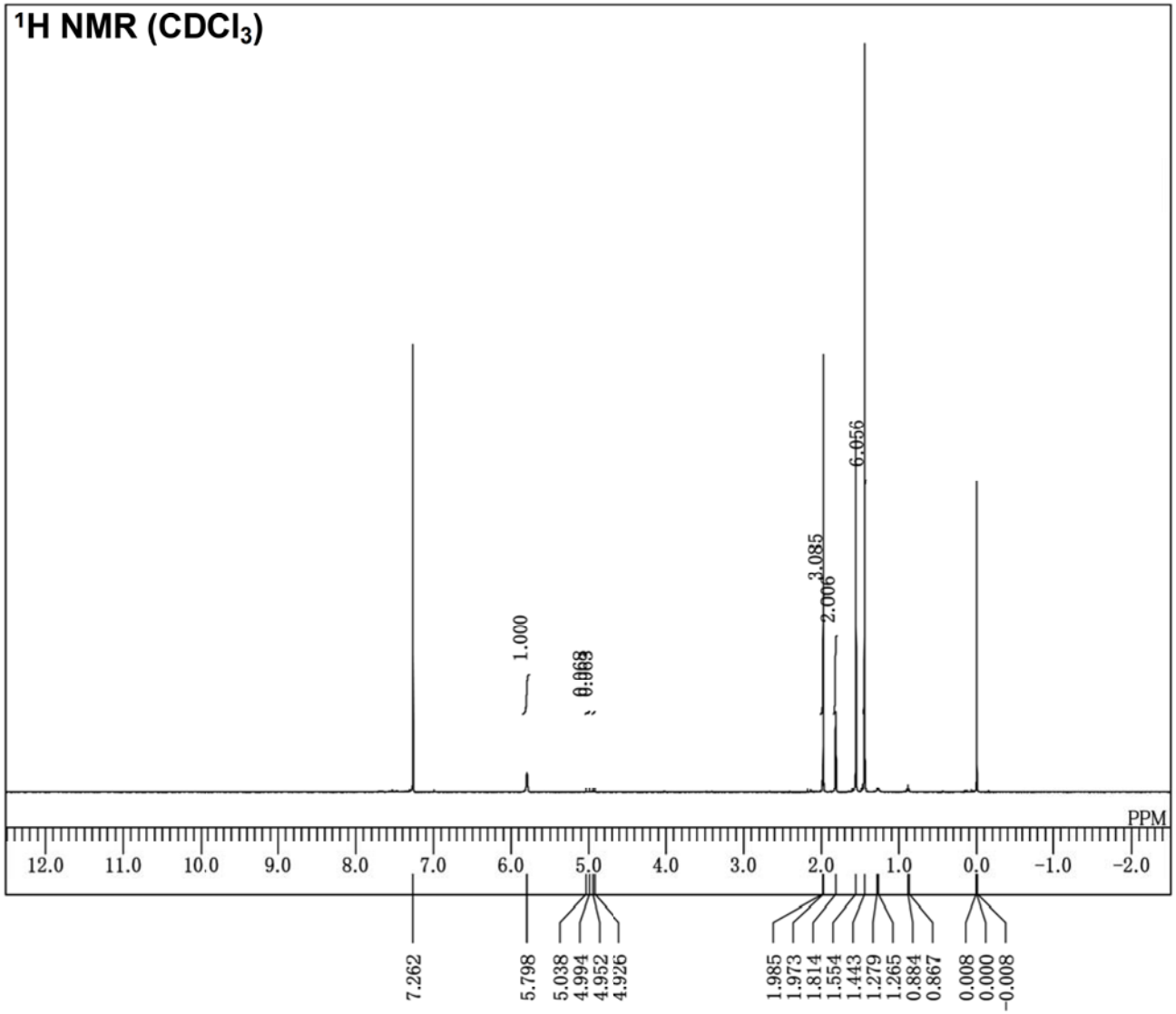
1H NMR (CDCl3)
1.000
3.085
2.006
6.056
PPM
12.0
11.0
10.0
9.0
8.0
7.0
6.0
5.0
4.0
3.0
2.0
1.0
0.0
-1.0
-2.0
7.262
5.798
5.038
4.994
4.952
4.926
1.985
1.973
1.814
1.554
1.443
1.279
1.265
0.884
0.867
0.008
0.000
-0.008

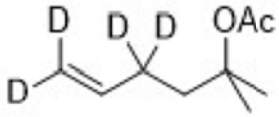
D
D
D
OAc
D

14-d_4

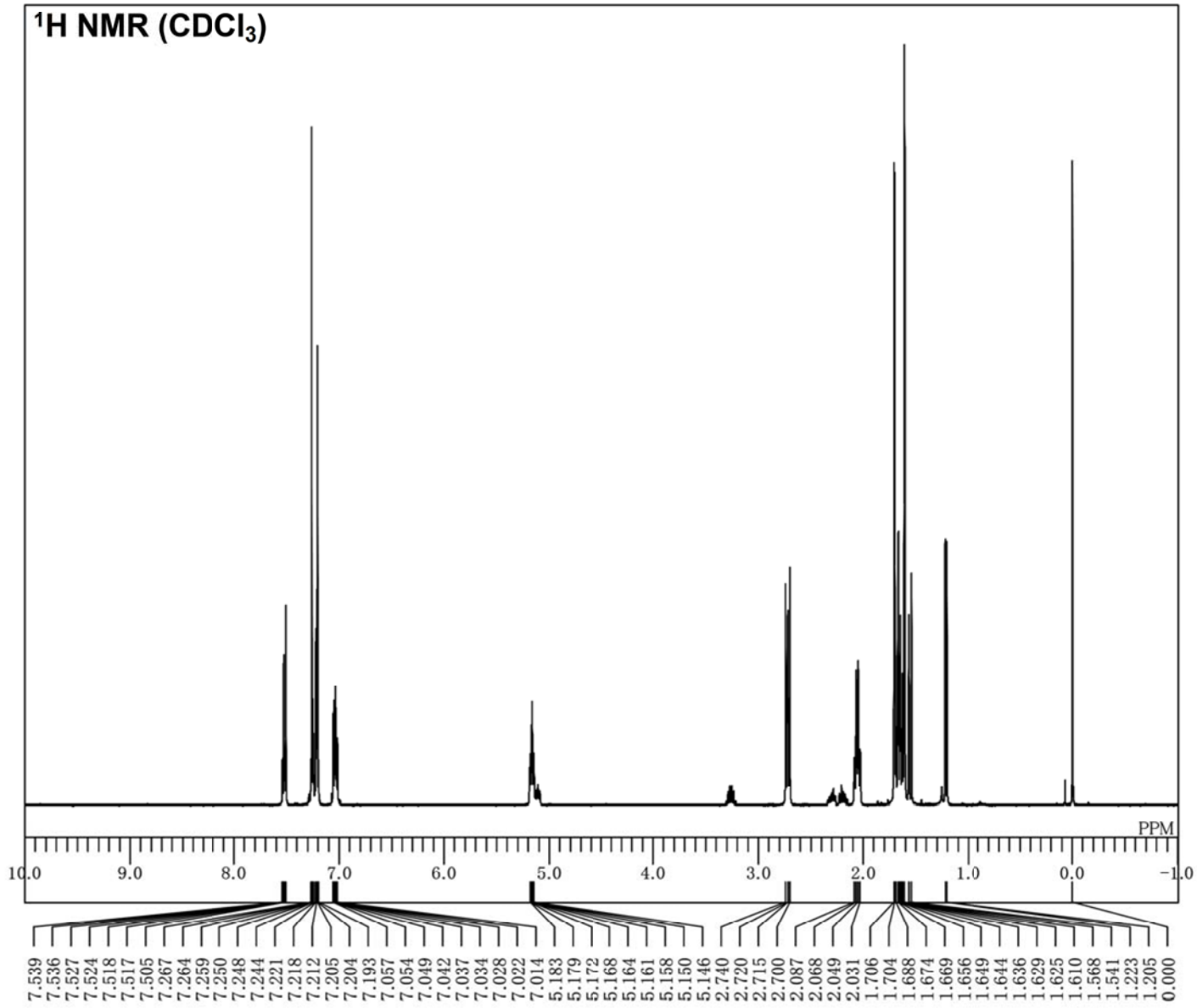
¹H NMR (CDCl₃)
PPM
10.0
9.0
8.0
7.0
6.0
5.0
4.0
3.0
2.0
1.0
0.0
−1.0
7.539
7.536
7.527
7.524
7.518
7.517
7.505
7.267
7.264
7.259
7.250
7.248
7.244
7.221
7.218
7.212
7.205
7.204
7.193
7.057
7.054
7.049
7.042
7.037
7.034
7.028
7.022
7.014
5.183
5.179
5.172
5.168
5.164
5.161
5.158
5.150
5.146
2.740
2.720
2.715
2.700
2.087
2.068
2.049
2.031
1.706
1.704
1.688
1.674
1.669
1.656
1.649
1.644
1.636
1.629
1.625
1.610
1.568
1.541
1.223
1.205
0.000

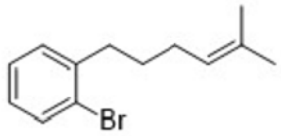
Br

16

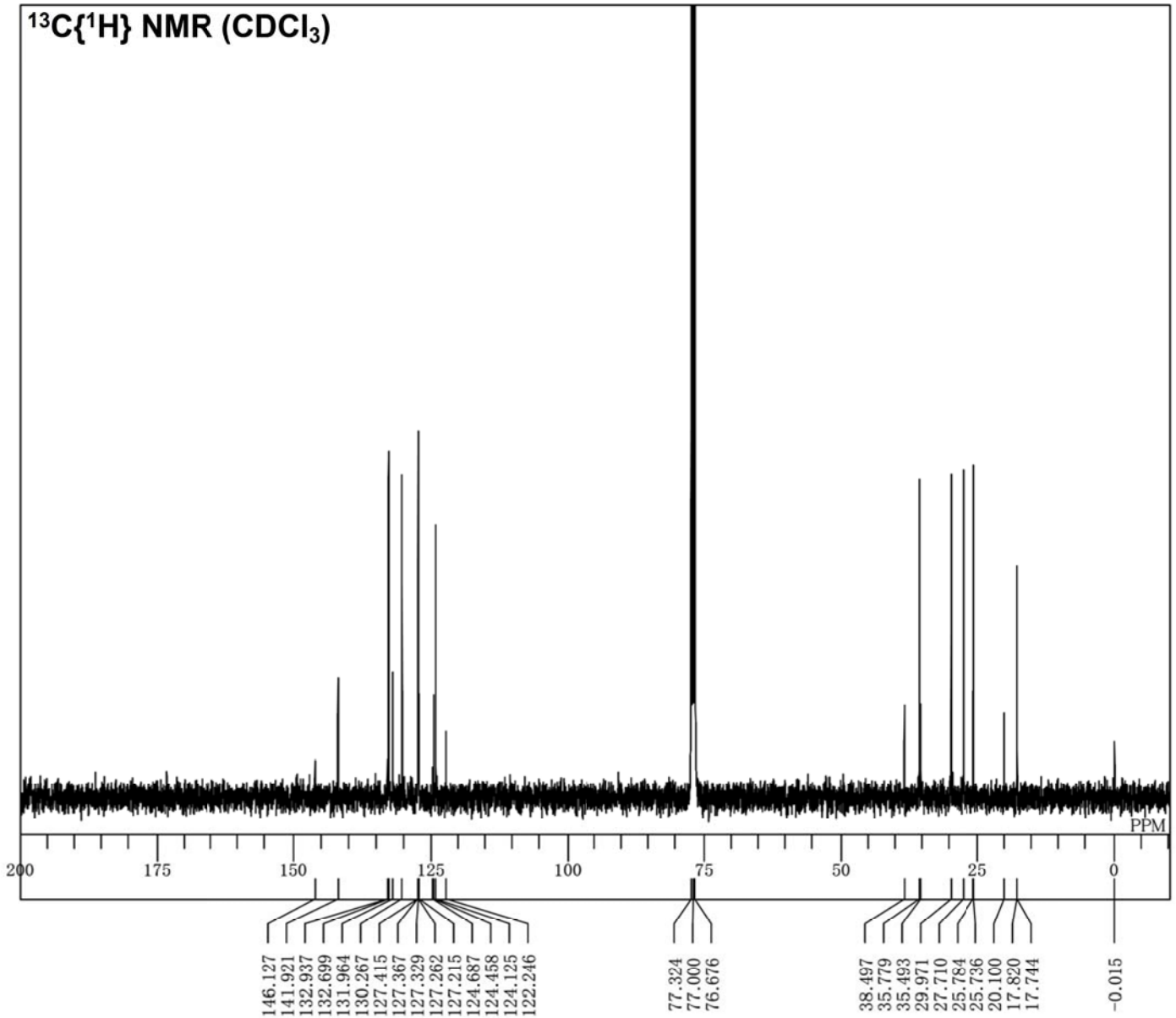
13C{1H} NMR (CDCl3)
PPM
200
175
150
125
100
75
50
25
0
146.127
141.921
132.937
132.699
131.964
130.267
127.415
127.367
127.329
127.262
127.215
124.687
124.458
124.125
122.246
77.324
77.000
76.676
38.497
35.779
35.493
29.971
27.710
25.784
25.736
20.100
17.820
17.744
-0.015

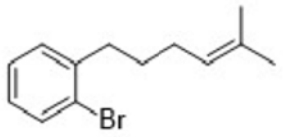
Br

16

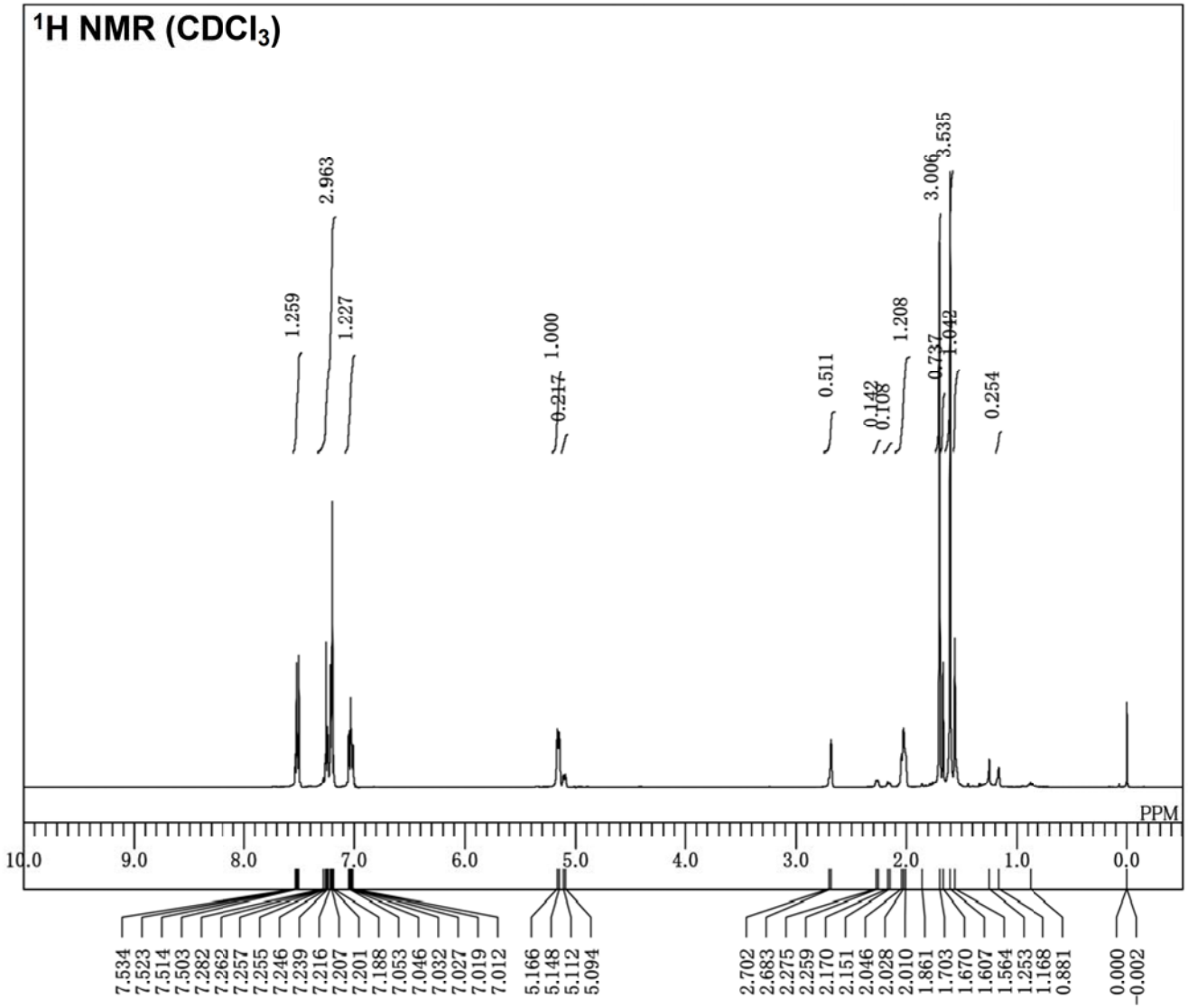
1H NMR (CDCl3)
1.259
2.963
1.227
1.000
0.217
0.511
0.142
0.108
1.208
0.737
1.042
3.006
3.535
0.254
PPM
10.0
9.0
8.0
7.0
6.0
5.0
4.0
3.0
2.0
1.0
0.0
7.534
7.523
7.514
7.503
7.282
7.262
7.257
7.255
7.246
7.239
7.216
7.207
7.201
7.188
7.053
7.046
7.032
7.027
7.019
7.012
5.166
5.148
5.112
5.094
2.702
2.683
2.275
2.259
2.170
2.151
2.046
2.028
2.010
1.861
1.703
1.670
1.607
1.564
1.253
1.168
0.881
0.000
-0.002

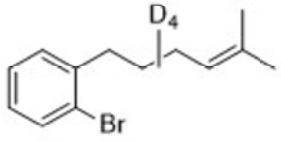
D4
Br

16-d_4

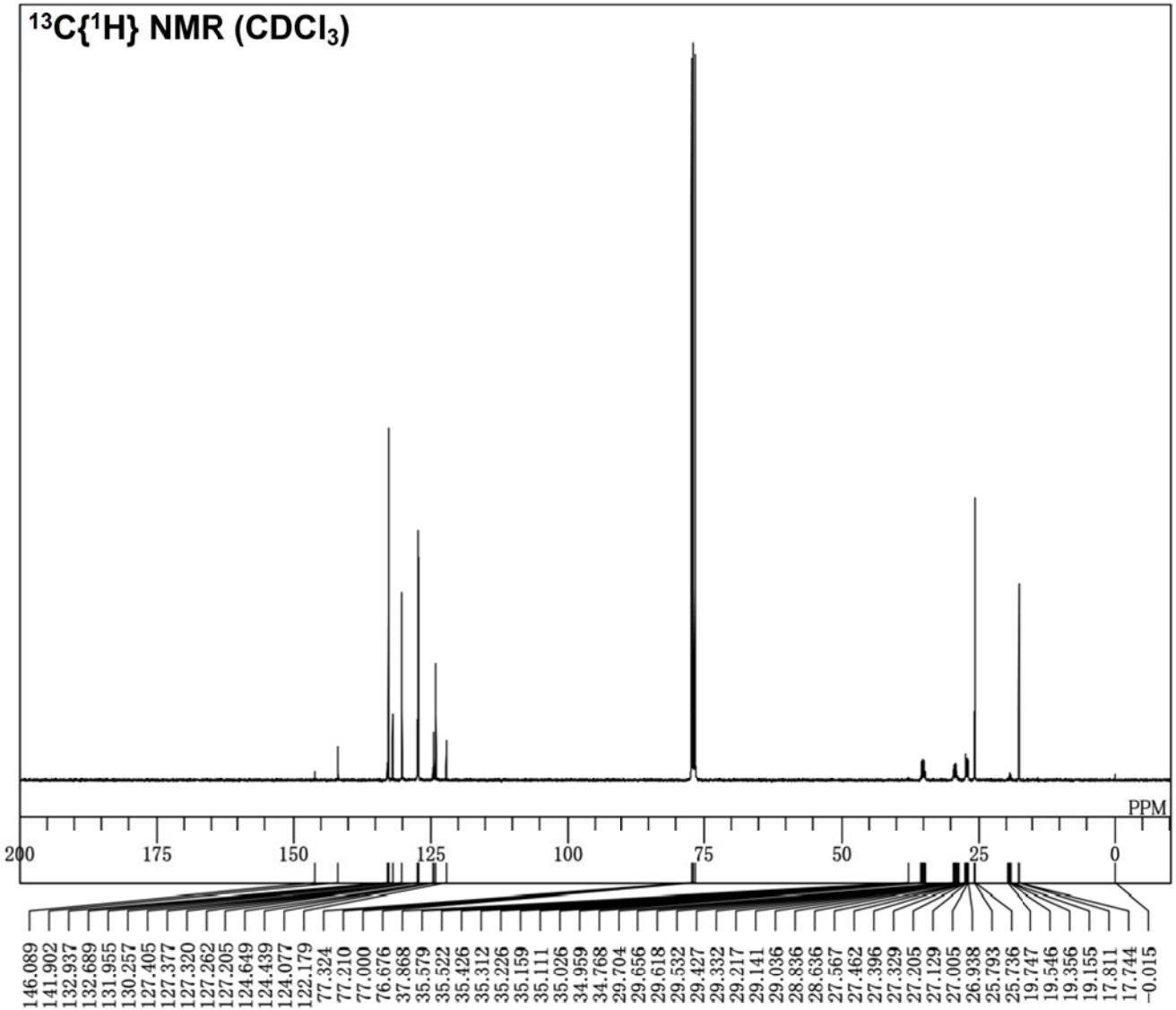
13C{1H} NMR (CDCl3)
PPM
200
175
150
125
100
75
50
25
0
146.089
141.902
132.937
132.689
131.955
130.257
127.405
127.377
127.320
127.262
127.205
124.649
124.439
124.077
122.179
77.324
77.210
77.000
76.676
37.868
35.579
35.522
35.426
35.312
35.226
35.159
35.111
35.026
34.959
34.768
29.704
29.656
29.618
29.532
29.427
29.332
29.217
29.141
29.036
28.836
28.636
27.567
27.462
27.396
27.329
27.205
27.129
27.005
26.938
25.793
25.736
19.747
19.546
19.356
19.155
17.811
17.744
-0.015

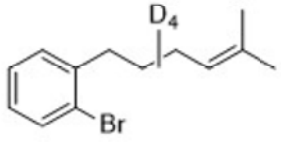
D4
Br

16-d_4

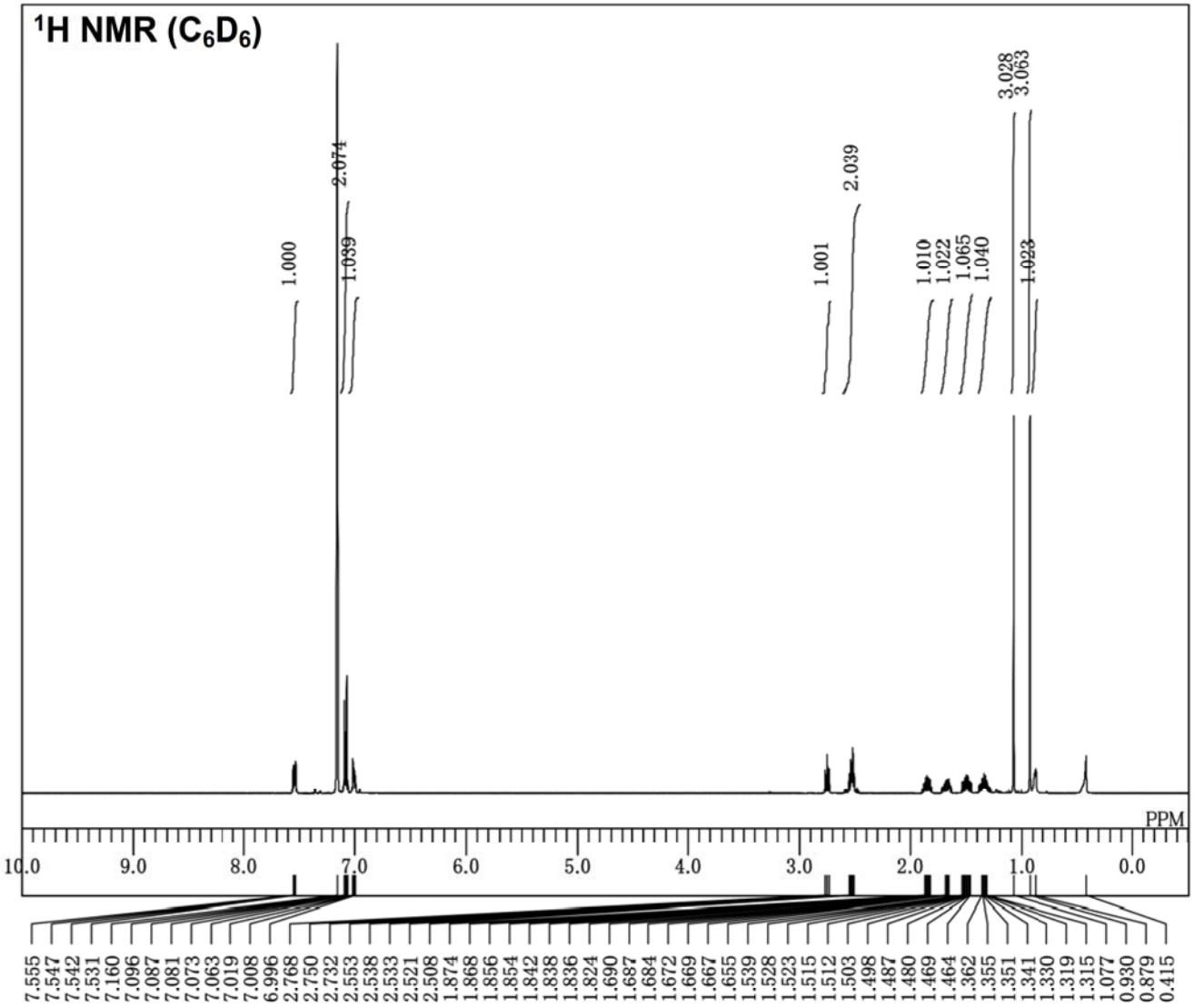
1H NMR (C6D6)
1.000
2.074
1.039
1.001
2.039
1.010
1.022
1.065
1.040
3.028
3.063
1.023
PPM
10.0
9.0
8.0
7.0
6.0
5.0
4.0
3.0
2.0
1.0
0.0
7.555
7.547
7.542
7.531
7.160
7.096
7.087
7.081
7.073
7.063
7.019
7.008
6.996
2.768
2.750
2.732
2.553
2.538
2.533
2.521
2.508
1.874
1.868
1.856
1.854
1.842
1.838
1.836
1.824
1.690
1.687
1.684
1.672
1.669
1.667
1.655
1.539
1.528
1.523
1.515
1.512
1.503
1.498
1.487
1.480
1.469
1.464
1.362
1.355
1.351
1.341
1.330
1.319
1.315
1.077
0.930
0.879
0.415

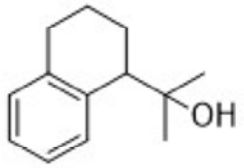
OH

18

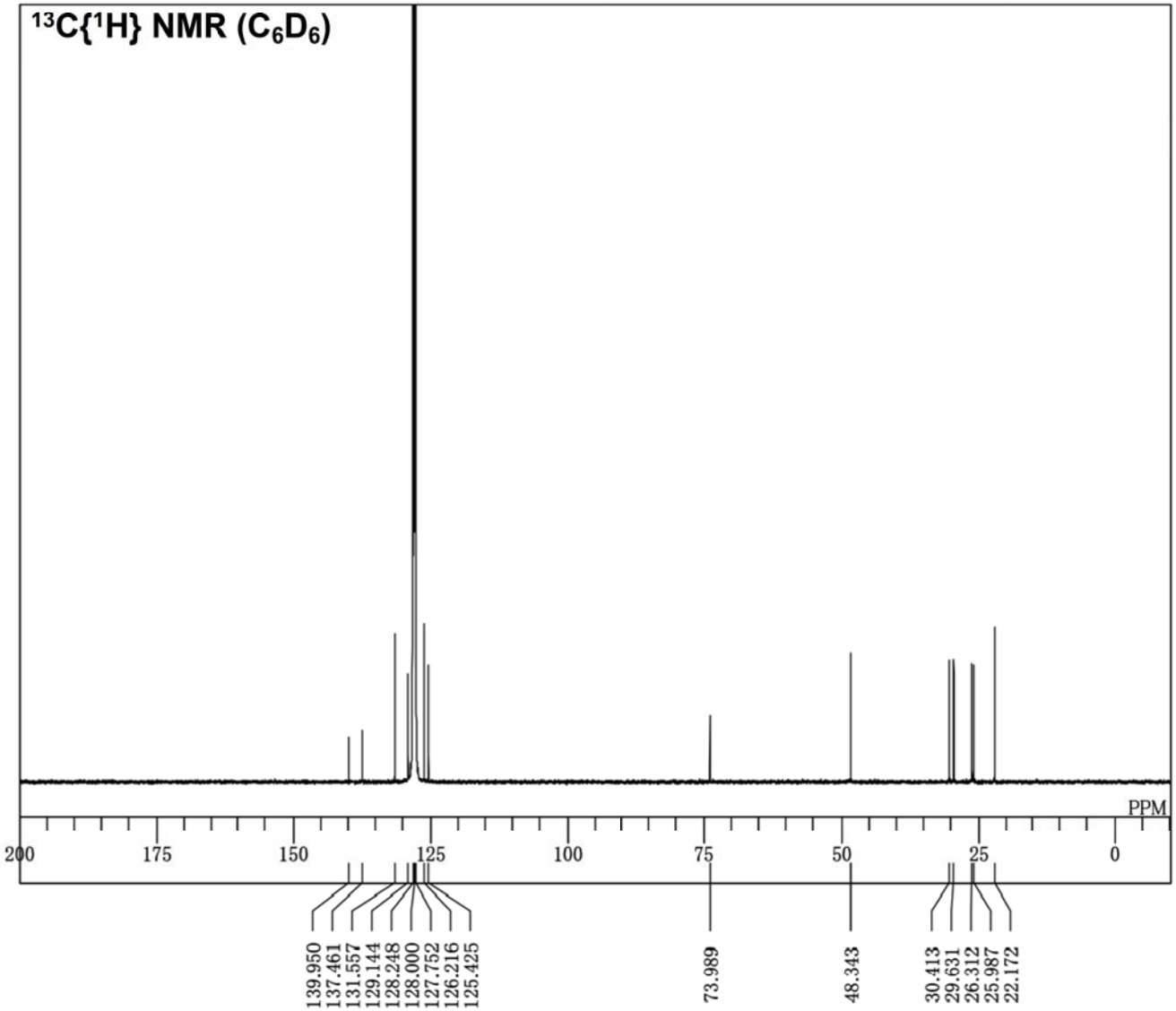
13C{1H} NMR (C6D6)
PPM
200
175
150
125
100
75
50
25
0
139.950
137.461
131.557
129.144
128.248
128.000
127.752
126.216
125.425
73.989
48.343
30.413
29.631
26.312
25.987
22.172

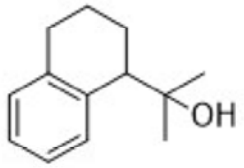
OH

18

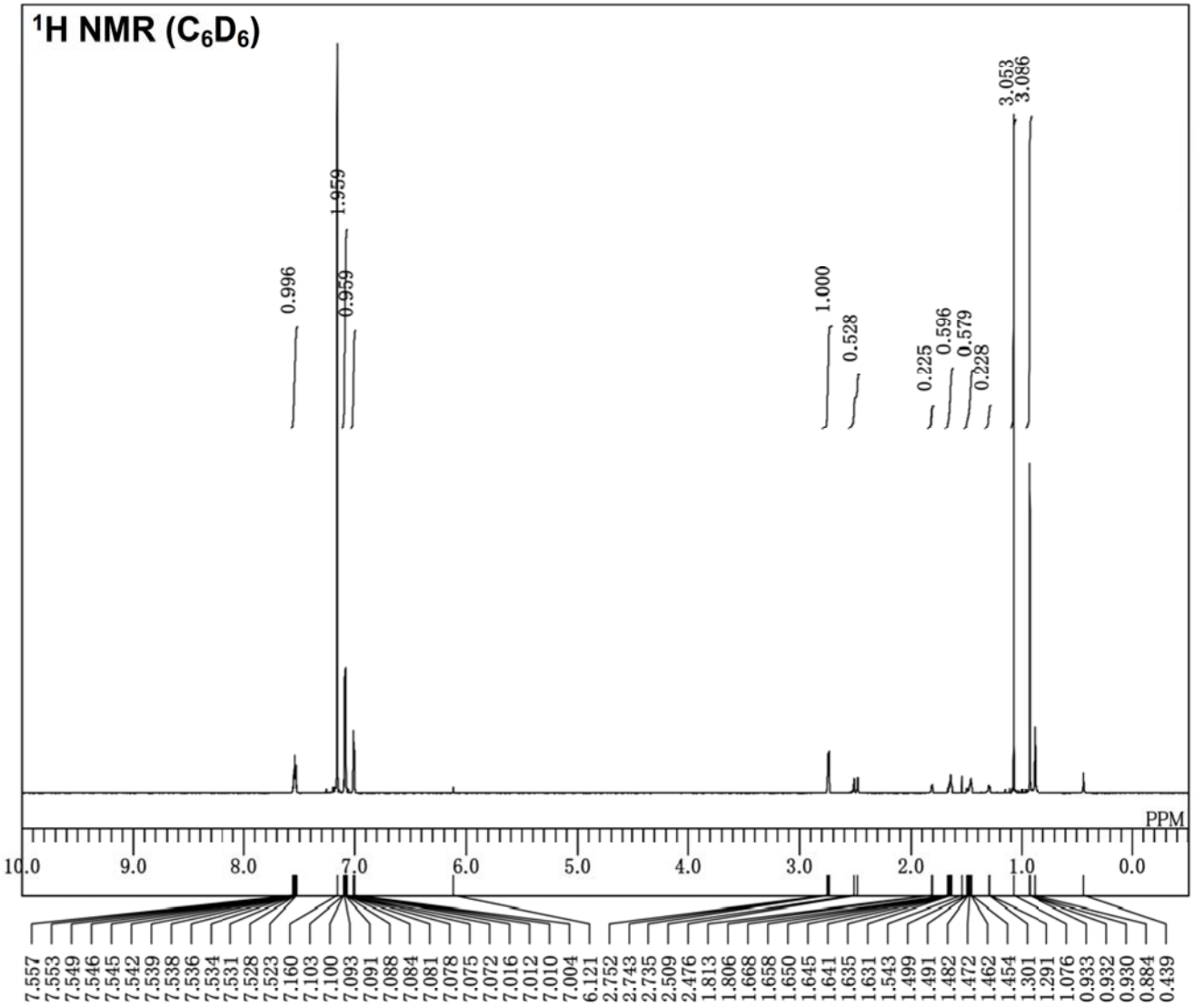
¹H NMR (C6D6)
0.996
1.959
0.959
1.000
0.528
0.225
0.596
0.579
0.228
3.053
3.086
PPM
10.0
9.0
8.0
7.0
6.0
5.0
4.0
3.0
2.0
1.0
0.0
7.557
7.553
7.549
7.546
7.545
7.542
7.539
7.538
7.536
7.534
7.531
7.528
7.523
7.160
7.103
7.100
7.093
7.091
7.088
7.084
7.081
7.078
7.075
7.072
7.016
7.012
7.010
7.004
6.121
2.752
2.743
2.735
2.509
2.476
1.813
1.806
1.668
1.658
1.650
1.645
1.641
1.635
1.631
1.543
1.499
1.491
1.482
1.472
1.462
1.454
1.301
1.291
1.076
0.933
0.932
0.930
0.884
0.439

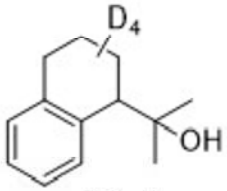
D4
OH

18-d_4

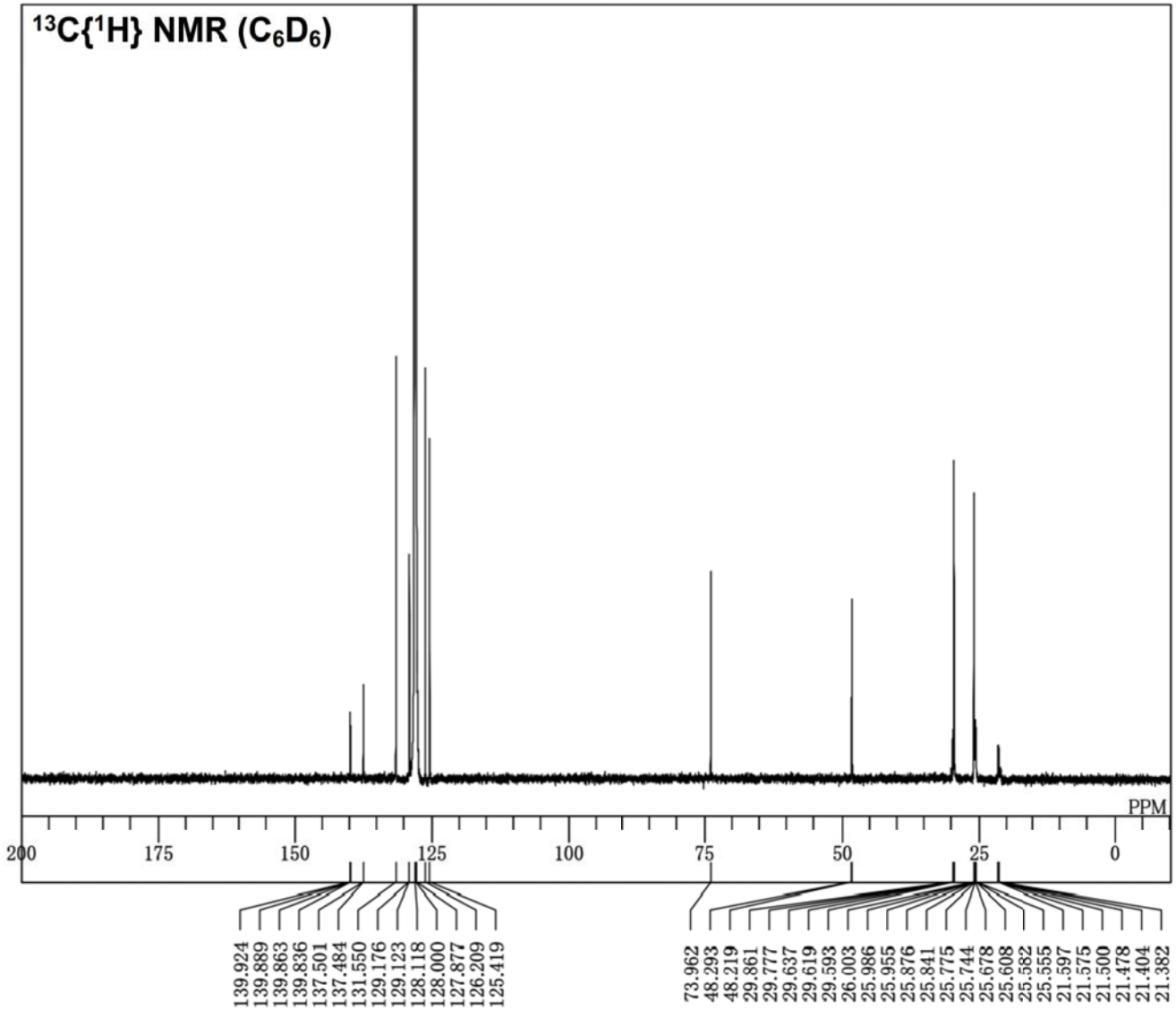
$^{13}C\{^{1}H\}$ NMR (C_6D_6)
PPM
200
175
150
125
100
75
50
25
0
139.924
139.889
139.863
139.836
137.501
137.484
131.550
129.176
129.123
128.118
128.000
127.877
126.209
125.419
73.962
48.293
48.219
29.861
29.777
29.637
29.619
29.593
26.003
25.986
25.955
25.876
25.841
25.775
25.744
25.678
25.608
25.582
25.555
21.597
21.575
21.500
21.478
21.404
21.382

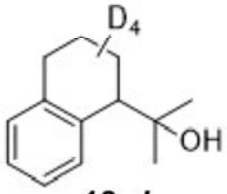
D4
OH

18-d_4